Deep Inelastic Scattering at High Energies

Luke Lippstreu

November 26, 2018

Contents

Outline of this thesis

The primary purpose of this thesis is to provide a pedagogical introduction into the general formalism for applying the theory of Quantum Chromodynamics (QCD) to collider phenomenology. To this end, we frame the discussion in terms of one of the simplest, yet still one of the most important collider observables, the process of deep inelastic scattering.

We begin by recounting three landmark experiments which lead to crucial breakthroughs in our understanding of the nucleus's' structure. We first describe the Geiger-Marsden experiment which provided the first evidence for the existence of the nucleus. We then describe the elastic electron-proton scattering experiments which first determined the scale of the nucleus. This is then followed by a discussion of the deep inelastic scattering experiments which gave the first evidence of Bjorken scaling. We then explain the theoretical line of reasoning which lead to the conclusion that Bjorken scaling implies that the field theory describing the nucleus must be of the Yang-Mills type.

In the next chapter we outline the theory of factorization, which is the central framework for any collider experiment prediction. We first develop the tools necessary for the proof of factorization in DIS. This involves the general investigation of infrared singularities in a quantum field theory by use of the theory of pinch singular surfaces (PSS). We describe how PSS offer a useful tool for understanding many aspects of field theories such as the cancellation of infrared divergences in certain observables, as well as the existence of jets in collider experiments. We then outline the proof of factorization in DIS. We then describe the definitions and properties of the parton distribution functions and the hard scattering co-efficients used in factorization theorems.

In the final chapter we study the cusp anomalous dimension which governs the large Bjorken-x behavior of parton distribution functions. We first motivate the use of a cusped Wilson line in the kinematic regime of large-x scattering. We then perform the one-loop calculation of a double cusped Wilson line. We then study the renormalization properties of lightlike Wilson lines. In so doing we are lead to an important QCD quantity the lightlike cusped anomalous dimension. Finally we indicate how this quantity governs the large-x behavior of the DGLAP splitting functions.

1 Introduction: A Brief History of the Nucleus

In this section we retrace the steps which lead from the discovery of the nucleus in the Cavendish laboratory in 1909, to the theory which describes the nucleus' structure, Quantum Chromodynamics, in 1973. The historical overview will also serve to introduce many of the key formula's for the rest of this thesis. We will recount three of the landmark experiments which revealed key aspects of the nucleus. We first describe Geiger and Marsden's 1909 α particle scattering experiment, which lead Ernest Rutherford to deduce that the positive charge of the atom must be concentrated in a very small core. We then turn to Hofstadter and McAllister's 1956 elastic electron-proton experiments which implied that the smallest nucleus, the proton, has a finite size of roughly a femtometre. We then turn to the 1967 SLAC-MIT deep inelastic scattering experiments which indicated that the proton is composed of *pointlike* constituents. This experiment also indicated that these constituents do not interact with one another. This striking featuring, called Bjorken scaling, was the essential observation which lead to the discovery of Quantum Chromodynamics. We conclude by summarizing the theoretical line of reasoning which lead theorists to deduce that Bjorken scaling implied that the theory of the strong interactions must be of the Yang-Mills type.

1.1 Geiger, Marsden and Rutherford (1909-1913)

In 1909, Geiger and Marsden [1] performed the following experiment, see Fig(1.1): a radioactive source of Radon (A) was placed below a $4 \times 10^{-7} m$ thick gold foil reflector (R) below which a florescent screen (S) and observational microscope were placed. The Radon source was known to produce α particles at a velocity of approximately $2 \times 10^{7} m/s$ and thus a kinetic energy of around 8 MeV. The radioactive source (A) was placed upon a lead plate in order to prevent the α particles from approaching the screen directly. The configuration was such that any α which reached (S) would need to be deflected by the gold foil by an angle greater than $90°$. They found that, of the α particles which struck the reflector, about 1 in $20,000$ were deflected though an average angle of $90°$.

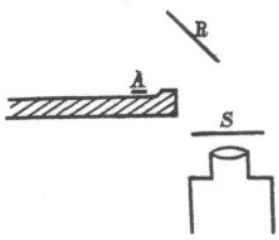

Figure 1.1: Geiger and Marsden's experimental setup. Figure taken from their paper [1].

Ernest Rutherford contemplated the implications of these results for the following two years. He came to the conclusion [2] that these large angle deflections of such energetic particles could only arise if the positive charge distribution of the atom were concentrated in a region at least 10^4 times smaller than the size of the atom. This was in stark contrast to Lord Kelvin's "plum-pudding" model, which saw the atom as a sphere filled with a uniform positive charge distribution in which the electrons were embedded.

Rutherford first argued that one could ignore the influence of the atomic electrons as they were known to be approximately 8000 times lighter than the α particles, and with the innermost electrons binding energy being on the order of 100 KeV, the large difference in the energy scales between the two particles kinematically forbade the electron from imparting a large momentum to the α. In the opposite limit, it was known that the gold atom is 50 times heavier than the α particle and thus it was a good approximation to assume that the positive charge of the atom did not recoil when scattering against the α particle. If one then supposed that the positive charge of an atom Q_a were uniformly spread out throughout it's radius R, then the electric force experienced by an α particle a distance r away from the center of the atom would be

$$F = \frac{Q_\alpha Q_a}{4\pi\epsilon_0}\frac{r}{R^3} \tag{1.1}$$

Approximating the time an α particle of velocity v spends in the vicinity of the atom to be $\Delta t \approx \frac{2R}{v}$, an impulse approximation yields a momentum transfer of

$$\Delta p = F\Delta t = \frac{Q_\alpha Q_a}{4\pi\epsilon_0}\frac{2r}{vR^2} \tag{1.2}$$

Thus the greatest momentum is imparted for scattering at grazing distance $r = R$. Supposing that the α particle scatters at this distance and that the force only acts orthogonally to the momentum of the α, the angular deflection can approximated to be

$$\theta \approx \frac{\Delta p}{p} = \frac{1}{T}\frac{Q_\alpha Q_a}{4\pi\epsilon_0}\frac{1}{R}\ , \tag{1.3}$$

where T is the kinetic energy of the α particle. The radius of atoms was known at the time (from experiments in kinetic theory) to be of the order of $10^{-10}m$. Substituting in this value for R and taking $Q_\alpha = 2e$, $Q_{Au} = 79e$ and $T = 8$ MeV one obtains a deflection angle of

$$\theta \approx 0.0004^\circ\ . \tag{1.4}$$

J.J. Thompson had proposed that large angle scattering arose from multiple scatterings. Rutherford pointed out that as the gold foil was only 400 atoms thick, one could only expect a variance in the total scattering angle of $\theta_{total} = \sqrt{400}\cdot\theta = 0.008^\circ$ about an average total scattering angle of zero. Thus a diffuse atom was not sufficient for producing large angle deflections. Referring to Eq.(1.3), the only way to increase the scattering angle to 90° would be to decrease R by five orders of magnitude.
This motivated Rutherford to model the positive charge of the atom to be pointlike, producing a Coulomb potential

$$V(r) = \frac{1}{4\pi\epsilon_0}\frac{Q_a}{r}\ . \tag{1.5}$$

The hyperbolic solution for scattering on a $\frac{1}{r}$ potential was well known from celestial mechanics, thus allowing Rutherford to make a precise prediction for his model. Presuming that the large angle deflection occurred due to a single interaction, and averaging over the impact parameter, Rutherford arrived at the prediction that the number of α particles falling on a unit area per second on a screen a distance r away from the gold foil should be equal to

$$y = \frac{Fnt}{4r^2} \frac{Q_{Au}^2 Q_\alpha^2}{m^2 v^4 \sin^4(\frac{\theta}{2})} \ , \tag{1.6}$$

where F is the number of α particles per second striking the gold foil, t is the thickness of the material, n is the number of atoms in a unit volume of the material and m, v, E are respectively the mass, velocity and charge of the α particle. Rutherford thereby introduced the concept of the differential cross for the first time in physics.
Geiger and Marsden designed four experiments [3] to test four of the features of Eq.(1.6): the $\sin^{-4}(\frac{\theta}{2})$ angular dependence, the v^{-4} velocity dependence, the linear dependence on the thickness t of the material and the charge dependence of the cross section. They published their results in 1913 [3] with excellent agreement between the data and the model.
Thus by 1913 the picture of the atom as consisting of a concentrated positive charge at least 10^4 times smaller than the atom had been firmly established. It was yet to be determined whether the nucleus was a pointlike object or whether it had any spatial extent.

***

To better appreciate the subsequent experiments it will be instructive to interpret Geiger and Marsden's experiment in terms of the Born approximation of non-relativistic quantum mechanics. The Born approximation tells us that the cross section for a particle of momentum $\vec{p_i}$ to scatter elastically on a potential $V(r)$ into a final momentum $\vec{p_f}$ is proportional to the square of the momentum imparted $\vec{q} \coloneqq (\vec{p_f} - \vec{p_i})$ Fourier mode of the potential

$$\frac{d\sigma}{d\Omega} \propto \left| \int d^3r \, e^{iq\cdot r} V(r) \right|^2 \quad ; \quad V(r) = \int d^3r' \frac{\rho(r')}{|r - r'|} \tag{1.7}$$

Thus a charge density equally distributed over a region of the order R, will only have Fourier modes on the order of $\frac{1}{R}$ and hence cannot impart a momentum greater than $\vec{q} \lesssim \frac{1}{R}$. However, a pointlike distribution has Fourier modes at all momenta and hence is capable of producing the large angle deflections seen in the Geiger-Marsden experiment.

1.2 Elastic Electron-Proton Scattering (1956-1966)

To resolve the structure of the nucleus on the smallest possible distance scale, one would like to take the smallest possible nucleus (a proton), the smallest possible probe (an electron) and collide them at the highest possible energy. This leads to high energy $e^- p^+$ collisions. In 1956 McAllister and Hofstadter [4] scattered 188 MeV electrons elastically off of a stationary target of hydrogen gas and measured only the electrons final state momentum. Their experiment indicated that at sufficiently high momenta, the proton was incapable of producing large angle deflections, hence indicating that the proton has a finite size. Their results indicated a proton radius on the order of a femtometre. To appreciate their results, see Fig(1.3), we must first parameterize the elastic electron-proton cross section in terms of variables which can be inferred from only measuring the final state electrons momentum.

Let us first build up the physical meaning of all the terms in the Rosenbluth formula Eq.(1.16) which describes the elastic scattering of an electron off of a proton. If the proton were structureless, spinless, infinitely heavy and the electron spinless, then the elastic $e^- p$ scattering cross section would, in the framework of quantum field theory, at tree level, be the relativistic Rutherford formula

$$\left(\frac{d\sigma}{d\Omega}\right)_{Lab} = \frac{\alpha_e^2}{4E^2 \sin^4 \frac{\theta}{2}}\,, \tag{1.8}$$

where E is the relativistic energy of the incident electron and θ is the scattering angle of the electron. Taking account of the electron's spin gives the Mott cross section, see curve (a) of Fig(1.3)

$$\left(\frac{d\sigma}{d\Omega}\right)_{Lab} = \frac{\alpha_e^2 \cos^2 \frac{\theta}{2}}{4E^2 \sin^4 \frac{\theta}{2}} \tag{1.9}$$

Rutherford was therefore rather lucky in that alpha particles have zero spin in their ground state. Had he used particles with spin as a probe of the nucleus he would have found that his prediction Eq.(1.6) would have failed terribly.
If the electron is scattered by a static source, it's final energy E' is the same as it's incident energy E. If the target has a finite mass M, and thus recoils, then for elastic scattering the final electron energy is

$$E' = \frac{E}{1 + \frac{2E}{M} \sin^2 \frac{\theta}{2}}\,. \tag{1.10}$$

Including this recoil effect, and also accounting for the spin-$\frac{1}{2}$ of the proton

$$\left(\frac{d\sigma}{d\Omega}\right)_{Lab} = \frac{\alpha_e^2 \cos^2 \frac{\theta}{2}}{4E^2 \sin^4 \frac{\theta}{2}} \cdot \frac{E'}{E}\left(1 + \frac{Q^2}{2M^2} \tan^2 \frac{\theta}{2}\right) \tag{1.11}$$

where we have introduced the positive quantity $Q^2 \coloneqq -q^2$. The $\tan^2 \frac{\theta}{2}$ term arises due to the spin-spin interaction. This magnetic type of scattering causes

a leveling off in the decrease of the elastic cross section as a function of the scattering angle at high energies of the incident electron (compare curves (a) and (b) of Fig(1.3)). Note that Eq.(1.11) approaches the Mott cross section as the target mass increases.
Thus far we have considered the proton to be structureless. If we presume that the interaction between the electron and proton proceeds via a single photon exchange, then the amplitude reads

$$\mathcal{M} = \frac{4\pi\alpha}{q^2} J^e_\mu(q) J^\mu_p(q)\,, \tag{1.12}$$

where J^e_μ and J^μ_p are respectively the electron and proton electromagnetic currents. Without loss of generality one can always parameterize an electromagnetic current in the form

$$J_\mu = \bar{u}(p_f)\left[F_1(q^2)\gamma_\mu + i\frac{q^\nu \sigma_{\mu\nu}\kappa}{2M} F_2(q^2)\right] u(p_i)\,. \tag{1.13}$$

Here p_i and p_f are the initial and final particles momenta, $q \coloneqq p_f - p_i$ is the four momentum transfer and κ is the anomalous magnetic moment of the particle ($\kappa = 1.79$ for the proton). Eq.(1.13) assumes only the QED Ward identity and that the incoming and outgoing proton are on-shell. The functions F_1 and F_2 are referred to as *form factors*. In the non-relativistic limit $\frac{q^2}{4M_p^2} \ll 1$ they are related to the Fourier transforms of the charge ρ and magnetic moment μ distributions of the target[1]

$$G_E(q^2) \coloneqq F_1(q^2) - \frac{Q^2\kappa}{2m_p^2} F_2(q^2) = \int d^3\mathbf{r}\ \ e^{i\mathbf{q}\cdot\mathbf{r}}\rho(\mathbf{r}) \tag{1.14}$$

$$G_M(q^2) \coloneqq F_1(q^2) + \kappa F_2(q^2) = \int d^3\mathbf{r}\ \ e^{i\mathbf{q}\cdot\mathbf{r}}\mu(\mathbf{r}) \tag{1.15}$$

For example the electron has $F_1(0) = 1$ and $F_2(0) = 0$, indicating the total charge and magnetic moment of the electron. If we use the current parameterization Eq.(1.13) for the proton in Eq.(1.12) one arrives at the Rosenbluth formula for the elastic differential cross section[2]

$$\left(\frac{d\sigma}{d\Omega}\right)_{lab} = \left(\frac{d\sigma_0}{d\Omega}\right)\left\{\left(F_1^2 + \frac{\kappa^2 Q^2}{4m_p^2}F_2^2\right) + \frac{Q^2}{2m_p^2}\left(F_1 + \kappa F_2\right)^2 \tan^2\frac{\theta}{2}\right\} \tag{1.16}$$

$$\frac{d\sigma_0}{d\Omega} \coloneqq \frac{\alpha_e^2 \cos^2\frac{\theta}{2}}{4E^2 \sin^4\frac{\theta}{2}}\frac{E'}{E} \tag{1.17}$$

[1] To see this, one compares the result Eq.(1.16) to the Born approximation of non-relativistic quantum mechanics for scattering on a classical charge and magnetic moment distribution.

[2] The Rosenbluth formula ignores the form factor and bremsstrahlung contributions of the electron current. McAllister and Hofstadter could ignore these effects when comparing theory to data as the electron form factors are known to scale very slowly (logarithmically) and hence modified the angular dependence very weakly over the kinematic range covered in their experiment [4]. However, in the region of a particle resonance, such effects cannot be ignored.

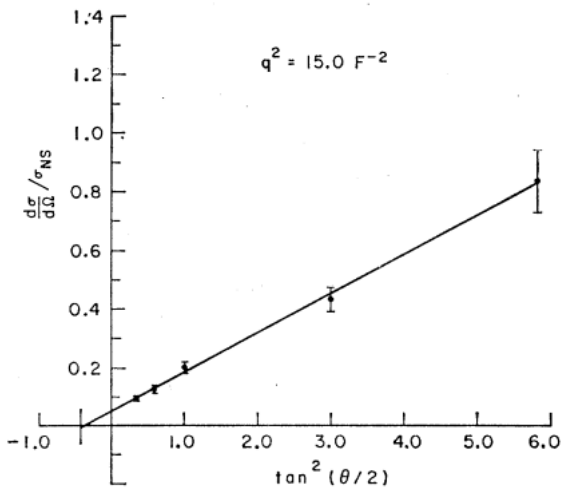

Figure 1.2: Rosenbluth plot of the neutron for a momentum transfer $q^2 = 15.0F^{-2}$. The straight line behavior agrees with the single photon exchange approximation which is implicit in Eq.(1.16). Plot taken from [5].

The formula Eq.(1.16) followed from an assumption of single photon exchange between the target and the electron. The validity of this assumption can be tested experimentally by dividing the observed cross section by $\frac{d\sigma_0}{d\Omega}$ and plotting the result at fixed q^2 as a function of $\tan^2\frac{\theta}{2}$. The result should be a straight line. Fig(1.2) taken from [5] indicates that the approximation holds at the energies relevant to the McAllister and Hofstadter experiment. Furthermore, the form factors can be readily inferred from such Rosenbluth plots by measuring the slope and intercept of the line.
Before turning to the experimental data, let us briefly consider what one could mean by a pointlike particle in a quantum theory. In a classical field theory a point charge distribution $\rho(r) = \delta^3(r)$ would have a constant Fourier transform and hence also constant structure function. In this case the Rosenbluth formula reduces to Eq.(1.11). However, in a quantum theory, a point particle has a logarithmically dependent charge and magnetic moment distribution induced by quantum effects. For example, the τ lepton is considered to be a more massive version of the electron and in $e^-\tau^- \to e^-\tau^-$ scattering one finds, both in theory and experiment, that it has a logarithmically dependent form factor

$$F_1(q_1^2) - F_1(q_2^2) \approx -\frac{e^2}{16\pi^2}\ln\frac{q_1^2}{q_2^2}, \qquad |q_1^2|, |q_2^2| \gg m_\tau^2 \tag{1.18}$$

However, a logarithm does not indicate any inherent scale and thus one can continue to refer to the τ as a pointlike particle. If a particle has some finite extent L then one expects the Fourier transform of it's charge distribution to fall off after $q \gtrsim \frac{2\pi}{L}$. Thus as the de Broglie wavelength of the photon approaches

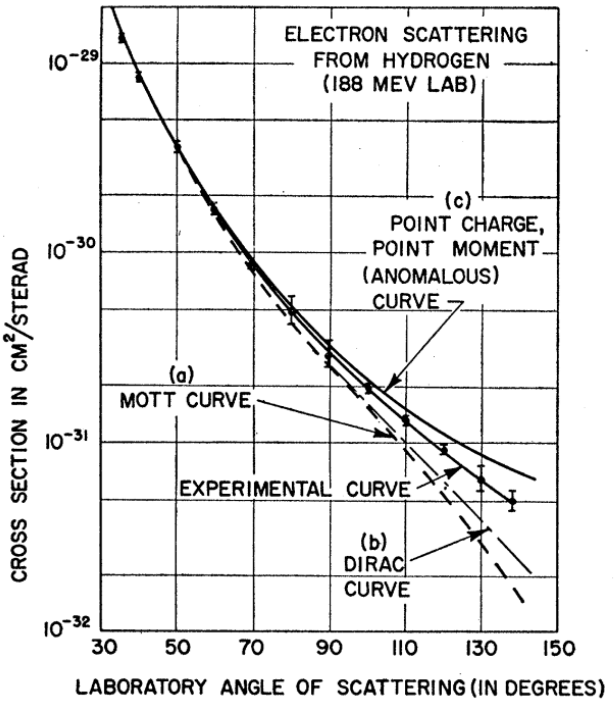

Figure 1.3: Curve (a) shows the theoretical Mott curve for a spinless point proton. Curve (b) shows the theoretical curve for a point proton with the Dirac magnetic moment (gyromagnetic ratio 2.00), curve (c) the theoretical curve for a point proton having the anomalous contribution in addition to the Dirac value of the magnetic moment (gyromagnetic ratio= 5.58). The experimental curve falls between curves (b) and (c). This deviation from the theoretical curves represents the effect of a form factor for the proton and indicates structure within the proton, or alternatively, a breakdown of the Coulomb law. The best fit indicates a size of 0.70×10^{-13}cm. Figure taken from [4]

the size of the target one expects the cross section to drop below that of a point particle's.

The results of McAllister and Hofstadters elastic electron-proton scattering experiments [4] are summarized in Fig(1.3). The data clearly demonstrated that at large scattering angles (and hence large momentum transfers) the cross section dropped below that of a constant structure functions cross section. One can observe in Fig(1.3) that the experimental curve lies below that of a point proton with a constant magnetic moment of 1.79. This suggested that the charge of the proton was diffusively spread out. At the energies used in these experiments one could not distinguish between a uniform, exponential, or Gaussian charge

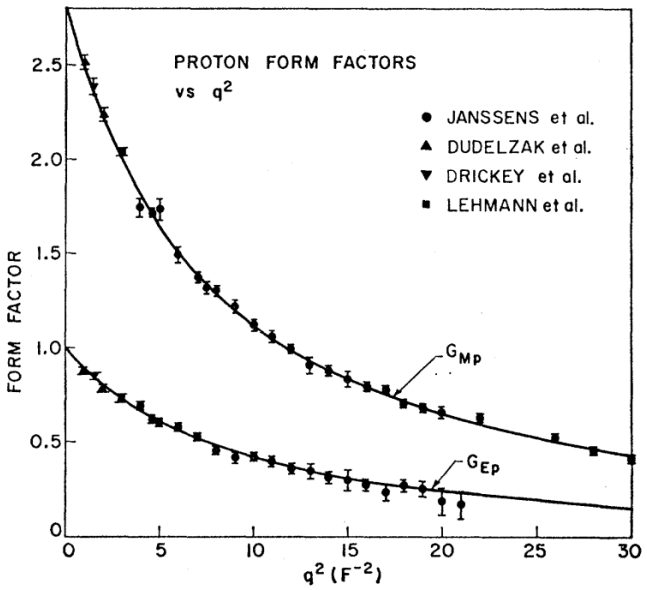

Figure 1.4: Proton form factors for elastic scattering in [5] were found to be fitted by Eq.(1.19) with the scale $0.71\,\mathrm{GeV}^2$ emerging for both form factors.

distribution. All that could be inferred was a root mean square radius of the proton. By measuring the form factors at low momentum transfer

$$\begin{aligned} F(q^2) &= \int d^3r\rho(r)e^{i\mathbf{q}\cdot\mathbf{r}} \\ &= \int d^3r\rho(r)[1 + i\mathbf{q}\cdot\mathbf{r} - \frac{1}{2}(\mathbf{q}\cdot\mathbf{r})^2 + \mathcal{O}(\mathbf{q}\cdot\mathbf{r})^4] \\ &= 1 - \frac{\mathbf{q}^2}{6}\langle r^2\rangle \end{aligned}$$

and assuming that the same $\langle r^2\rangle$ applied to both form factors, McAllister and Hofstadter found root mean square radius of $\langle r^2\rangle^{\frac{1}{2}} = 0.74 \pm 0.24$ fm. Subsequent studies [6] found that the form factors did indeed exhibit a characteristic length scale with the form factors found to be best fitted by the so-called dipole parameterization

$$G_{E_p}(q^2) \approx \frac{1}{\left(1 - \frac{q^2}{0.71GeV^2}\right)^2} \tag{1.19}$$

Here a definite scale of $0.71\,\mathrm{GeV}^2$ appears. Taking the Fourier transform implies the charge distribution

$$\rho(r) \approx e^{-\frac{r}{r_0}} \tag{1.20}$$

with $r_0 \approx 0.24\,fm$ implying a charge root mean square radius of $r_{rms} \approx 0.8\,fm$. What is important is that a length scale emerged at all, which is in contrast to a logarithmic structure function which would have indicated that the proton was a quantum point particle. Thus by 1966 it had unambiguously been determined that the proton did indeed have a size of roughly a femtometre. The question as to whether the proton was composite had to wait for inelastic scattering.

1.3 Deep Inelastic Scattering at SLAC (1967-1969)

In the late 1960's the Stanford Linear Accelerator Center (SLAC) opened a vast new energy domain for exploration. The two mile long accelerator produced electrons with energies up to about 18 GeV and collided them against a stationary liquid hydrogen target. At these high energies much of the scattering was inelastic, typically $ep \to ep\pi\pi...$ or $ep \to en\pi\pi....$ The SLAC data showed two surprising features of the proton: that it contained pointlike constituents and that these constituents appeared to not be interacting with one another, which seemed to be in contradiction with the fact that the strong interactions needed to be strong in order to overcome the electromagnetic repulsion between protons in a nucleus. The theoretical activity stimulated by these two observations would in a short period lead to the discovery of Quantum Chromodynamics. To appreciate their results we must first parameterize the total (inelastic and elastic) electron-proton cross section when only the final state electron is measured.

When the scattering is not elastic, the energy and direction of the scattered electron are independent variables, unlike the elastic scattering situation (that is Eq.(1.10) does not apply), thus the relevant differential cross section becomes $\frac{d^2\sigma}{d\Omega dE'}$. In a similar manner to the derivation of the Rosenbluth formula, one can write down the most general parameterization of the inelastic and elastic differential cross section when only the final state electron is measured

$$\left(\frac{d\sigma}{dE'\,d\Omega}\right)_{Lab} = \left(\frac{d\sigma}{d\Omega}\right)_{\text{MOTT}} \left[W_2(\nu, Q^2) + 2W_1(\nu, Q^2)\tan^2\frac{\theta}{2}\right] \tag{1.21}$$

$$\left(\frac{d\sigma}{d\Omega}\right)_{\text{MOTT}} \coloneqq \frac{\alpha_e^2}{4E^2}\frac{\cos^2\frac{\theta}{2}}{\sin^4\frac{\theta}{2}} \tag{1.22}$$

This expression depends on two *structure functions*[3], W_1 and W_2, related to the two possible polarizations of the virtual photon, see Eq.(A.27,A.28). As the energy and angle of the electron are no longer related[4], these structure functions depend on two variables. In Eq.(1.21) we have chosen to use the two variables $\nu \coloneqq \frac{P\cdot q}{M_p} = (E - E')_{lab}$, the energy lost by the electron in the laboratory frame, and Q^2 the virtuality of the photon, which determines the length scale $\frac{1}{Q}$ on

[3]The nomenclature is that functions which parameterize the cross section which depend on a single variable are referred to as a form factor, whereas functions of several variables are called structure functions.

[4]For elastic scattering one has that $(P+q)^2 = M_p^2$ and hence the two variables are related by $Q^2 = 2M_p\nu$

which the proton is probed. Eq.(1.21) is the most important expression in this thesis. All the theoretical ideas explored will be tested by making predictions for $W_2(\nu, Q^2)$. As such, we recall the derivation of Eq.(1.21) in Appendix.(A). Note that Eq.(1.21) follows from the approximation of a single photon exchange[5].
The experimental data from the 1967 run [7] at SLAC is reproduced in Fig(1.5). The differential cross section is plotted as a function of the mass of the hadronic system $W^2 \coloneqq (P+q)^2$. The low W region $W \lesssim 4\,\mathrm{GeV}$ showed the predicted behavior: peaks appeared as W approached the mass of one of the resonances in the sequence N^* ($I = \frac{1}{2}$ nonstrange baryons) or Δ ($I = \frac{3}{2}$ nonstrange baryons). These resonances can clearly be seen in Fig(1.5)(a) and (b). In terms of the parameterization of DIS discussed in Appendix(A), these resonances correspond to momentum values q^μ where the matrix element $\langle \mathcal{X}|\tilde{J}(q)|P\rangle$ is large. As the momentum transfer Q^2 was increased the resonances decreased about just as rapidly as the elastic proton form factor. This could be attributed to Q^{-1} no longer corresponding to the size of the hadrons.

The resonant behavior was as predicted. What was surprising was the behavior for W values beyond the resonances. As can be seen in Fig(1.5), the cross section in this region did not appear to be decreasing with increased Q^2. Further analysis of the data [8] indicated that the weak Q^2 dependence of the cross section was between one and two order of magnitude greater than expected. The Q^2 dependence of the cross section for scattering at 10° is plotted in Fig(1.6). The y-axis refers to the structure functions

$$\left(\frac{d^2\sigma}{d\Omega dE'}\right)\Big/\left(\frac{d\sigma}{d\Omega}\right)_{MOTT} = W_2(\nu, Q^2) + 2W_1(\nu, Q^2)\tan^2\frac{\theta}{2} \tag{1.23}$$

For comparison, the elastic form factors

$$\left(\frac{d\sigma}{d\Omega}\right)\Big/\left(\frac{d\sigma}{d\Omega}\right)_{MOTT} = \left(F_1^2 + \frac{\kappa^2 Q^2}{4m_p^2}F_2^2\right) + \frac{Q^2}{2m_p^2}\left(F_1 + \kappa F_2\right)^2 \tan^2\frac{\theta}{2} \tag{1.24}$$

are also plotted. The striking difference between the behavior of the deep inelastic and elastic cross sections can be vividly seen in this figure. Furthermore, as the hadronic mass W increased the Q^2 dependence decreased. Hofstadter's results on elastic scattering had suggested that the proton was a diffuse ball of charge. Thus the general expectation at the time [9] was that the structure functions would fall with increasing Q^2 about as rapidly as the elastic form factors. The fact that the electron did still scatter at large angles at these high energies indicated, just as in Rutherford's experiment, that the photon was hitting some pointlike substructure.

The second surprising feature in the data was found by following a suggestion by Bjorken [10], who, on the basis of models that satisfy *free* field theory

[5] Eq.(1.21) does not account for electron bremsstrahlung and form factors, both of which were important for the SLAC experiment. See [7] for how these effects were accounted for.

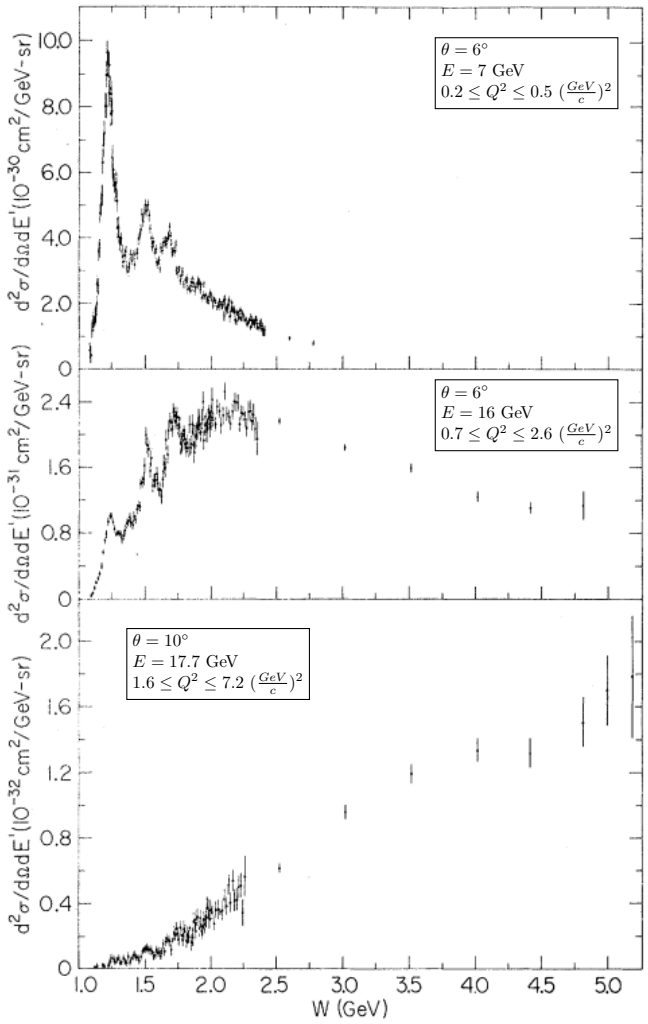

Figure 1.5: Three representative radiatively corrected spectra. The elastic peaks have also been subtracted. The first two peaks visible in both panels (a) and (b) correspond to the one and two pion production threshold. Note the decrease in both the cross section and the resonance behavior for increasing Q^2. The peaks have almost completely disappeared at the large momentum transfers of panel (c). What was striking about these results is that the $W \gtrsim 4$ GeV region is approximately constant with increasing Q^2. This slow fall off in the large W region was one of the first pieces of evidence for Bjorken scaling. Figure taken from [7]

current algebra, conjectured that in the limit of $\nu, Q^2 \to \infty$ with $\omega := \frac{2M_p\nu}{Q^2}$ held fixed, the two quantities νW_2 and W_1 should become functions only of the

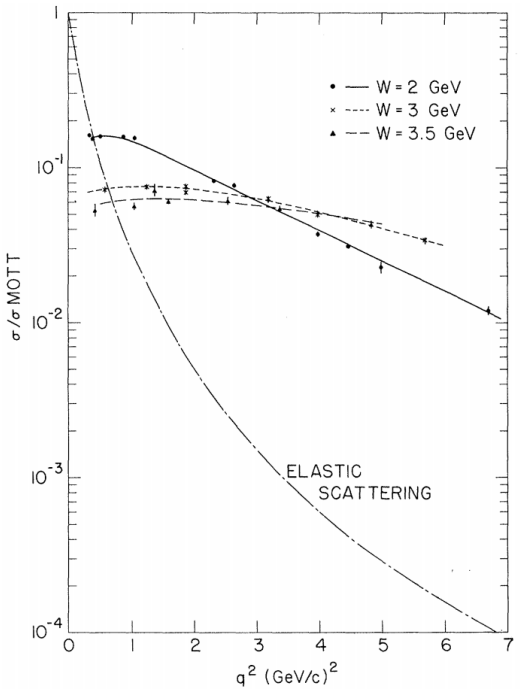

Figure 1.6: $(\frac{d^2\sigma}{d\Omega dE'})/(\frac{d\sigma}{d\Omega})_{mott}$ in GeV vs q^2 for $W = 2, 3$ and 3.5 GeV. The lines drawn through the data are meant to guide the eye. Also shown is the cross section for elastic $e\,p$ scattering divided by $(\frac{d\sigma}{d\Omega})_{mott}$, calculated for $\theta = 10°$, using the dipole form factor Eq.(1.19). The relatively slow variation with Q^2 of the inelastic cross section compared with the elastic cross section is clearly visible. This slow falloff suggests that the proton is composed of approximately pointlike (relative to the scale $1/Q^2$) substructures.

ratio ω; that is

$$2MW_1(\nu, Q^2) \to F_1(\omega) \tag{1.25}$$

$$\nu W_2(\nu, Q^2) \to F_2(\omega) \tag{1.26}$$

Scaling behavior was indeed found within experimental errors for $Q^2 > 2\,\mathrm{GeV}^2$ and $W > 2.6\,\mathrm{GeV}$. The first experimental evidence [8] for this phenomenon is displayed in Fig(1.7). Bjorken scaling proved to be the experimental jackpot. In a short period of time it would uniquely identify one class of field theories, non-abelian gauge theories, as the only possible candidate field theory for the strong interactions.

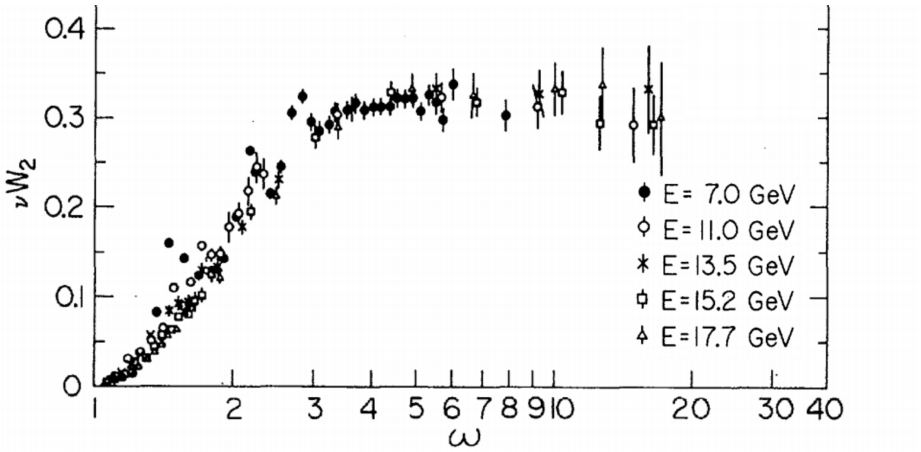

Figure 1.7: The first experimental evidence for Bjorken scaling [8]. νW_2 vs $\omega := \frac{2M_P\nu}{Q^2}$ for electrons scattering at 10° at momentum transfers $Q^2 > 0.5$ $({}^{GeV}/_c)^2$. The structure function appears to be independent of the incident energy E and a function of the single variable ω. This is consistent with Bjorken's suggestion that the charge distribution of the proton is approximately scale invariant at high energies.

1.4 The Discovery of Quantum Chromodynamics (1973)

Bjorken scaling appears to imply that the structure of the proton $\nu W_2(Q^2, \omega)$ is independent of the length scale $\frac{1}{Q}$ and time scale $\frac{1}{\nu}$ on which one probes it. This leads one to suspect that the underlying field theory must be reaching a fixed point of the renormalization group (R.G.). Pursuing this line of reasoning Gross and Callan [11] (1973) demonstrated that the only fixed point which could reproduce Bjorken scaling was free field theory. This was in line with Bjorken's presumption of using free field theory current algebra, but this then presents an apparent paradox: if the underlying field theory is free, why do the constituents of the proton not fly apart? This can be resolved if the theory is asymptotically free— at long distances the particles are strongly interacting and at short distances they are essentially free. Coleman and Gross [12] (1973) then proved that the *only* possible renormalizable asymptotically free theories in four dimensions are non-abelian gauge theories, thus singling out such theories as the unique candidate for the strong interactions. We now make this heuristic discussion more precise.

The Operator Product Expansion

Deep inelastic scattering is most naturally analyzed with the aid of Wilson's operator product expansion (OPE), which expresses the product of two spatially

separated operators as a sum of local operators

$$T\left(\hat{J}(x;\mu_R)\hat{J}(0;\mu_R)\right) = \sum_n C_n(x,g;\mu_R)\hat{\mathcal{O}}_n(0;\mu_R) \tag{1.27}$$

where the $\hat{\mathcal{O}}_n$ are a complete set of local operators, T denotes time ordering, μ_R denotes the energy scale at which the individual operators have been renormalized and the C_n are c-number functions ("Wilson co-efficients") of the separation x^μ, the coupling constants g and the renormalization scale μ_R. Typically, products of operators, such as the LHS of Eq.(1.27), diverge as they approach one another $x^\mu \to 0$. As the Wilson co-efficients now carry the spatial dependence of the operator, they also contain this short distance singularity structure. One expects that at high energies it is this short distance singularity structure which dictates the gross features of scattering amplitudes. The virtue of the OPE is that it allows one to extract the most important features of the product of operators by retaining only the most singular terms in the expansion. One can infer, up to logarithmic corrections, which Wilson co-efficients are the most singular by examining the canonical (naive) dimensions of the operators $\hat{J}$ and $\hat{\mathcal{O}}$

$$C_n(x,g;\mu_R) \underset{x_\mu \to 0}{\sim} |x|^{d_n - 2d_J} f(\ln x\mu_R, g) \tag{1.28}$$

Where $f(\ln \mu_R x, g)$ is a dimensionless function and d_J, d_n refer respectively to the mass dimension of the operators $\hat{J}$ and $\hat{\mathcal{O}}$. Eq.(1.28) suggests that it is the operators of the lowest mass dimension which dominate at short distances. However, the logarithms can, and often do, sum to a power thus modifying the naive dimensional analysis. We will resum these logarithms in the next section by means of the renormalization group, but for the moment we will be guided by the naive dimensions of operators. Products of operators often also diverge when approaching a lightlike separation. One can again perform an operator expansion for this case, however one finds that the OPE takes the form

$$T\left(\hat{J}(x;\mu_R)\hat{J}(0;\mu_R)\right) = \sum_{n,j} C_{n,j}(x^2,g;\mu_R)x^{\mu_1}x^{\mu_2}...x^{\mu_j}\hat{\mathcal{O}}_{(n)\mu_1\mu_2...\mu_j}(0) \tag{1.29}$$

In this instance, the singularities of the Wilson co-efficients are not dictated by the mass dimension of the operators but by

$$C_{n,j}(x^2,g;\mu_R) \underset{x^2 \to 0}{\sim} (x^2)^{\frac{d_n - j - 2d_J}{2}} f_{n,j}(\ln x^2\mu_R^2, g) \tag{1.30}$$

their twist ($\tau \coloneqq d_n - j$). The operators of lowest twist therefore contain the leading lightcone singularities. Eq.(1.29) indicates that the leading operators of the lightcone OPE are trace-free and symmetric in their Lorentz indices, thus j refers to the spin of the operators. In four dimensions the mass dimension of a field is bounded from below by 1, thus adding more fields without Lorentz indices can only increase the twist of an operator. Adding a derivative to an operator, whilst symmetrizing on all Lorentz indices, does not affect the twist.

Thus the lowest twist of an operator in four dimensions is 2 and there are infinitely many such operators.

In deep inelastic scattering, the product of operators featuring in the hadronic tensor $W^{\mu\nu}$ are not time ordered, see Eq.(A.10), and hence one cannot immediately apply the OPE. Instead, we first define the forward Compton scattering tensor as

$$T^{\mu\nu} \coloneqq \int d^4x \; e^{iq\cdot x} \, \langle P|T(J^\mu(x)J^\nu(0))|P\rangle \tag{1.31}$$

which is time ordered. In Appendix (A) we use dispersion relation techniques to prove that the two are related by

$$Disc_\nu(T^{\mu\nu}(\nu, Q^2)) = i\, W^{\mu\nu}(\nu, Q^2) \tag{1.32}$$

Next, we should determine the singularity structure of the product of operators featuring in the forward Compton tensor when working in the Bjorken limit. The dominant contribution to the integral Eq.(1.31) is the region in x which leaves the leaves the phase $e^{iq\cdot x}$ stationary. Setting $q^\mu = \lambda n^\mu - q_0^\mu$ where n^μ is a lightlike vector and q_0^μ is fixed, then as $\lambda \to \infty$ we have

$$\begin{aligned} Q^2 &= 2\lambda(q_0 \cdot n) \; \to \infty \\ \nu &= \frac{\lambda(p\cdot n)}{M_p} \quad \to \infty \\ \xi &= \frac{1}{M_P}\frac{q_0\cdot n}{p\cdot n} \to \text{fixed} \end{aligned} \tag{1.33}$$

therefore achieving the Bjorken limit. The exponent in Eq.(1.31) will then be stationary if $n\cdot x \sim \mathcal{O}\frac{1}{\lambda}$, which implies that $x^\mu \sim n^\nu + (\frac{1}{\lambda})x_0^\mu$. Thus as $\lambda \to \infty$ we have that

$$(x^\mu)^2 \sim \frac{1}{\lambda} n\cdot x_0^\mu \to 0 \tag{1.34}$$

The Bjorken limit is therefore dictated by the lightcone structure of the operator product. The relevant OPE is therefore of the form Eq.(1.29), which in Fourier space reads

$$\int d^4x \; e^{iq\cdot x}\, T(\hat{J}(x)\hat{J}(0)) = \sum_{n,j} \bar{C}_{n,j}(q^2, g) q^{\mu_1} q^{\mu_2} ... q^{\mu_j} \; \hat{\mathcal{O}}^{(n,j)}_{\mu_1\mu_2...\mu_j}(0) \tag{1.35}$$

Dimensional analysis then suggests

$$\int d^4x \; e^{iq\cdot x}\, T(\hat{J}(x)\hat{J}(0)) = \sum_{n,j} \tilde{C}_{n,j}\left(\frac{Q^2}{\mu_R^2}, g\right) \frac{q^{\mu_1} q^{\mu_2} ... q^{\mu_j}}{(Q^2)^j} \hat{\mathcal{O}}^{(n,j)}_{\mu_1\mu_2...\mu_j}(0) \tag{1.36}$$

where the $\tilde{C}$ are dimensionless functions. We need not be specific what the twist two operators are at the moment, only that they are necessarily symmetric and

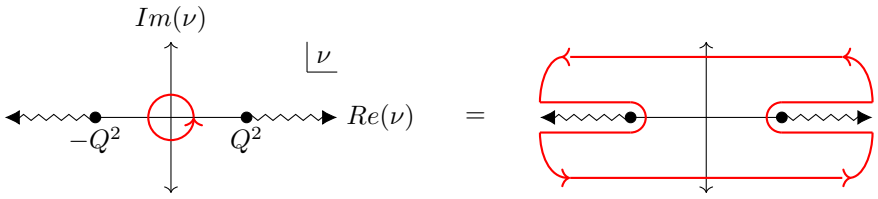

Figure 1.7: The analytic structure of $T^{\mu\nu}(\nu, Q^2)$ for fixed Q^2: it has branch cuts beggining in the physical region $\nu \geq Q^2$ and no poles off of the real axis. The integration contour seen in the left panel does not correspond to a kinematically allowed scattering configuration, however the operator product expansion is convergent in this region. The contour can be stretched without changing the value of the integral as no poles are enclosed. The right panel's contour evaluates to the $2Disc(T^{\mu\nu}) = 2ImT^{\mu\nu} = 2W^{\mu\nu}$ in the physical region.

trace-free. These two conditions imply that their relevant matrix for DIS are uniquely fixed to the form

$$\langle P|\hat{\mathcal{O}}^{(n,j)}_{\mu_1\mu_2...\mu_j}(0)|P\rangle \coloneqq \mathcal{A}^{(n,j)}\left(\frac{M_p}{\mu_R}\right)P^{\mu_1}P^{\mu_2}...P^{\mu_j} \tag{1.37}$$

where this equation defines the dimensionless variable $\mathcal{A}^{(n,j)}$. Plugging this into Eq.(1.36) gives

$$T^{\mu\nu}(Q^2, \nu) = \sum_{n,j}\left(\frac{\nu}{Q^2}\right)^j \tilde{C}_{(n,j)}\mathcal{A}^{(n,j)} \tag{1.38}$$

However this sum will not converge in the physical region as elementary kinematic constraints indicate that $\frac{\nu}{Q^2} > 1$. Fortunately, we can circumnavigate this by dispersing in ν. To pick out the spin j contribution to Eq.(1.38) we can integrate and use Cauchy's theorem

$$\frac{1}{2\pi i}\oint_C d\nu\ \frac{T^{\mu\nu}(Q^2, \nu)}{\nu^{j+1}} = \tilde{C}_{(n,j)}\mathcal{A}^{(n,j)}\frac{1}{Q^{2j}} \tag{1.39}$$

where the contour C is chosen to encircle the unphysical region $\nu < 1$, see left panel of Fig(1.7). We have used that $T^{\mu\nu}$ exhibits no poles in the unphysical region. In this region, the summation on the RHS of Eq.(1.38) is convergent. We can then exploit the analytic structure of $T^{\mu\nu}$ to deform the contour. It has been shown that[6] $T^{\mu\nu}$ is an analytic function except in regions along the real ν axis associated with scattering processes where it has branch cuts. The physical region for $T^{\mu\nu}(\nu, Q^2)$ is $\nu > Q^2$. But because Eq.(1.31) is symmetric under the

[6]See Sect 13.2 of [13] for the proof.

interchange $(q,\mu) \to (-q,\nu)$ we must also have[7]

$$T_2(-\nu, Q^2) = T_2(\nu, Q^2) \tag{1.40}$$

Thus T_2 must also have a branch cut along the negative real ν axis. The two regions enveloping the branch cuts pick out the $Disc(T^{\mu\nu}) = iW^{\mu\nu}$ which is precisely what we measure in deep inelastic scattering. Expressing the integrals in terms of ξ we have found that

$$2\int_0^1 d\xi\, \xi^{j-1}\, \nu W_2(\xi, Q^2) = \tilde{C}_{(n,j)}\mathcal{A}^{(n,j)} \tag{1.41}$$

This important relation tells us that the j^{th} Mellin moment[8] of the hadron structure functions measures the spin-j Wilson co-efficients of the twist 2 operators.

Asymptotic Freedom

Bjorken scaling puts a severe restriction on these Mellin moments. If $W_2(Q^2,\xi)$ tends towards a function which is independent of Q^2 then

$$\int_0^1 \xi^{j-1} W_2(Q^2,\xi) \underset{Q^2\to\infty}{\to} \text{constant} \tag{1.42}$$

implying that the Wilson co-efficients of the twist two operators also become Q^2 independent. Callan and Gross [11] (1973) proved that this can only occur in a free field theory. As this was a crucial step towards the discovery of QCD we summarize their arguments below.

Recall that our naive power counting in Eq.(1.30) could be spoiled by the logarithms summing to a power. One can resum these logarithms by applying the Callan-Symanzik [14, 15] renormalization group equations to the Wilson co-efficients [16, 17]

$$\left[\mu\frac{\partial}{\partial\mu} + \beta(g)\frac{\partial}{\partial g} + [\gamma_n(g)]_{ij} - 2\gamma_J(g)\right] C_j^n(x,g;\mu) = 0 \tag{1.43}$$

where γ_J is the anomalous dimensions of the current operator $\hat{J}$, which is in fact identically zero since the conserved charge $Q = \int d^3x J^0(x)$ must be dimensionless. $[\gamma^n(g)]_{ij}$ is the anomalous dimension *matrix* of the twist two spin-n operators. This term reflects that the renormalization procedure mixes operators with the same quantum numbers (spin, charge, mass dimension etc). If we define the effective coupling constant $\bar{g}(g,t)$ by

$$\frac{d\bar{g}}{dt} = \beta(\bar{g}), \qquad \bar{g}(g,0) = g \tag{1.44}$$

[7] This is a consequence of crossing symmetry which relates photon-proton scattering to photon-anti-proton scattering.

[8] For an arbitrary function $f(x)$, it's j^{th} Mellin moment f_j is defined as $f_j := \int_0^1 \partial x\; x^{j-1} f(x)$

then the explicit solution to Eq.(1.43) is

$$C_i^n(e^{-t}x_R^2, g, \mu) = e^{t(2d_J - d_n)}\mathcal{P}_t \exp\left[-\int_0^t dt' \gamma_n(\bar{g}(t'))\right]_{ij} C_j^n(x_R^2, \bar{g}(t), \mu) \quad (1.45)$$

where $\mathcal{P}_t$ denotes path ordering in the t parameter. If the β function has a UV stable fixed point g_f i.e. $\beta(g_f) = 0,\ \beta'(g_f) < 0$, then the high energy behavior of the theory is controlled by this fixed point and Eq.(1.45) has the asymptotic behavior

$$C_i^n(e^{-t}x_R^2, g, \mu) = e^{t(2d_J - d_n)} \exp\left[-t\gamma_n(g_f)\right]_{ij} C_j^n(x_R^2, \bar{g}(t), \mu) \quad (1.46)$$

We can then take linear combinations of the spin-j, twist-2 operators which diagonalizes the anomalous dimension matrix. For these eigenvectors, the net effect of the logarithms, when the coupling is in the vicinity of the fixed point, is to modify the naive dimension of the Wilson co-efficients to $d_n + \gamma_n(g_f)$, hence the name anomalous dimension. Our dimensional analysis at Eq.(1.36) should then also contain a factor of $(Q^2)^{-\gamma(g_f)/2}$. This modifies the Q^2 dependence of our expression for the Mellin moments of the structure functions Eq.(1.41) to

$$\int_0^1 d\xi\ \xi^{j-1}\, \nu W_2(Q^2, \xi) \underset{Q^2\to\infty}{\sim} (Q^2)^{-\gamma_j(g_f)/2} \quad (1.47)$$

However, if the right hand side is to be Q^2 independent, as Bjorken scaling would require, then all the anomalous dimensions of the twist two operators must vanish at the fixed point $\gamma_j(g_f) = 0$. This appears to be very unlikely as it imposes an infinite set of conditions on functions of a single parameter g_f. Via the following argument, Callan and Gross [11] proved that this can only occur if the UV fixed point is the origin of coupling space $g_f = 0$. Hence if a field theory were to reproduce Bjorken scaling it would need to be asymptotically free.

First note that the positivity of the $\nu W_2(Q^2, \xi)$ ensures that it's Mellin moments are a decreasing function of j and hence that the γ_j increase with j. Callan and Gross then assumed that the energy-momentum tensor is the unique twist-2, spin-2 operator. The energy momentum tensor is constrained to have canonical dimensions ($\gamma_2(g) = 0$) as it's zero components are Noether charges. Then the above to statements imply the following inequality:

$$0 = \gamma_2 \leq \gamma_3 \leq \gamma_4 \leq ... \leq \gamma_n \quad (1.48)$$

Thus if the large j anomalous dimensions vanish, then all of them do. Callan and Gross then proved a conjecture originally due to Parisi that for large spin-j, the anomalous dimension of the twist two operators approaches twice the anomalous dimension of the field

$$\lim_{j\to\infty} \gamma_j(g) = 2\gamma_\psi(g) \quad (1.49)$$

The intuition for this proof is simple: composite operators such as the twist-2 spin-n operators $\hat{\mathcal{O}}^j = \phi^* \overset{\leftrightarrow}{\partial}_{\mu_1} ... \overset{\leftrightarrow}{\partial}_{\mu_n} \phi$, do not have mass dimension $2d_\phi + j$ because they involve the product of fields at the same spacetime point and hence

require subtractions at some arbitrary renormalization scale μ, thus introducing another mass scale. However, one might intuitively expect that for large j the derivatives effectively act to separate the two fields, thus reinstating the naive dimensional analysis. The formal proof can be found in [11].
Relations Eq.(1.48) and Eq.(1.49) then imply that Bjorken scaling requires $\gamma_\psi(g_f) = 0$. If one then examines the Callan-Symanzik equation for the propagator $D(p^2, \mu, g)$ of any theory

$$\left[\mu\frac{\partial}{\partial\mu} + \beta(g)\frac{\partial}{\partial g} - 2\gamma_\psi(g)\right]D(p^2, \mu^2, g) = 0 \tag{1.50}$$

Using $\beta(g_f) = 0$, $D(p^2, \mu^2, g) = (i/p^2)f(p^2/\mu^2)$ (by dimensional analysis) and Parisi's conjecture $\gamma_\psi = 0$, we deduce that the above implies

$$D(p^2, \mu^2, g_f) = \frac{i}{p^2} \tag{1.51}$$

Callan-Gross then invoked the Federbush-Johnson theorem [18], which informs us that if the full propagator is equal to the free propagator then the theory is a free-field theory. We therefore conclude that the vanishing of the anomalous dimensions of the twist-2 operators implies that the theory is asymptotically free.

Non-Abelian Gauge Theory

This observation motivated Gross and Coleman [12] to investigate whether there are any renormalizable asymptotically free theories in four dimensions. The expectation was that there were none [19]. The renormalizabilty condition severely restricts the class of theories that need to be considered to only those involving fields of spin $0, \frac{1}{2}$ and 1. It also constrains the number of types of interactions to four. The three types of interactions which they studied were: abelian gauge fields coupled to a conserved current, general ϕ^4 theory and Yukawa couplings of fermions to scalars

$$\mathcal{L}_{int} = A^\mu J_\mu \tag{1.52}$$

$$\mathcal{L}_{int} = -\lambda_{ijkl}\phi^i\phi^j\phi^k\phi^l + \bar{\psi}^a(A^k_{ab} + iB^k_{ab}\gamma^5)\psi^b\phi_k \tag{1.53}$$

The problem was amenable to perturbative techniques as to investigate the stability of the origin of coupling space under R.G. flow one need only use first order perturbation theory (this is in contrast to a generic fixed point). The proof proceeded by brute force, computing the β function for the first three classes of theories. It was found for these three theories that, for a sufficiently small domain around the origin, the fixed point is UV repulsive[9] $\beta'(g \sim 0) > 0$

[9]There are many asymptotically free theories in dimensions less than four which are not non-abelian gauge theories: all super-renormalizable interactions as well as the $(\bar{\psi}\psi)^2$ coupling in two dimensions are asymptotically free.

't Hooft had recently [20] (1967) proven that Yang-Mills theory in four dimensions is renormalizable, thus leaving one possible exception to Coleman and Gross's proof that there are no sensible asymptotically free theories in four dimensions. They had omitted the calculation of the β function of Yang-Mills theory as the calculation is made much more formidable by the interface between renormalization and maintaining gauge invariance.
In 1973 Gross and Wilczek [21] and independently Politzer [22] as well as 't Hooft (unpublished) calculated the β function of Yang-Mills theory and found that

$$\beta(g) = -\frac{g^3}{(4\pi)^2}\left[\frac{11}{3}C_2(G) - \frac{4}{3}n_f C(r)\right] \tag{1.54}$$

where $C_2(G)$ is the quadratic Casimir of the adjoint representation of the group ($C_2(SU(N)) = N$), n_f is the number of fermion flavors and $T(R)$ is the normalization convention for the generators in the R representation of the gauge group $\mathrm{Tr}(t^a t^b) \coloneqq T(R)\delta^{ab}$ (for the fundamental representation of $SU(N)$, $T(R) = N$). Thus for sixteen triplets of fermions or less *Yang-Mills theory is asymptotically free*. Thus Bjorken scaling implied that the theory governing the strong interactions must be of the Yang-Mills type.
With the conceptual breakthrough of asymptotic freedom, many other problems were also resolved: if one identified the fermions of Yang-Mills theory with Gell-Mann's quarks, then one could qualitatively explain why no-one had ever seen a quark—the increase in the coupling at large distances would energetically favor the production of a hadron rather than two well separated quarks. Furthermore, the Yang-Mills Lagrangian contains a massless spin-1 boson, but no-one had ever seen in experiments such a particle associated with the strong interactions. But this was now to be expected, again by energy considerations.

***

To summarize, Bjorken scaling could only occur if the anomalous dimensions of the twist two operators of the theory vanished. Gross and Callan [11] proved that this can only occur for asymptotically free theories. Coleman and Gross [12] then proved that the only renormalizable asymptotically free theories in four dimensions are non-abelian gauge theories. The minimum number of colors was 3 due to considerations of baryon spectroscopy and hence $SU(3)$ was singled out as the most likely candidate for the strong interactions.

2 The parton model and DIS factorization

Almost every perturbative QCD prediction for collider experiments rely on the parton model, or to be more precise, its generalization known as factorization. The goal of this chapter is to outline the framework of factorization in one of the simplest realistic examples, deep inelastic scattering. Our primary reference has been the review paper [23] but we have also benefited greatly from the lectures and textbooks [24, 13, 25].

2.1 Brief statement of the parton model and factorization in DIS

The factorization theorem for DIS in the Bjorken limit, is that the hadronic tensor, as defined at Eq.(A.10), for a nucleus N, carrying a momentum p^μ, can be expressed as a simple one-dimensional convolution

$$W_N^{\mu\nu}(q^\mu, p^\mu) = \sum_a \int_{x=\frac{Q^2}{2p\cdot q}}^1 \frac{\mathrm{d}\xi}{\xi}\ f_{a/N}(\xi, \mu_R, \mu_F) H_a^{\mu\nu}(q^\mu, \xi p^\mu, \mu_F, \mu_R, \alpha_s(\mu_R)) + \text{remainder} \quad (2.1)$$

where the remainder is down by a power of Q^{-2} modulo logarithms. Heuristically, one can interpret the *parton distribution functions* (PDF's) $f_{a/N}(\xi)$ as the number density of type-a partons (a = gluons, quarks, anti-quarks, and in principle all other particles in the Standard Model) found in nucleus N, carrying a momentum fraction ξ of the nucleus's momentum. The *hard co-efficient* $H_a^{\mu\nu}$ is similar to, but not precisely equal to, the total virtual-photon-parton cross section $\sigma^{a\gamma^*}$, where the parton is taken to be massless, on-shell, collinear to the nucleus, and carrying a momentum fraction ξ of the nucleus's momentum. We give the precise definitions of $f_{a/N}$ and $H_a^{\mu\nu}$ at Eq.(2.60) and Eq.(2.57) respectively, and find that these heuristic interpretations are helpful but slightly inaccurate. In Eq(2.1) μ_R and μ_F respectively refer to the renormalization and factorization scales. The meaning of the factorization scale is explained in Sect(2.5).

We will often make reference to the factorization theorems for the DIS structure functions, which can be obtained by projecting Eq.(2.1) with the relevant tensors (see Eq's.(A.17,A.18))

$$F_1(x, Q^2) = \sum_a \int_x^1 \frac{\mathrm{d}\xi}{\xi}\ f_{a/N}(\xi, \mu) H_{1a}\left(\frac{x}{\xi}, \frac{Q}{\mu}, \alpha_s(\mu)\right) + \text{remainder} \quad (2.2)$$

$$F_2(x, Q^2) = \sum_a \int_x^1 \mathrm{d}\xi\ f_{a/N}(\xi, \mu) H_{2a}\left(\frac{x}{\xi}, \frac{Q}{\mu}, \alpha_s(\mu)\right) + \text{remainder} \quad (2.3)$$

where the integral measure in F_2 does not contain a factor of $\frac{1}{\xi}$ as the relevant tensor multiplying F_2 contains a factors of the target momentum.

The predictive power of the formalism stems from two key properties: the perturbative calculability of the hard co-efficients and the *universality of the PDF's*. We will now outline how one uses these two properties to make predictions.

Whereas the hard co-efficients are perturbatively calculable, as we explain in Sect(2.5), the PDF's are inherently non-perturbative objects that must be extracted from experiment. One does this by formulating factorization theorems of the form Eq.(2.1) for many different processes. Then once the physical quantities such as $W^{\mu\nu}$ have been measured, and the hard co-efficients calculated, one uses the factorization theorem to deduce the PDF's. For example, the following factorization theorem for the Drell-Yan process (lepton pair production in hadron-hadron collisions) has been proven [26, 27, 28, 29]

$$\frac{\mathrm{d}\sigma}{\mathrm{d}Q^2\mathrm{d}y} = \sum_{a,b} \int_{x_A}^1 \mathrm{d}\xi_A \int_{x_B}^1 \mathrm{d}\xi_B \times f_{a/N}(\xi_A,\mu) H_{ab}\left(\frac{x_A}{\xi_A}, \frac{x_B}{\xi_B}, Q; \frac{\mu}{Q}, \alpha_s(\mu)\right) f_{b/N}(\xi_B,\mu) \quad (2.4)$$

where Q^2 and y refer respectively to the invariant mass and rapidity of the produced lepton pair. The crucial point is that it has been proven that the same PDF's apply in Eq.(2.4) and Eq.(2.1), and thus one can use measurements made in DIS to make a prediction for the Drell-Yann process.

The factorization formalism makes predictions of a second kind. Granted that we measure the DIS structure functions $F_{1,2}(x,Q)$ at some initial Q_0, one can predict the structure functions at another value of Q. This follows from all the Q dependence in Eq.(2.1) sitting in the hard co-efficient, which itself is perturbatively calculable. We should mention that it is common to refer to the Q-dependence of the PDF's, which appears to contradict our Eq .(2.1) where the PDF's are Q independent. However, if we set $\mu_F = \mu_R = Q$ then all of the Q dependence is shifted from the hard scattering co-efficient into the PDF's.

Let us outline some questions to be answered in the following sections:

- Why are the partons on-shell and massless if the quarks and gluons in the nucleus are neither?
- Why are the partons collinear to the nucleus and why do they carry a momentum fraction bounded between $0 < \xi < 1$?
- Why does scattering occur upon a single parton?
- Why does the factorization formula not involve details that occur after the hard scattering, such as pion production rates? Shouldn't the subsequent evolution interfere quantum mechanically with the short distance scattering?

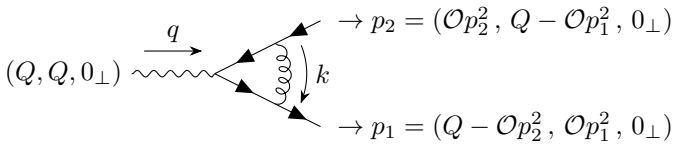

Figure 2.1: Feynman graph contributing to the Sudakov amplitude. We have chosen to refer to the center of mass co-ordinate system so that the large Q effects can be seen clearly in both quark propagators. Our lightcone variables are $(0^+, 0^-, 0^\perp)$

2.2 Pinch singular surfaces and infrared divergences

2.2.1 Pinch singular surfaces

There are two distinct causes for divergences in Feynman diagrams; UV divergences and IR divergences. The UV divergences arise due to allowing arbitrarily large momentum to flow through loops in a graph. These divergences are systemically dealt with by means of counterterms. It is however the study of IR divergences which indicate how the parton model emerges in a QFT. We will thus suppose in what follows that all UV divergences have already been renormalized and that only the IR divergences remain.

The IR divergences arise as follows: a given Feynman graph will contain a product of propagator denominators, $\frac{1}{p^2-m^2+i\epsilon}$, which appear to contribute a divergent amount to the graph as the momentum goes onshell. However, as the $i\epsilon$ indicates, the integrand of a Feynman graph is to be considered a complex function of the loop momentum, in which case a contour deformation away from the pole is often possible, thus indicating only a finite contribution to the graph. It is when there is a barrier to such a deformation that a region of loop momentum space can give a large, sometimes infinite, contribution to a diagram. These regions of momentum space are referred to as *pinch singular surfaces* (PSS's).

Before turning to a systematic study of PSS's let us first give an example of how such a barrier can arise: consider the denominator factors of the graph in Fig(2.1)

$$\mathcal{M} = \int \mathrm{d}^n k \, \frac{numerator}{(k^2 + i\epsilon)[(p_1 - k)^2 - m_f^2 + i\epsilon][(p_2 + k)^2 - m_f^2 + i\epsilon]} \tag{2.5}$$

The numerator is model dependent and is in any event irrelevant for determining the locations of the PSS's. In order to study the effects of the large Q limit we work in the center of mass frame where both quark propagators contain a Q-dependence. We orientate our co-ordinate system such that each quark does not have any transverse momentum in lightcone variables. We do not necessarily take the external quarks to be onshell. Inspecting the integrand in Eq.(2.5) we

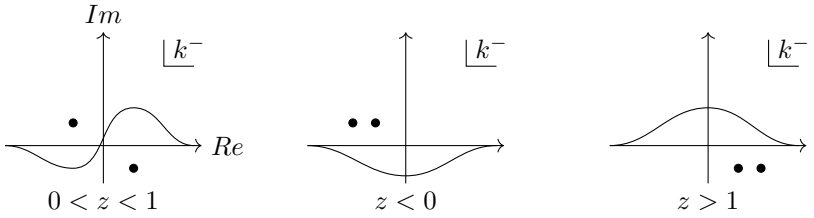

Figure 2.2: Analytic structure of the integrand in Eq.(2.6) in the k^- plane. The k^- contour can deformed away from the poles when either $z < 0$ or $z > 1$. If $0 < z < 1$ then the contour is trapped between two coalescing poles and therefore represents a PSS. This PSS represents a region of k space which provides a large contribution to the Sudakov graph Fig(2.1). There is a pole due to the third propagator in Eq.(2.6), which occurs at $k^- \sim p_2^-$ and thus are far away from those indicated here. However this pole prevents a contour deformation all the way to infinity in the second and third diagrams.

find that one of the momentum regions where two of the propagators go onshell is when the gluon is collinear to the quark. To examine this region let us change co-ordinates on the gluons plus momentum to $k^+ = zp_A^+$, in which case

$$\mathcal{M} = \int \mathrm{d}z\ \mathrm{d}^{d-2}k_\perp\ \mathrm{d}k^- \frac{numerator}{2(p_2^- + k^-)(zp_1^+ + p_2^+) - k_\perp^2 - m_f^2 + i\epsilon} \cdot \frac{1}{[2zp_1^+k^- - k_\perp^2 + i\epsilon][2(1-z)p_1^+(p_1^- - k^-) - k_\perp^2 - m_f^2 + i\epsilon]} \tag{2.6}$$

Consider the k^- contour integral, and in particular note the location of the poles of the gluon and quark propagators. The analytic structure is depicted in Fig (2.2). When $z < 0$ or $z > 1$ both poles lie on the same side of the contour and we can thus deform the contour away from the poles, making manifest that these regions do not contribute a singular amount to the integral Eq.(2.6). There is however a barrier to deforming the contours all the way to infinity as the pole coming from the $(p_2 + k)$ denominator occurring at $k^- \approx -p_2^-$ prevents this. These two regions therefore contribute a finite amount. However, when $0 < z < 1$ the k^- contour is trapped between the two poles thus preventing a contour deformation away from the poles. The real distance in k^- between these two poles is

$$(\Delta k^-)^* = \frac{k_\perp^2 + m_f^2}{p_1^+}\left(\frac{1}{z} + \frac{1}{1-z}\right) + p_1^- \tag{2.7}$$

As $\frac{m_f^2}{p_1^+} \to 0$, $\frac{k_\perp^2}{p_1^+} \to 0$ and $p_1^- \to 0$, this distance vanishes and thus this region contributes singularly to the integral. Note that the non-zero quark mass prevents the poles from actually meeting thus rendering this contribution to the

integral finite. However, as $p_1^+ \sim Q$, even if the quark has a non-zero mass, the contour necessarily comes within a distance of $\Delta k^- \sim \frac{m_f^2}{Q}$ of the PSS. Hence in the large Q limit, the integral receives large contributions from the regions of momentum space in the immediate vicinity of the PSS.[10]

Studying Eq.(2.7) allows us to preempt many of the parton model properties: if we consider the gluon to be the parton of the quark (or visa-versa) then in the immediate vicinity of the PSS the parton is massless (or more precisely, the ration $\frac{m^2}{Q}$ is negligible), onshell, carries a collinear momentum fractions bounded by $0 < z < 1$ and has zero transverse momentum.

Examining the denominators in Eq.(2.6) further will indicate that the integrand contains five PSS's in total. Briefly, these are when the gluon is collinear to the quark or anti-quark, or when either of the gluons,quarks or anti-quarks momenta is soft. The soft PSS's are in fact endpoints/sub-manifolds of the collinear PSS's. These configurations where two PSS's overlap give rise to enhanced singularities such as the soft-collinear $\frac{1}{\epsilon_{IR}^2}$ double poles encountered in IR-dimensional regularization.

We will now provide a systematic procedure for identifying the location of all the PSS's for any Feynman graph.

2.2.2 The Landau-Coleman-Norton conditions

As we learnt from the case in Fig(2.1) with the gluon collinear to the quark, it was not sufficient for a set of propagators to go on-shell in order for a PSS to form. The restriction that $0 < z < 1$ came from the condition that the poles must be approaching one-another and from opposite sides of the contour. The Landau conditions [30, 31] determine the necessary and sufficient conditions on the *integrand* for a pinch to form, thus producing a genuine singularity in the *integral*. The proof [32] is straightforward, and may be adequately understood by a simple example: let us rewrite the set of denominators in Eq.(2.5) in terms of a single denominator D, by introducing a set of Feynman parameters (now working in the massless limit)

$$\mathcal{M} = 2 \int \mathrm{d}^d k \int_0^1 \frac{\mathrm{d}\alpha_1 \mathrm{d}\alpha_2 \mathrm{d}\alpha_3 \; \delta(1 - \sum_{i=1}^3 \alpha_i)}{D^3} \tag{2.8}$$

$$D \coloneqq \alpha_1 k^2 + \alpha_2 (p_1 - k)^2 + \alpha_3 (p + k)^2 + i\epsilon, \tag{2.9}$$

we therefore seek the poles of D in$\{ \alpha_i, k^\mu \}$ space. Note that D is quadratic in each of the components of k^μ, thus the condition for two of the zeros of D to

[10] We have glossed over the fact that the contour occurs not in a 1-dimensional complex space as Fig(2.2) suggests, but in a 4-dimensional complex space, and thus it is not apriori clear whether a contour deformation away from the coalescing poles is possible. This issue is not fully resolved in the literature, see Sect(5.4.3) of [24]

occur at the same point is the same as that for a quadratic form:

$$\frac{\partial}{\partial k^\alpha} D(k^\mu, \{\,\alpha_i\,\}, \{\,p_i\,\}) = 0, \tag{2.10}$$

at the location of the zeros[11]. What does not immediately follow, but is nevertheless true, and proved in [32], is that Eq.(2.10) is in fact sufficient for the poles to be approaching one another from opposite sides of the real contour. If we then assume that a multi-dimensional contour deformation away from the coalescing poles is not possible, then we conclude that the Landau conditions are sufficient for the formation of a PSS. In summary, the Landau conditions read

$$\boxed{D = 0 \qquad ; \qquad \frac{\partial}{\partial k^\alpha} D = 0} \tag{2.11}$$

Applying Eq.(2.10) to our example Eq.(2.5) we obtain the condition

$$\alpha_1 k^\mu - \alpha_2 (p_1 - k)^\mu + \alpha_3 (p_2 + k)^\mu = 0 \tag{2.12}$$

$$\Updownarrow$$

$$t_1 v_k^\mu - t_2 v_{p_1 - k}^\mu + t_3 v_{p_2 + k}^\mu = 0 \tag{2.13}$$

Eq.(2.12) is the statement that the three vectors $\alpha_i p_i^\mu$ must form a closed loop. Coleman and Norton [32] pointed out that Eq.(2.12) rewritten in the form Eq.(2.13) takes on a very simple interpretation. To explain their procedure we first introduce the concept of a reduced diagram: for an arbitrary Feynman graph we meet the first Landau condition $D = 0$ by picking some subset of propagators which we put on-shell. For all other propagators we set their Feynman parameters to zero. Then in the Feynman graph we contract all off-shell propagators into one of their vertices. For example, the reduced diagram of the Fig(2.1) associated with the PSS where the gluon is collinear to the quark is constructed in Fig(2.3). Now if we assign each vertex in the reduced graph a space-time point x_i^μ, and each propagator a time $t_i \coloneqq \alpha_i p_i^0$ and velocity $v_i^\mu \coloneqq \frac{p_i^\mu}{p_i^0}$ then Eq.(2.13) is the statement that the points are connected by classical propagation. That is, the spacetime separation between vertices x_i and x_j connected by a propagator $\alpha_a p_a$ must be $\Delta x_{ij} = t_a v_a$. If one can construct a consistent spacetime picture, then the Landau conditions are met.

Let us interpret the example in Fig(2.3) of the collinear quark-gluon pair in terms of the CLN criterion: we put the k^2 and $(p_1 - k)^2$ propagators onshell whilst setting $\alpha_3 = 0$ in order to produce a zero of D. Then Eq.(2.13) requires

$$t_1 v_k^\mu = t_2 v_{p_1 - k}^\mu \tag{2.14}$$

[11] We do not need to consider the possibility of two coalescing poles in the α_i plane as D is only linear in the α_i. Hence if one holds all parameters except one α_i in D fixed, then there is at most one solution for $D = 0$. With only one pole in the α_i plane, the contour can only be trapped if the pole occurs at an endpoint $\alpha_i = 0$ or 1.

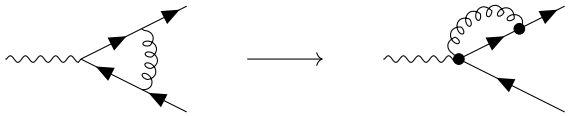

Figure 2.3: Constructing the reduced graph associated with the PSS where the gluon is collinear to the quark. As the anti-quark propagator is off-shell it is contracted to a point

and thus we find again that the particles must be collinear in order for a pinch to form. This is obvious in terms of the spacetime picture: as the particles emerge from a common vertex, the only way they can recombine at a later time, as the reduced graph requires, is if the particles are traveling in the same direction. In terms of a spacetime picture the bounds on the possible momentum fraction carried by the gluon is set by noting the velocities of the two particles are in opposite directions if either $k^\mu < 0$ or $k^\mu > p_1^\mu$, and thus they could never recombine after splitting.

2.2.3 The relation between the massless limit and the high energy limit

Libby and Sterman [33, 34, 35] pointed out that there is a useful one-to-one correspondence between the IR singularity structure occurring in the high energy limit of a theory involving massive particles, and the IR singularity structure occurring for the corresponding massless theory where the external lines do not not necessarily have large energies. As we will see in the next section, this correspondence simplifies the search for PSS's considerably. Hence we review their arguments briefly here.

Consider an arbitrary Feynman graph F containing L-loops, particles of mass $\{ m_i \}$, external momenta $\{ p_i \}$, loop momenta $\{ k_i \}$ and one external line with momenta q^μ

$$F\Big(\{ p_i \}, \{ m_i \}, \mu_R, q^\mu \Big) = \int \mathrm{d}^{dL} \{ k_i \} \;\; I\Big(\{ p_i \}, \{ k_i \}, \{ m_i \}, \mu_R, q^\mu \Big) \tag{2.15}$$

where we are interested in studying the non-UV singularity structure of the integrand I in the limit of $\sqrt{q^2} := Q \to \infty$. Let us choose to set the UV renormalization scale to $\mu_R = Q$. This has the effect of effectively cutting off all loop momenta with virtuality and energy greater than Q. The regions of loop momentum space which give rise to singularities is where some subset of propagator momenta $\{ l_i \}$, where the l_i, which are functions of the loop k and external p momenta, approach their mass shell $\{ l_i^2 \} \to \{ m_i^2 \}$. Let us now scale

all variables by a factor of Q

$$\{\,\tilde{p}_i\,\} = \frac{\{\,p_i\,\}}{Q}, \quad \{\,\tilde{k}_i\,\} = \frac{\{\,k_i\,\}}{Q}, \quad \{\,\tilde{m}_i\,\} = \frac{\{\,m_i\,\}}{Q}, \quad \tilde{q}^\mu = \frac{q^\mu}{Q} \tag{2.16}$$

In these variables the important regions of loop momentum space are where $\{\,\tilde{l}_i^2\,\} \to \{\,\tilde{m}_i^2\,\}$. The singularities in the $Q \to \infty$ limit therefore correspond to $\{\,\tilde{l}_i^2\,\} \to 0$, which equivalent to the $m \to 0$ with Q fixed limit. Thus the non-UV divergences of I in the $Q \to \infty$ limited can be located by studying the Q-fixed $m \to 0$ instead.

This observation motivates us to introduce some terminology that will aid the further discussion. We will refer to any subset of propagators with virtuality much less than Q as providing a "long distance" contribution to F and any subset of propagator with virtuality on the order of Q as providing a "short distance" contribution. In this terminology the claim of factorization Eq.(2.1) is that in the leading regions of momentum space for a given DIS graph, the momentum routes itself through the graph such that the long and short distance contributions are almost independent of one another, related only by a single momentum convolution. The following two sections will reinforce this interpretation.

2.2.4 The Landau criterion in the massless limit

The massless limit simplifies the search for PSS's considerably. As all particles in the reduced diagram either travel at the velocity of light or have zero momentum, we can derive a very simple set of rules for all the possible reduced diagram.

1. Two lightlike lines which emerge from a common vertex can never recombine.
2. As the sum of two lightlike on-shell momenta in the *same direction* form another on-shell lightlike momentum, lightlike lines can split and recombine into arbitrarily many lightlike lines in the same direction.
3. Adding a zero momentum line to a consistent reduced graph leaves all momenta unchanged, thus producing another consistent reduced graph.
4. Two lightlike on-shell lines with different directions always combine to form an off-shell line

We thus recognize that in the massless limit PSS's only form due to soft and/or collinear interactions. As a first example, these rules immediately make it clear that the PSS's of the Sudakov graph in Fig(2.1) are where any one of the internal lines are soft,

$$\begin{aligned} k^\mu = 0, \qquad & \alpha_2 = \alpha_3 = 0 \\ (p_2 + k)^\mu = 0, \qquad & \alpha_1 = \alpha_2 = 0 \\ (p_1 - k)^\mu = 0, \qquad & \alpha_1 = \alpha_3 = 0 \end{aligned} \tag{2.17}$$

or where the gluon is collinear to one of the internal fermions,

$$\alpha_1 k^\mu - \alpha_2 (p_1 - k)^\mu = 0, \quad \alpha_3 = 0, \quad , k^2 = p_1 \cdot k = 0$$
$$\alpha_1 k^\mu + \alpha_3 (p_2 + k)^\mu = 0, \quad \alpha_2 = 0, \quad , k^2 = p_2 \cdot k = 0$$

The quark and anti-quark do not form a pinch when simultaneously put on-shell as they necessarily travel in different directions (unless the incoming photon is lightlike) and thus would not be able to recombine at a point again (as the reduced diagram would require).

2.2.5 Jet structures

In many QCD collider events, the final state consists of sets of beams of roughly collinear particles. Furthermore, the angular distribution of these jets tend to resemble the angular distribution of an underlying partonic event. For example, the partonic process $e^+e^- \to q\bar{q}$ exhibits a $(1 + \cos^2\theta)$ angular distribution, where θ is the angle between the incoming electron and outgoing quark in the center of mass frame. For center of mass energies of around 7 GeV and above, the two jet angular distribution arising in e^+e^- collisions begins to resemble this distribution. This then implies there must be a cutoff on the transverse momentum exchanges within the jets during the hadronization process.

The tools we have just developed indicate why this is the case. The rules stated above for reduced diagrams in the massless limit indicate that immediately after two lightlike lines emerge from a common vertex in the reduced diagram they become spacelike separated and hence can no longer exchange finite momenta and can never recombine again. Within the jet, lines can split and recombine arbitrarily as long as they are collinear to one another. In this way the final state jet structure will resemble the orientation of the particles emerging from the hard vertex. Even-though the jets may not be able to exchange momenta, the possibility of a soft-subgraph, means that other quantum numbers such as color can still be exchanged between jets.

2.2.6 Unitarity, final state cancellations and factorization in DIS

Let us first introduce some terminology. In DIS, the scattering of the highly virtual photon occurs on a very short time and distance scale, roughly of the order $\sim \frac{1}{Q}$. Thus one can categorize interactions which occur before and after the hard scattering vertex as "initial state interactions" and "final state interactions ".

On a process by process level, the total DIS cross section receives contributions which are IR divergent. For example the three jet production process depicted in Fig(2.4) has a highly pinched reduced diagram as it corresponds to a consistent classical scattering process. Further power counting will indeed indicate that the contribution from this configuration is IR singular. Outside

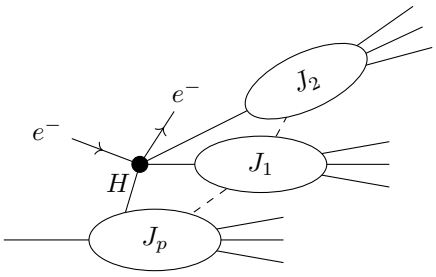

Figure 2.4: Typical reduced diagram contributing to σ_{DIS}^{tot}. Each jet gives rise to a PSS and subset of IR divergences.

of perturbation theory, confinement in fact renders the QCD parts of these amplitudes finite by providing an IR cutoff, but the pinch analysis nevertheless indicates the presence of large logarithms $\log \frac{Q}{m_N}$ and also that long distance final state interactions have a large influence on the value of the amplitude. At first sight then, it is unclear why the factorization formula Eq.(2.1) can determine the total cross section by making reference only to the short distance hard scattering $H^{\mu\nu}$ and the initial state parton distributions $f_{a/N}$. Why, for example, do we not need to know the amplitudes for pion production rates to calculate the total cross section?

Unitarity implies the generalized/off-shell optical theorem[12] which allows one to relate total $\sigma^{\gamma^* N}$ cross section to the imaginary part of their forward scattering amplitude which itself can be obtained by summation over Cutkosky cuts of the forward amplitude. Furthermore, this relation holds on a diagram by diagram basis. If we compute the total cross section via the the forward $\gamma^* N \to \gamma^* N$ amplitude, then class of reduced diagrams which are pinched reduces considerably. For example, consider the reduced forward scattering diagram in Fig(2.5) in which jets J_1 and J_2 are not collinear, due to the photon imparting a large momentum transfer. This clearly does not have a Coleman-Norton classical propagation interpretation as the two jets immediately become spacelike separated after the hard scattering vertex and hence will not be able to recombine at a later stage as the forward scattering would require. We therefore conclude that although each individual cut over the final state interaction lines in Fig(2.5) may contain highly pinched contributions giving rise to $\frac{1}{\epsilon_{IR}^n}$ poles in the integral, when we sum over all cuts, these final state poles must cancel amongst one another[13].

The physics of this is clear; as the hard scattering occurs is well localized in spacetime it cannot interfere quantum mechanically with the subsequent long

[12]The usual optical theorem requires the external lines of a Feynman diagram to be on-shell, whereas in DIS the external photon is virtual.

[13]It should be noted that this cancellation occurs only once the amplitudes are averaged over an interval in Bjorken-x as the KLN theorem would require

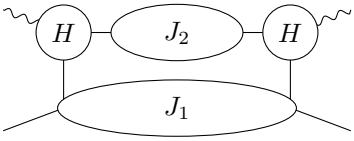

Figure 2.5: Example of a reduced graph contributing to the inclusive DIS but which is not pinched as the requirement of physical scattering cannot be realized.

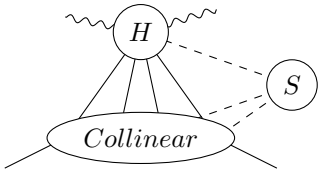

Figure 2.6: The class of reduced graphs contributing to the PSS of the inclusive DIS cross section. The lines connecting the collinear and hard subgraphs are necessarily collinear to the hadron and there can be arbituarily many such connections. The hard scattering should be contracted to a point in the reduced graph as all its internal lines in the associated Feynman graph are off-shell by an amount $\approx Q^2$. All lines in the reduced collinear subgraph are on-shell and parallel to the hadron's momentum.

distance processes. And by the constraint of unitarity, we have that the sum of all subsequent processes must sum to unity.

In this manner we can rule out the possibility of multiple jets in the reduced forward scattering graph for DIS. Furthermore the virtuality of the photon implies that there are no jets which are collinear to the photon. We can always attach a soft line to any consistent DIS reduced graph to obtain another consistent graph. We therefore conclude that the set of reduced graphs contributing to the total DIS cross section can contain only a single jet line which is collinear to the incoming hadron, and a single hard scattering vertex, with soft attachments at arbitrary points as depicted in Fig(2.6).

Although the final state infrared divergences in DIS do cancel amongst one another, the total DIS cross section is *not infrared safe* due to the remaining initial state interactions of the hadron. This is due to the fact that we do perform a sufficient average over the initial states for the KLN theorem to hold [13]. The physical consequence of these remaining large logarithmic enhancements will be the Q dependence of the PDF's and is summarized in the DGLAP evolution equations described in Sect(2.7).

2.2.7 IR versus UV divergences

Let us briefly comment on the different manners in which one treats UV and IR divergences and their different physical interpretations.

UV divergences occur when one sends the UV cutoff on loop momenta to infinity. This is in all likelihood an unphysical procedure as the renormalization group suggests that the Standard Model is just an effective field theory with some physical cutoff. We can nevertheless take the cutoff to infinity, as the Standard Model is renormalizable, so long as we include counterterms which undo the effects of the unphysically high Fourier modes. Taking the cutoff to infinity may not be physical, but it aids the calculation of manifestly Lorentz and gauge invariant quantities.

IR divergences however represent genuine physics in QED, and one therefore does not cancel these infinities by means of counterterms. For example, the $\sigma(\mu^+\mu^- \to e^+e^-\gamma)$ cross section vanishes after resumming all leading contributions (at each order in perturbation theory one encounters divergent contributions, however these terms exponentiate leading to a vanishing result). Clearly one of the assumptions of QFT is being violated. The culprit is the definition of the S-matrix. The in/out states of the S-matrix are defined such that at early and late times they resemble *direct products* of one particle states. That is to say, the states are non-interacting at early and late times[14]. However, the $\bar{\psi}\gamma^\mu\psi A_\mu$ interaction of QED acts approximately as a $\frac{1}{r}$ potential. As this potential has an infinite range, the soft-collinear photons never decouple from the electrons. This suggests that we should rather instead ask what is the amount of energy flowing into a given direction, as opposed to what the S-matrix for single collinear photon production is. Indeed as the KLN theorem indicates, when we average over all final state and initial state emissions which are consistent with prescribed energy flow (for example a lower bound on detector energy) one obtains an IR finite result.

In QCD the story is different due to confinement. Soft-collinear gluons again induce IR divergences at low orders of perturbation theory, but we know that confinement, which may be outside the realm of perturbation theory, puts an effective IR cutoff on gluon momenta. One could attempt to model this situation phenomenologically by using a gluon mass in low orders of perturbation theory.

In summary, UV divergences represent our choice to work with an unphysical theory (one with an infinite cutoff) and hence are dealt with by means of counterterms. IR divergences however represents genuine physics in QED, but in QCD they result due to our use of low order perturbation theory, and in neither case do we use counterterms to render the quantities finite. In order to make testable predictions one should therefore search for infrared finite quantities.

[14] See for example the discussion of the Lippmann-Schwinger equations in [36] at Eq.(3.1.21)

2.3 Power counting for the leading graphs of DIS

For an integral to be truely IR divergent it is necessary but not sufficient for the integrand to be pinched. In order for an IR divergence to form one requires that the strength of the singularity not be outweighed by the remaining factors in the integrand. This leads us to a power counting analysis.

A powerful power counting formalism has been developed [34, 35] in which one uses local co-ordinates in the immediate vicinity of the PSS in order to evaluate the strength of a singularity. We will however employ a different technique, as found in [37], based rather on general properties of dimensional analysis and Lorentz transformations.

We have already deduced that Fig(2.6) is the class of DIS reduced graphs which contain PSS's. As the hard, collinear and soft subgraphs exhibit very different kinematics, we will analyze each individually.

For the hard subgraph, all momenta are by definition far off-shell, thus the usual UV power counting provides an appropriate estimate to its Q dependence. If we set the UV renormalization scale to Q, then the naive UV power associated with the hard subgraph is [38] Q^{D-N_E} where D is the dimension of space time, N_E is the number of external lines and we have not included the external line propagator factors in the power counting. We therefore have that the power of the hard subgraph in DIS is

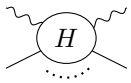

$$\approx \; Q^{D-\frac{3}{2}(N_F+CH_F)-(N_B+CH_B)} \tag{2.18}$$

where N_F, N_B respectively refer to the number of external fermion and boson lines and CH_F, CH_B refer respectively to the number of fermion and boson lines connecting the hard and collinear subgraphs. This already indicates the rational for the parton model assumption that the hard scattering involves a single parton as Eq.(2.18) indicates a Q power suppression for increasing the number of $CH-$lines. Note that this power only depends on the number of external lines and not on the internal details of the graph. Furthermore we deduce that there is a Q power suppression of any external soft lines attaching to the hard subdiagram.

For power counting the collinear subgraph we can exploit the fact that all lines emerging from the graph have a common direction and common order of magnitude. Thus we can begin with the collinear subgraph in its rest frame where all external line momenta are on the order of hadron's mass. As this graph is insensitive to the photon momentum it can only scale as some power of the mass

$m^{dimension}$, in particular there is no Q dependence in this frame,

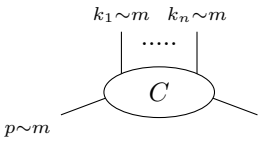

$$\approx \; m^{dimension} \tag{2.19}$$

We can then boost the graph to the overall centre of mass frame where the external lines have momenta on the order $(Q, \frac{m^2}{Q}, m)$ in $(+,-,\perp)$ momentum variables. We thus only need to analyze the Poincaré transformation properties of these graphs. For example, the sum of all forward scattering graphs where the proton emits a quark of momentum k^μ and helicity α followed by an absorption of an anti-quark of momentum k^μ of helicty β is given by the matrix element

$$S_{\beta\alpha}(k^\mu, P) \coloneqq$$

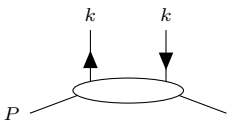

$$= \int \mathrm{d}^d x \; e^{ik\cdot x} \, \langle P|T(\bar{\psi}_\beta(x)\psi_\alpha(0))|P\rangle \tag{2.20}$$

Where $S_{\beta\alpha}$ does indeed transform as a Dirac tensor of the second rank. Note that the matrix element contains the denominator factors of $\frac{1}{k^2}$ which we ommited when calculating the hard subgraphs $Q-$power dependence. The general analysis of direct products of such representations of the Poincaré group indicate that the largest component of the tensor scales as $((\beta)^s)^r$ where s is the spin of the field, r is the rank of the tensor and β is the boost parameter which in our case is of the order $\frac{Q}{m}$. Therefore, the largest scaling component $S_{\beta\alpha}$ scales as $S_{\beta\alpha} \to (\frac{Q}{m})S_{\beta\alpha}$ under such a boost. We therefore have that the largest component of the collinear subgraph exhibits a Q power dependence of the order

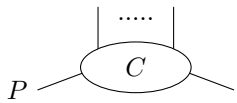

$$\approx \; Q^{CH_g^s + \frac{1}{2}CH_f^s} \tag{2.21}$$

where the CH_g^s, CH_f^s refer respectively to the number of gluon and fermion lines connecting the collinear and hard subgraphs. The superscript s reminds us that it is only the helicity component of each field which receives the largest enhancement under a boost that exhibits this scaling power. These helicity components are often referred to as having "scalar polarization"[15].

We must account for the possibility of the soft subgraph attaching to the collinear subgraph. To this end we must decide on an appropriate scale for when a line is considered soft. This issue has not entirely been solved satisfactory in the literature [37]. In the hadrons rest frame, we will regard a momenta

[15]These arguments indicate why the high spin operators form an important contribution to the DIS OPE on the lightcone, and furthermore reinforce the Regge ideas that cross sections involving the exchange of spin-j Reggeons scale as $\sigma \approx s^{j(t)-1}$ where s and t are the usual Mandelstam variables.

to be soft if its momenta is less than $\frac{m^2}{Q}$. The disadvantage of this choice is that it forces us to include momenta which are unphysically soft in a confining theory. If we include the propagator and loop integral factors in the soft subgraph then its power in this frame is is just given by the canonicaly dimensions of the fields exiting the graph

$$\left(\frac{m^2}{Q}\right)^{\frac{3}{2}CS_f+CS_g} \tag{2.22}$$

If we now boost to the center of mass frame and account for the Lorentz transformation properties of the fields we obtain

$$\left(\frac{m^2}{Q}\right)^{\frac{CS_f}{2}} \tag{2.23}$$

and thus there is a Q power suppression for fermions connecting the soft and collinear subgraphs, whereas there is no such suppression for gluon connections. However, soft fermion loops may circulate within the soft subgraph.

Combing then the power counting of Eq.(2.21) and Eq.(2.18) we find that the overall power for a given DIS graph is

$$Q^{2-CH_f^s} \tag{2.24}$$

The minimum number of fermion lines connecting the hard to collinear graph is two and hence we expect a $\log(Q)$ dependence for this configuration[16]. We will refer to any contribution to the DIS cross section as "leading" if it contributes logarithmically in Q. Note that it appears that when two scalar polarized gluons are exchanged between the CH graphs we obtain an overall Q^2 dependence. However as was shown in [39] this superleading region cancels, so the actual leading power remains Q^0. Thus the leading regions of DIS occur for two transverse gluons or two scalar polarized fermions connecting the CH graphs, with an arbitrary number of extra scalar polarized gluons connecting the CH graphs. Note that the scalar polarization field is a pure gauge field (gauge equivalent to the vacuum), as it consists only of longitudinally/unphysically polarized gluons.

By Eq(2.24) we have a $Q-$power suppression for increasing the number of fermion lines or transverse polarized gluon lines connecting the hard and collinear subgraphs: this provides the rationale for the parton model assumption that the hard scattering occurs upon a single parton. The leading class of graphs to be considered is depicted in Fig(2.7). As the soft subgraph only connects to the collinear subgraph, it will be convenient henceforth to absorb the soft subgraph into the collinear subgraph, as has been done in Fig(2.7).

[16]In terms of OPE terminology, exchanges involving more than two fermions would be considered higher twist contributions.

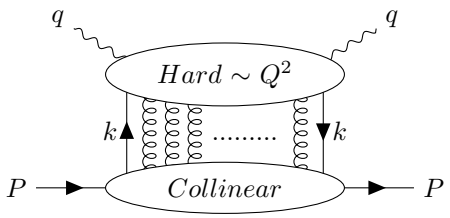

Figure 2.7: Leading graphs for DIS. The particles connecting the hard and collinear subgraphs have scalar polarization. Note that we have absorbed the soft subgraph into the collinear graph. One must also consider graphs where the two quarks are replaced by transversely polarized gluons.

Fig(2.7) seems to invalidate the parton model property that scattering occurs upon a single parton. The presence of the extra exchanges will occur in any theory involving vector fields (or any higher rank tensor fields). This appears to be a barrier to factorization taking the form of a single convolution between the hard and collinear graphs. However, as QCD has the extra color "symmetry", and therefore associated Slavnov-Taylor identities, we will be able to decouple these extra gluon attachments, thus restoring the parton model property of scattering upon a single parton (see Sect(2.4)).

2.4 Proof of Factorization in DIS

The choice of gauge has a large influence on the approach taken to proving factorization in DIS. In lightcone gauge $A^+ = 0$ all the CH_g^s gluons disappear, thus one only needs to prove factorization for the set of diagrams with only two CH connecting gluons. Furthermore, in this gauge, ghosts decouple (as there are no unphysical polarizations for them to cancel). However, an axial gauge introduces unphysical singularities in the gluon propagator

$$D_{\mu\nu}^{ab} = \delta^{ab} \frac{-g_{\mu\nu} + k_\mu u_\nu / k \cdot n + u_\mu k_\nu / k \cdot u}{k^2 + i\epsilon} \tag{2.25}$$

where $u^\mu = g_-^\mu$ in lightcone gauge. These singularities introduce additional PSS which produce difficulties which are as of yet not fully understood [40]. We will proceed in Feynman gauge following the proof found in [23]. Let us state the basic approach to disentangling the large number gluons connecting the CH graphs: as the CH_g^s gluons are longitudinally polarized and approximately on-shell in the leading region, they are perfectly suited for applying Slavnov-Taylor identities. We will find that this insight will allows us to decouple the CH_g^2 gluons from the hard subgraph. Now to the proof:

Given a cut Feynman diagram G contributing to DIS, we can specify a leading region L of momentum space; that is we specify which lines are considered to

be part of the H graph and those that are within the C graph. Note that a single graph can have multiple such decompositions. We denote this amplitude as G^L. Suppose that to the left of the cut we have n such CH_g gluons of momenta $\{ l_i^{\mu_i} \}$ and a single parton of momenta $k - \sum_i^n l_i$. To the right of the cut we have n' connecting gluons of momenta $\{ l'^{\nu_j}_j \}$ and a parton of momenta $k - \sum_j l'_j$. We take all momenta to the left of the cut as flowing into the hard subgraph and momenta to the right of the cut as flowing out. Denoting a particular cut of G^L as $G^{(L,C)}$ we can write the sum over all cuts which preserve n and n' as

$$\begin{aligned} G^L &= \sum_{Cuts\, C} G^{(L,C)} \\ &= \int_L \frac{\mathrm{d}^4 k}{(2\pi)^4} \prod_i \int_L \frac{\mathrm{d}^4 l_i}{(2\pi)^4} \prod_j \int_L \frac{\mathrm{d}^4 l'_j}{(2\pi)^4} \\ &\times \sum_{C_H} H^{(C_H,L)}(q^\nu; k^\mu - \sum l_i^\mu, \{ l_i^{\alpha_i} \}; k^\mu - \sum l'^\mu_j, \{ l'^{\beta_j}_j \})^{\{ \mu_i, \nu_j \}}_{\eta,\eta'} \\ &\times \sum_{C_J} J^{(C_J,L)}(p^\nu; k^\mu - \sum l_i^\mu, \{ l_i^{\alpha_i} \}; k^\mu - \sum l'^\mu_j, \{ l'^{\beta_j}_j \})^{\eta,\eta'}_{\{ \mu_i, \nu_j \}} \end{aligned} \tag{2.26}$$

where η, η' denote the polarizations of the parton to the left and right of the cut respectively, and $\{ \mu_i, \nu_j \}$ respectively refer to the set of polarization indices of the $\{ l_i, l'_j \}$ gluons. Note that the cuts on the J and H subgraphs can be carried out independently. The superscript L on the $J^{(C_J,L)}, H^{(C_H,L)}$ and its subscript on the momentum integrals are there to remind us that the momenta of the lines within each of these subgraphs are to restricted to the given leading region. That is, we introduce an energy scale μ, later to be identified with the renormalization scale, for which all virtualities within H must be greater than or equal to μ and all transverse momenta within J must be less than or equal to μ.

In the leading region, all of the CH_g gluons are approximately on-shell and collinear to the jet momentum. The function $J^{(C_H,L)}$ is sensitive to deviations of $\{ l, l' \}$ away from exact collinearity, however the hard function $H^{(C_H,L)}$ does not share such a sensitivity. Thus we will project the momenta entering $H^{(C_H,L)}$ to be onshell and collinear to the jet lightcone, that is, both the parton and gluons momenta. Furthermore we will project the polarizations of the $\{ l, l' \}$ gluons onto their longitudinal component. The correction to this approximation being suppressed by a power of Q^2. To implement this, we introduce the projection vectors

$$v^\mu = g_+^\mu \ , \ u^\mu = g_-^\mu \tag{2.27}$$

and define

$$u \cdot l_i = \lambda_i \quad , \quad u \cdot k = \kappa \quad , \quad u \cdot l'_i = \lambda'_i \tag{2.28}$$

The approximation is that

$$\sum_{C_H} H^{(C_H,L)}(q^\nu; k^\mu - \sum l_i^\mu, \{\, l_i^{\alpha_i} \,\}; k^\mu - \sum l'^\mu_j, \{\, l'^{\beta_j}_j \,\})^{\{\,\mu_i,\nu_j\,\}}_{\eta,\eta'}$$
$$\longrightarrow \hat{H}(q^\nu; (\kappa - \sum \lambda_i)v^\mu, \{\, \lambda_i v^{\alpha_i} \,\}; (\kappa - \sum \lambda'_j)v^\mu, \{\, \lambda'_j v^{\beta_j} \,\})_{\eta,\eta'}$$
$$\prod_i u^{\mu_i} \prod_j u^{\nu_j} \tag{2.29}$$

where

$$\hat{H}(q^\nu; (\kappa - \sum \lambda_i)v^\mu, \{\, \lambda_i v^{\alpha_i} \,\}; (\kappa - \sum \lambda'_j)v^\mu, \{\, \lambda'_j v^{\beta_j} \,\})_{\eta,\eta'} :=$$
$$\sum_{C_H} H^{(C_H)}(q^\nu; (\kappa - \sum \lambda_i)v^\mu, \{\, \lambda_i v^{\alpha_i} \,\}; (\kappa - \sum \lambda'_j)v^\mu, \{\, \lambda'_j v^{\beta_j} \,\})^{\{\,\gamma_i,\delta_j\,\}}_{\eta,\eta'}$$
$$\prod_{i'} v_{\gamma_i} \prod_{j'} v_{\delta_j} \tag{2.30}$$

Note that $\hat{H}$ contains the sum over cuts of the approximated H. This approximation is represented diagrammatically in Eq.(2.31)

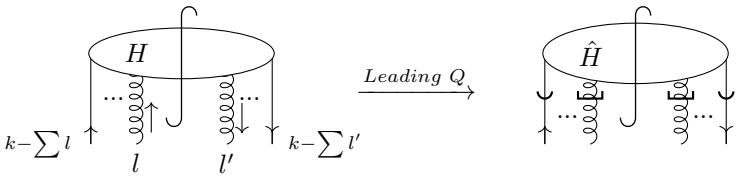

(2.31)

where the upwards brackets on the gluons on the RHS of Eq.(2.31) indicate that the gluon's momenta above the bracket is projected onto it's component parallel to the jet momentum and its polarization is projected onto its longitudinal component. The upwards braces on the partons indicate that above the brace the parton is made massless, it's momentum is put on-shell and collinear to that of the jet, with its helicity unaffected.

The graph is now in a form appropriate for the application of Ward identities, as we have on-shell momenta momenta being contracted into a graph in the location of the gluon attachments. The Ward identities tell us that once one sum over all the insertion points of the momenta we should get zero. Let us consider the simplest case where there is one gluon to the left of the cut, and we will ignore whatever is happening to the right of the cut at the moment. Then we have[17]

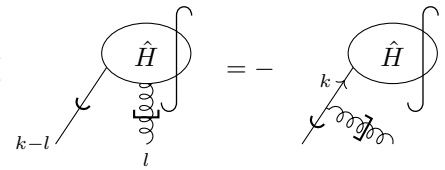

(2.32)

[17]Here we provide a simplified version of the proof where we ignore the influence of ghosts and BRST variations. The full proof can be found in Chapter 11 of [24]

where the sum over A_g denotes the sum over all attachments of the gluon momentum to the hard diagram. Note on the RHS of Eq(2.32) that after summing over all the attachment points the *total momentum is carried into the hard diagram by the parton*. As the parton and gluon are now collinear we can use the eikonal identity (see App.(C) and Sect(2.6)) that

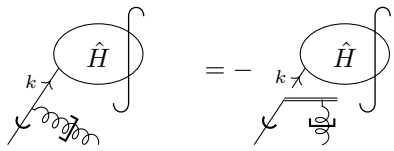

(2.33)

in which the parton gluon interaction is equivalent to that of an eikonal line in a direction opposite to the jet. Combining Eq.(2.32) and Eq.(2.33), and suppressing the Cutkosky cut, the bracket and brace adornments from now on (they are understood to be implicitly present) we arrive at

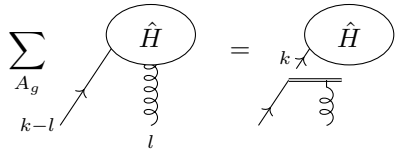

(2.34)

The longitudinal gluon has decoupled from the hard graph and coupled to an eikonal line instead. We can continue this process for two gluon attachments as follows.

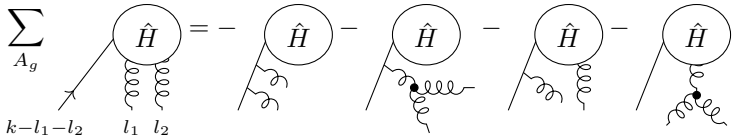

(2.35)

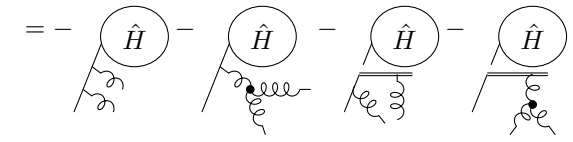

(2.36)

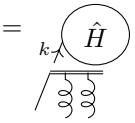

(2.37)

Note that on the RHS of the equality when the two gluons fuse they may produce a gluon of a different polarization. However, in Feynman gauge Lorentz invariance requires the resultant gluon to be longitudinally polarized as there are no other vectors on which it could depend (as opposed to an axial gauge). We may thus use Eq(2.34) applied to the third and fourth diagrams to produce the second equality. Note that we have not shown diagrams where the two gluons are interchanged. We can repeat this procedure for arbitrary many gluons to

arrive at

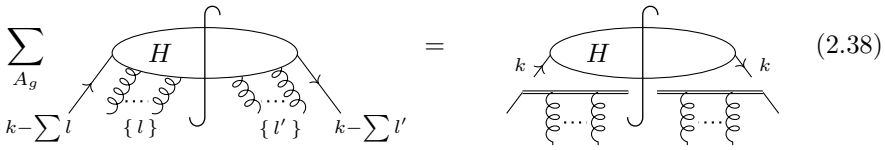

(2.38)

Thus after summing over all possible gluon attachments, the hard diagram can be decomposed as

$$\hat{H}(q^\nu;(\kappa-\sum\lambda_i)v^\mu,\{\,\lambda_i v^{\alpha_i}\,\};(\kappa-\sum\lambda'_j)v^\mu,\{\,\lambda'_j v^{\beta_j}\,\})_{\eta,\eta'}\prod_i u^{\mu_i}\prod_j u^{\nu_j}$$
$$=\tilde{H}(q^\nu,\kappa v^\mu)_{\eta,\eta'}\mathcal{E}(u,\{\,\lambda_i\,\})^{\{\,\mu_i\,\}}\mathcal{E}^*(u,\{\,\lambda'_j\,\})^{\{\,\nu_j\,\}} \tag{2.39}$$

where $\mathcal{E}(u,\{\,\lambda_i\,\})^{\{\,\mu_i\,\}}$ is an eikonal line in the u direction (opposite to the jet), coupled to the n gluons $\{\,l_i\,\}$, and similarly $\mathcal{E}^*(u,\{\,\lambda'_j\,\})^{\{\,\nu_j\,\}}$ is an eikonal line in the same direction coupled to the n' gluons $\{\,l'_j\,\}$. In particular, the function $\tilde{H}$ is only a function of the plus component of the total momentum flowing into and out of the hard graph. It is natural to associate the eikonal lines with the jet graph and then to define

$$\begin{aligned}\tilde{J}(\xi)^{\eta,\eta'} = &\int_L\frac{\mathrm{d}^4k}{(2\pi)^4}\delta(\xi p\cdot u/k\cdot u-1)\prod_i\int_L\frac{\mathrm{d}^4l_i}{(2\pi)^4}\prod_j\int_L\frac{\mathrm{d}^4l'_j}{(2\pi)^4}\\ &\times\mathcal{E}(u,\{\,\lambda_i\,\})^{\{\,\mu_i\,\}}\mathcal{E}^*(u,\{\,\lambda'_j\,\})^{\{\,\nu_j\,\}}\\ &\times\sum_{C_J}J^{(C_J,L)}(p^\nu;k^\mu-\sum l_i^\mu,\{\,l_i^{\alpha_i}\,\};k^\mu-\sum l'^\mu_j,\{\,l'^{\beta_j}_j\,\})^{\eta,\eta'}_{\{\,\mu_i,\nu_j\,\}}\end{aligned} \tag{2.40}$$

In particular $\tilde{J}$ and $\tilde{H}$ are now only linked through a convolution in ξ and the parton indices η,η'. Combining Eq's.(2.26,2.29,2.40) we arrive at the factorized form of the contribution to the leading region L of G

$$G^{(L)}(\mu)=\int_{\frac{Q^2}{2P\cdot q}}^1\frac{\mathrm{d}\xi}{\xi}\;\tilde{H}(q^\nu,\xi p\cdot u\,v^\mu)_{\eta,\eta'}\;\tilde{J}(\xi)^{\eta,\eta'} \tag{2.41}$$

Where the lower bound on the integral follows from the positive energy condition on the particles passing through the final state cut in the hard vertex $\theta(q^+ + \xi P^+)$, and the lower bound following following from a similar positive energy condition on the target remnants $\theta(P^+ - \xi P^+)$. Note that this derivation indicates that the summation over leading regions in $\tilde{J}$ can be carried out independently of the summation in $\tilde{H}$. To bring the result to the final factorized form we must still decouple the helicity indices. If the incoming hadron is unpolarized, then by Lorentz invariance the jet co-efficient must be diagonal in its spin indices, hence we can sum over the polarizations of the parton exiting the jet and average over the polarizations entering the hard subdiagram, thereby

decoupling these indices. Summing over Feynman diagrams $G^{(L)}$ and restoring the photon polarization indices gives our final result Eq.(2.1)

$$\boxed{W_N^{\mu\nu}(q^\mu, p^\mu) = \sum_a \int_{x=\frac{Q^2}{2p\cdot q}}^1 \frac{\mathrm{d}\xi}{\xi}\ f_{a/N}(\xi, \mu_F) H_a^{\mu\nu}(q^\mu, \xi p^\mu, \mu_F)}$$

Note how the proof may have failed: without the use of gauge invariance one would have obtained a different PDF and hard co-efficient for each number of gluon exchanges, in which case the factorization formalism would have very little predictive power as there would be an infinite set of PDF's to measure.

2.5 The Hard co-efficient

2.5.1 General procedure for determining the hard coefficient

In the section we will indicate the various possible definitions of the hard co-efficient and how to perturbatively calculate it. The primary condition on the hard co-efficient is that it must be insensitive to infrared momenta. To ensure the infrared safety of the hard co-efficient one employs the following strategy: first one observes that the derivation of the DIS factorization formula indicates that the hard co-efficient is *independent of the target hadron*—it is only a function of the two incoming parton lines. Thus we can calculate the hard co-efficient using a more convenient target state, such as a quark or gluon. For an elementary particle target, such as a quark, we again have a factorization theorem for DIS scattering,

$$W^{\mu\nu}_{\gamma^* q}(q^\mu, p^\mu) = \sum_{a=\{\, q,\bar{q},g\,\}} \int_{x^-}^{1^+} \frac{\mathrm{d}\xi}{\xi}\; H^{\mu\nu}_{\gamma^* a}\left(\frac{x}{\xi}, \frac{Q}{\mu_r}, \frac{\mu_F}{\mu_r}, \alpha_s(\mu_r)\right) \times f_{a/q}\left(\xi, \mu_F, \alpha_s(\mu_r), m_q\right) \tag{2.42}$$

where here the PDF's are now the number density of *partons in a quark*. With an elementary in/out state we can now calculate $W^{\mu\nu}_{\gamma^* q}(q^\mu, p^\mu)$ from first principles. We perform the calculation in $d = 4+\epsilon_{IR}$ dimensions. After renormalizing the UV contributions to $W^{\mu\nu}_{\gamma^* q}(q^\mu, p^\mu)$, the remaining $\frac{1}{\epsilon_{IR}}$-poles will indicate to us which contributions to $W^{\mu\nu}_{\gamma^* g}(q^\mu, p^\mu)$ are to be associated with long-distance phenomena. At each order in perturbation theory we then partition any quantities which contain IR poles into the $f_{a/q}$ in Eq.(2.42). With both $W^{\mu\nu}_{\gamma^* g}(q^\mu, p^\mu)$ and $f_{a/g}$ determined, Eq.(2.42) then determines the $H^{\mu\nu}_{\gamma^* a}$. We can then use this hard co-efficient in the factorization formula for a real target hadron[18].

In particular then, we pick a physical observable quantity for which a factorization theorem has been proven. For example, the factorization theorem for the hadronic tensor for virtual photon scattering on a nucleon N reads

$$W^{\mu\nu}_{\gamma^* N}(q^\mu, p^\mu) = \sum_{a=\{\, q,\bar{q},g\,\}} \int_{x^-}^{1^+} \frac{\mathrm{d}\xi}{\xi}\; H^{\mu\nu}_{\gamma^* a}\left(\frac{x}{\xi}, \frac{Q}{\mu_r}, \frac{\mu_F}{\mu_r}, \alpha_s(\mu_r)\right) \times f_{a/N}\left(\xi, \mu_F, \alpha_s(\mu_r), m_q\right) \tag{2.43}$$

$$\coloneqq H^{\mu\nu}_{\gamma^* a} \otimes f_{a/N} \tag{2.44}$$

where the second equality defines the meaning of the convolution symbol $\otimes$. The target in this case is a real nucleon N. Next we expand all quantities in

[18] This freedom in determining the hard co-efficient from an arbitrary in/out state corresponds to the freedom one has in deducing the Wilson co-efficients in an operator product expansion from any convenient set of in/out states.

powers of α_s

$$W^{\mu\nu} = W^{[0],\mu\nu} + \alpha_s W^{[1],\mu\nu} + ... \coloneqq \sum_{n=0}^{\infty} (\alpha_s)^n W^{[n],\mu\nu}$$
$$f_{a/n} = \sum_{n=0}^{\infty} (\alpha_s)^n f_{a/N}^{[n]} \quad , \quad H_{\gamma^* a}^{\mu\nu} = \sum_{n=0}^{\infty} (\alpha_s)^n H_{\gamma^* a}^{[n],\mu\nu} \tag{2.45}$$

In a power expansion Eq.(2.43) now reads (suppressing the Lorentz indices)

$$W_{\gamma^* N}^{[0]} + W_{\gamma^* N}^{[1]} + ... = H^{[0]} \otimes f_{a/N}^{[0]} + \alpha_s H^{[1]} \otimes f_{a/N}^{[0]} + \alpha_s H^{[0]} \otimes f_{a/N}^{[1]} + ... \tag{2.46}$$

Similarly, we have a factorization theorem for photon scattering on an elementary particle Eq.(2.42), and we can again perform a power expansion of the form Eq.(2.43). The crucial point is that the $H_{\gamma^* a}^{[n],\mu\nu}$ featuring in either expansion are the same. As the in/out states are now elementary quark fields one can calculate $W_{\gamma^* q}^{\mu\nu}$ perturbatively from first principles. For example, if we take our target to be a quark then the F_2 structure function at zeroth order is

$$F_2^{[0]\gamma^* q}(x, Q^2) = Q_f^2 x \delta(1-x) \tag{2.47}$$

and the PDF of a quark inside of a quark at zeroth order is naturally

$$f_{q/q'}^{[0]}(\xi) = \delta_{qq'} \delta(1-\xi) \tag{2.48}$$

Then comparing the zeroth order terms on the LHS and RHS of Eq.(2.46) implies that the hard co-efficient must be[19]

$$H_2^{[0]}(x/\xi) = Q_q^2 \delta(1 - x/\xi), \tag{2.49}$$

where the subscript 2 reminding us that this is the hard co-efficient for the F_2 structure function. At this order the hard co-efficient agrees with the cross section for the hard scattering of a quark on a virtual photon, hence the name hard co-efficient. However, as we will find Eq(2.57) which iteratively defines H, this identification with hard scattering is ruined at higher orders hence the terminology should not be taken literally.

At the next order there are many ways to proceed with the only requirement that the hard co-efficient be IR finite. To illustrate this we give two examples of factorization schemes, $\overline{MS}$ and DIS-factorization, before stating the factorization scheme which we will use, which will be to use predefined definitions of the PDF's in terms of Wilson lines.

[19] note that the measure for the structure function is $\mathrm{d}\xi$ and not $\frac{\mathrm{d}\xi}{\xi}$

Examples of factorization schemes: $\overline{MS}$ and DIS

In [41] a detailed derivation of the $F_2^{\gamma^* q}$ *quark* structure function gives

$$\begin{aligned} F_2^{\gamma^* q} = Q_f^2 x \Big\{ & \delta(1-x) \\ & + \frac{\alpha_s}{2\pi} C_F \left[\frac{1+x^2}{1-x} (\ln \frac{(1-x)}{x} - \frac{3}{4}) + \frac{1}{4}(9+5x) \right]_+ \\ & + \frac{\alpha_s}{2\pi} C_F \left[\frac{1+x^2}{1-x} \right]_+ (4\pi\mu_r^2 e^{-\gamma_E})^{\epsilon_r} \int_0^{Q^2} \frac{\mathrm{d}k_\perp^2}{k_\perp^{2+2\epsilon_{IR}}} \Big\} \end{aligned} \tag{2.50}$$

where at intermediate stages of the calculation the $\frac{1}{\epsilon_{IR}^2}$ double poles due to soft-collinear final state radiation have canceled amongst one another. This expression has already been renormalized in the UV; the upper cutoff of Q^2 on the $k_\perp$ integral arose from setting $\mu_R^2 = Q^2$. As we have used dimensional continuation both for renormalizing the UV region and for quantifying the IR poles, we have indicated the origins of the various ϵ's by their subscripts[20]. Nevertheless, $F_2^{\gamma^* q}$ is still IR divergent due to the collinear singularity in the $k_\perp$ integral, arising from real and virtual gluon radiation in the initial state. This was to be expected as the DIS cross section is not infrared safe as we do not perform a sufficient averaging over initial states for the KLN theorem [42, 43] to apply. This integral is finite in a theory where we include quark masses, producing a large logarithm $\ln \frac{Q^2}{m^2}$, however we are only interested in extracting the mass and infrared insensitive parts of F_2.

Let us break up this integral into an IR divergent piece and a finite piece

$$\begin{aligned} \int_0^{Q^2} \frac{\mathrm{d}k_\perp^2}{k_\perp^{2+2\epsilon_{IR}}} &= \int_0^{\mu_F^2} \frac{\mathrm{d}k_\perp^2}{k_\perp^{2+2\epsilon_{IR}}} + \int_{\mu_F}^{Q^2} \frac{\mathrm{d}k_\perp^2}{k_\perp^{2+2\epsilon_{IR}}} \\ &= \int_0^{\mu_F^2} \frac{\mathrm{d}k_\perp^2}{k_\perp^{2+2\epsilon_{IR}}} + \log \frac{Q^2}{\mu_F^2} \end{aligned} \tag{2.51}$$

At the moment the choice of μ_F is arbitrary. It will soon be identified with the factorization scale. As per Eq.(2.46) we must now partition the order α_s terms of Eq.(2.50)

$$F_2^{[1],\gamma^* q} = H_{\gamma^* q}^{[1]}(x) + Q_q^2 x f_{q/q}^{[1]}(x) \tag{2.52}$$

This step is arbitrary so long as $H^{[1]}$ is insensitive to the IR. In the $\bar{M}S$ factorization scheme one absorbs all of the μ_F-independent terms into the hard

[20] It is interesting to note that the transverse integral is actually zero before UV renormalization $(\frac{\mu^2}{4\pi} e^\gamma)^{\epsilon_{uv}} \int_0^\infty \frac{\mathrm{d}^{2-2\epsilon} k_\perp^2}{(2\pi)^{2-2\epsilon}} \frac{1}{k_\perp^{2-2\epsilon}} = \frac{1}{4\pi}(\frac{1}{\epsilon_{uv}} - \frac{1}{\epsilon_{ir}}) = 0$. However, it is not the case that the IR and UV poles cancel one another in their contribution to F_2 as after removing the UV pole by means of a counterterms, the remaining integral is still IR divergent. In Sect(3.2) we encounter this cancellation in position space when calculating contributions to the cusp anomalous dimension.

co-efficient:

$$\bar{MS}: \qquad f^{[1]}_{q/q}(x,\mu_F^2,\mu_r) = (4\pi\mu_r^2 e^{-\gamma_E})^{\epsilon_r} P_{qq}(x) \int_0^{\mu_F^2} \frac{\mathrm{d}k_\perp^2}{k_\perp^{2+2\epsilon_{IR}}} \tag{2.53}$$

$$H^{[1]}_{2,\gamma^* q}(x) = Q_f^2 x P_{qq}(x) \ln\left(\frac{Q^2}{\mu_F^2}\right) + \mu_F - \text{independent} \tag{2.54}$$

where we have defined the splitting function

$$P_{qq}(x) \coloneqq \frac{\alpha_s C_F}{2\pi}\left[\frac{1+x^2}{1-x}\right]_+ \tag{2.55}$$

which is an important ingredient in the Q dependence of the PDF's, and in the following chapter, we will come to recognize the $\frac{\alpha_s C_F}{\pi}$ co-efficient as the anomalous cusp dimension.

In the $DIS-$factorization scheme one partitions all of the μ_F independent terms into $f^{[1]}_{q/q}$. Either way, one arrives at an IR finite $H^{[1]}_{2,\gamma^* q}(x)$ co-efficient. We could now use this co-efficient in the factorization formula for a real nucleon target.

When performing the perturbative calculations it is helpful to set the quark masses to zero. This will have the effect of converting the large logarithms $\log(\frac{Q}{m_q})$ into genuine singularities. This is actually an aid and not a hindrance, as the resultant $\frac{1}{\epsilon_{IR}}$ poles will make clear which terms are to be associated with the hadrons wavefunction.

Factorization by using PDF definitions

The factorization scheme we will follow will be to work with predefined definitions of the PDF's in terms of Wilson line matrix elements. We give these definitions in Sect(2.6). Thus with $W^{\mu\nu}_{\gamma^* q}$ and $f_{a/q}$ unambiguously defined and calculable for *an elementary target*, one can infer from the expansion

$$W^{[n],\mu\nu}_{\gamma^* q}(x,Q) = \sum_{n'=0}^{n} \sum_{a=\{\,q,\bar{q},g\,\}} \int_{x^-}^{1^+} \frac{\mathrm{d}\xi}{\xi} H^{[n'],\mu\nu}_{\gamma^* a}(x/\xi,Q) f^{[n-n']}_{a/q}(\xi) \tag{2.56}$$

that the n^{th} order hard-scattering co-efficient must be

$$\boxed{H^{[n],\mu\nu}_{\gamma^* q}(z,Q) = W^{[n],\mu\nu}_{\gamma^* q}(z,Q) - \sum_{n'=0}^{n-1} \sum_a \int_{z^-}^{1^+} \frac{\mathrm{d}\rho}{\rho} H^{[n'],\mu\nu}_{a}(z/\rho,Q) f^{[n-n']}_{a/q}(\rho)} \tag{2.57}$$

Thus starting with the zeroth order hard co-efficients Eq.(2.49) and PDF's Eq.(2.48) we can iteratively determine the hard co-efficients using Eq.(2.57). The subtractions in Eq.(2.57) then ensure that the resultant hard scattering co-efficient is infrared finite.

It is common in the literature to refer to this procedure as "absorbing" the singularities into the PDF's. It should be clear however that the PDF's of real hadrons are of-course finite, due to the hadron radius providing an effective cutoff in the infrared, and it is only in the calculation involving pseudo-in/out states that the PDF's are infinite.

By construction H is now fermion mass independent, and hence we need not worry about large $\log(\frac{Q}{m})$ logarithms spoiling the hard co-efficients perturbative expansion. Note that within this formalism a perturbative expansion of H is justified if one sets $\mu_F \approx \mu_R \approx Q$. These are the only three energy scales on which H depends and hence only ratios of these scales can appear in the arguments of logarithms.

In summary, we ensure that $H^{\mu\nu}$ is IR finite and infrared safe, by calculating it in $d = 4 + \epsilon_{IR}$ dimensions for an elementary target, isolate the $\frac{1}{\epsilon_{\rm IR}}$ poles, and subtract them out into the PDF. This is physically appropriate as the $\frac{1}{\epsilon_{\rm IR}}$ poles indicate to us which regions of momentum space are associated with long-distance phenomena and hence, in the case of a real hadron, should be genuinely associated with hadron's wavefunction.

2.5.2 Using the theory for real hadrons

Having calculated the hard scattering co-efficients $H^{\mu\nu}$, one can now substitute these hard co-efficients into the factorization formula for scattering on a real nucleon target

$$W^{\mu\nu}_{\gamma^* N}(q^\mu, p^\mu) = \sum_{a=\{\, q,\bar{q},g\,\}} \int_{x^-}^{1^+} \frac{\mathrm{d}\xi}{\xi}\; H^{\mu\nu}_{\gamma^* a}\left(\frac{x}{\xi}, \frac{Q}{\mu_r}, \frac{\mu_F}{\mu_r}, \alpha_s(\mu_r)\right) \times f_{a/N}\left(\xi, \mu_F, \alpha_s(\mu_r), m_q\right) \tag{2.58}$$

where the PDF's $f_{a/N}$ are unknown. One could then in principle measure $W^{\mu\nu}_{\gamma^* N}$ in experiment and from the result infer the PDF's of nucleon N. One could then make a prediction for any nuclear collision in which these same PDF's apply. For example, a factorization theorem for the Drell-Yann process has been proven [26, 27, 28, 29]

$$\frac{\mathrm{d}\sigma}{\mathrm{d}Q^2 \mathrm{d}y} = \sum_a \int_{x_A}^1 \mathrm{d}\xi_a \int_{x_B}^1 \mathrm{d}\xi_B\; f_{a/A}(\xi_A) f_{\bar{a}/B}(\xi_B) \sigma(Q^2, y) \tag{2.59}$$

Thus with the $\sigma(Q^2, y)$ being perturbatively calculable, we now have a genuine prediction for the cross section. The process of inferring the PDF's from experiment is a highly non-trivial procedure as it is often only certain quark flavor combinations that can be deduced from a given observable, and hence one uses must use multiple different observables to infer the PDF's.

2.6 PDF's operator definitions

As we saw in Sect(2.5), the primary purpose of the PDF's is to factor out the leading IR sensitive regions of the relevant class of Feynman graphs. Other than this constraint, there is a freedom in how one exactly defines the PDF's [44]. In this section we will illustrate a convenient choice for the PDF definitions [45] in terms of hadronic matrix elements of certain bi-local operators involving Wilson lines. We will then motivate this definition by demonstrating that this choice reproduces many of the intuitive features of the parton model.

Working in a frame where the target has no transverse momentum and has a minus momentum component $P^- = \frac{m^2}{2P^+}$, we will take our definitions of the PDF's for a spin-averaged nucleon N of momentum P as

$$f_{q/N}(\xi) = \frac{1}{4\pi}\int \mathrm{d}x^-\ e^{-i\xi P^+x^-}\mathrm{Tr}_f\Big\{\ \langle P|\bar{\psi}_a(0,x^-,0_\perp)\gamma^+W_{ab}(x^-)\psi_b(0,0,0_\perp)|P\rangle_c\ \Big\} \tag{2.60}$$

$$f_{\bar{q}/N}(\xi) = \frac{1}{4\pi}\int \mathrm{d}x^-\ e^{-i\xi P^+x^-}\mathrm{Tr}_f\Big\{\ \langle P|\gamma^+\psi_a(0,x^-,0_\perp)W_{ab}(x^-)\bar{\psi}_b(0,0,0_\perp)|P\rangle_c\ \Big\} \tag{2.61}$$

$$f_{g/N}(\xi) = \frac{1}{2\pi\xi P^+}\int \mathrm{d}x^-\ e^{-i\xi P^+x^-}\ \langle P|F_a(0,x^-,0_\perp)^{+\nu}W_{ab}(x^-)F_b(0,0,0_\perp)_\nu^{\ +}|P\rangle_c \tag{2.62}$$

where Tr_f is a trace over the spinor indices, $F_a^{\mu+}$ refers to components of the QCD fields strength tensor, the subscript c reminds us to only take connected Feynman graphs when computing S-matrix contributions, and the Wilson lines are defined as

$$W_{ab}(x^-) \coloneqq \mathcal{P}\exp\left(ig\int_0^{x^-}\mathrm{d}y^-\ A_c^+(0,y^-,0_\perp)t^c\right)_{ab} \tag{2.63}$$

where the $\mathfrak{su}[3]$ generators are in the representation of whichever field they are acting upon. The path ordering orders the x^- earliest fields to the furthest right. The normalizations in Eq(2.60,2.62) are chosen such that in a theory of free quarks and gluons the PDF's are

$$f_{a/b}(\xi) = \delta_{ab}\delta(\xi-1) \tag{2.64}$$

Note that we have not presented the definitions in a co-ordinate covariant manner— we have made specific reference to the + polarization indices in the definition. A coordinate covariant definition is however certainly possible [24].

Notice that the presence of the γ^+ in the quark PDF definitions ensure that the PDF's only involve the good components of the fermion field (see appendix (B)). Furthermore, these components coincide with components of the spinor field which receive the greatest enhancement under a boost in the plus direction.

These are precisely the components described in our power counting analysis of Sect(2.3).

Note that the primary purpose of the PDF's, to absorb the soft-collinear singularities, has been met. The Wilson-lines correspond to the summation of soft-collinear radiation emitted and absorbed by whichever particles are at the beginning and endpoints of the Wilson lines , see App(C) and [46]. As such, they contain the IR singularity structure encountered when calculating structure functions for an elementary target. We will now describe how these definitions implement many of the intuitive features of the parton model.

2.6.1 Support and analytic properties

The definitions Eq(2.60, 2.62) are best motivated in lightcone quantization, see App.(B). Henceforth we will assume that the fields have been canonically quantized on the surface $x^+ = 0$.

First notice the support property that

$$f_{a/N}(\xi) = 0, \text{ if } \quad \xi > 1 \tag{2.65}$$

This follows from the fact that the remaining energy $(1-\xi)P^+$ of the target remnants after emitting the ξP^+ parton is negative. Thus either one encounters a negative energy particle passing through the final state cut or, if there is gluon exchange such that all particles passing the cut have positive energy, then one can always locate a closed momentum loop where the energy is positive all the way around the loop (in the direction of the loop) and hence all the poles lie on the same side of the real k^- (recall by Lorentz invariance the two momenta always feature as k^+k^-) axis hence one can always close the k^- contour in the opposite plane to give zero.

Next, we can derive the inter-relations

$$f_{q/N}(-\xi) = -f_{\bar{q}/N}(\xi) \tag{2.66}$$

$$f_{g/N}(-\xi) = -f_{g/N}(\xi) \tag{2.67}$$

These follow from the canonical commutation relations in lightfront quantization

$$\gamma^+\{\psi_G(0, x^-, 0_\perp), \bar{\psi}_G(0)\}\gamma^+ = \gamma^+\delta(x^-)\delta(x^\perp) \tag{2.68}$$

$$[A_a(0, x^-, x^\perp)^i, A_b(0)^j] = -\frac{1}{4}\delta_{ab}\delta_{ij}\epsilon(x^-)\delta(x^\perp), \quad (i, j = 1, 2) \tag{2.69}$$

where all the fields featuring here are bare. The renormalized fields will contain two extra factors of the field strength renormalization on the RHS's of the Eq.(2.68,2.69). As $f(\xi)$ is gauge invariant, if we establish the relations Eq.(2.66,2.67) in $A^+ = 0$ gauge where the Wilson lines are not present, then

the identities will have been proven in any gauge. In this gauge, the anti-commutator within the hadronic expectation value is zero

$$\langle P|\gamma^+\{\psi_G(0,x^-,0_\perp),\bar{\psi}_G(0)\}|P\rangle_c = 0 \tag{2.70}$$

since the anti-commutator of the good fields is just the unit operator times a number and hence only contributes to disconnected Feynman graphs. Using Eq.(2.70) in Eq.(2.60) followed by a shift in co-ordinates establishes Eq.(2.66). Likewise for the gluon distributions the relevant hadronic commutator is zero

$$\begin{aligned}\langle P|[F^+_\nu(0,x^-,0),F^{\nu+}(0)]|P\rangle &= -\langle P|[\partial_- A^j(0,x^-,0),\partial_- A_j(0)]|P\rangle_c \\ &= 0\end{aligned}$$

again due to the connectivity requirement, thus establishing Eq.(2.67). Furthermore, we see that relations Eq(2.66,2.67) hold if we use renormalized fields in the PDF definitions as the commutation relations are only modified by multiplication by the field strength renormalization constants, which are c-numbers and hence the relevant hadronic commutation relations still vanish.

2.6.2 Sum rules

With these support and analytic properties established one can demonstrate that our choice of PDF definitions satisfy the parton sum rules. The basic observations is that integrating over all ξ produces a delta function in y^- thus bringing all operators to the same point. The first two Mellin moments then produce Noether currents.

Using the fact that the PDF's vanish for $|\xi|> 1$ we can extend the region of integration of the difference between the q and $\bar{q}$ PDF's

$$\begin{aligned}\int_0^1 \mathrm{d}\xi\ f_q(\xi) - f_{\bar{q}}(\xi) &= \int_{-1}^1 \mathrm{d}\xi\ f_q(\xi) = \int_{-\infty}^{\infty} \mathrm{d}\xi\ f_q(\xi) \\ &= \int_{-\infty}^{\infty} \mathrm{d}\xi \int \frac{\mathrm{d}y^-}{4\pi} e^{-i\xi P^+ y^-} \cdot \langle P|\bar{\psi}_q(0,y^-,0_\perp)\frac{\gamma^+}{2}\psi_q(0)|P\rangle \\ &= \frac{1}{2P^+}\langle P|\bar{\psi}_q(0)\gamma^+\psi_q(0)|P\rangle\,,\end{aligned} \tag{2.71}$$

which is the plus component (and hence the conserved component) of the electromagnetic Noether current divided by the quark charge. For example, the up and down quark fields currents for the proton in/out states non-perturbatively evaluates to

$$\frac{1}{2P^+}\langle P|\bar{\psi}_u(0)\gamma^+\psi_u(0)|P\rangle_c = 2 \quad , \quad \frac{1}{2P^+}\langle P|\bar{\psi}_d(0)\gamma^+\psi_d(0)|P\rangle_c = 1 \tag{2.72}$$

Likewise taking the second Mellin moment produces the energy momentum tensor thus giving the momentum sum rule

$$\begin{aligned}\sum_a \int_0^1 \mathrm{d}\xi\ \xi f_{a/N}(\xi) &= \frac{1}{2(P^+)^2}\langle P|\bar{\psi}_f\gamma^+ iD^+\psi_f + F^{+\nu}F_\nu{}^+|P\rangle \\ &= \frac{1}{2(P^+)^2}\langle P|T^{++}(0)|P\rangle \\ &= 1\end{aligned}$$

where at an intermediate step we represented $\xi e^{-i\xi P^+x^-} = \frac{i}{P^+}\frac{\partial}{\partial x^-}e^{-i\xi P^+x^-}$ followed by an integration by parts in x^-.

Note that these current algebra relations depend crucially on the anti-commutation relations being c-number valued, which is only the case for the good components of the fermion fields. The γ^+ matrix in the quark PDF definitions project onto these components thus validating the use of current algebra. As Noether currents are unaffected by renormalization, so too are these relations.

2.6.3 Number density interpretation

In $A^+ = 0$ lightcone gauge our PDF definitions realize the parton model property that the PDF's count the number of quarks in the target state. In lightcone quantization, the operator

$$N_\alpha(k^+, k^\perp, x^+ = 0) \coloneqq \frac{1}{2\xi(2\pi)^3} b^\dagger_\alpha(k^+, k^\perp, x^+ = 0) b_\alpha(k^+, k^\perp, x^+ = 0) \quad (2.73)$$

counts the number of "good" quarks of helicity α, situated on the lightcone $x^+ = 0$, with momentum components $k^+, k^\perp$ (we cannot measure the k^- momentum as we have precisely located the conjugate position $x^+ = 0$). Note that we take $k^+ \coloneqq \xi^+ P^+$, and thus the number operator by this definition is specific to the in/out state's momentum. This number density interpretation follows from the anti-commutation relations of the Fourier co-efficients of the quark and anti-quark fields

$$\{b_{k,\alpha}, b^\dagger_{l,\alpha'}\} = \{d_{k,\alpha}, d^\dagger_{l,\alpha'}\} = (2\pi)^3 2k^+\delta(k^+ - l^+)\delta^{(2)}(k_\perp - l_\perp)\delta_{\alpha\alpha'} \quad (2.74)$$

with the other anti-commutators all zero. The $\frac{1}{2k^+}$ in Eq.(2.73) is therefore the correct normalization as it compensates the $2k^+$ in the anti-commutation relations Eq.(B.19). We will now show that this operator co-incides with our PDF definitions when evaluated between the nucleon in/out states. In order to correctly treat the infinity associated with norm of the pure momentum states $|P\rangle$, we will need to work with wavepackets centered around a momentum value of P and with a width on the order of Δ

$$|P, \Delta\rangle \coloneqq \sum_{P'} F(P'; P, \Delta)\,|P'\rangle \quad (2.75)$$

where we normalize the wavefunction F according to

$$\sum_{P'}|F(P';P,\Delta)|^2=1; \qquad \sum_{P'}\coloneqq\int_0^\infty\frac{\mathrm{d}p'^+}{2p'^+}\int\frac{\mathrm{d}^2p'_\perp}{(2\pi)^3} \tag{2.76}$$

At the end of the calculation we will take the limit of zero width. Let us examine the momentum space number density of flavor q quarks in such a wavepacket state. Using the Fourier transform in Eq.(B.17) one finds

$$\begin{aligned}\sum_\alpha\frac{\langle P,\Delta|\,b^\dagger_{k,\alpha,q}b_{k,\alpha,q}\,|P,\Delta\rangle}{2\xi(2\pi)^3}=\sum_{P',P''}\frac{2k^+}{2\xi(2\pi)^3}F^*(P'')F(P')\\ \cdot\int\mathrm{d}w^-\mathrm{d}^2w_\perp\mathrm{d}z^-\mathrm{d}^2z_\perp e^{-i\xi P^+(w^--z^-)+ik_\perp\cdot(w_\perp-z_\perp)}\\ \cdot\langle P''|\bar\psi_q(0,w^-,w_\perp)\gamma^+\psi_q(0,z^-,z^\perp)|P'\rangle\end{aligned} \tag{2.77}$$

where we have simplified the helicity sum according to $\sum_\alpha\gamma^+u_{k,\alpha}\bar u_{k,\alpha}\gamma^+=2k^+\gamma^+$. Next we rewrite the hadron matrix element as

$$\begin{aligned}&\langle P''|\bar\psi_q(0,w^-,w_\perp)\gamma^+\psi_q(0,z^-,z^\perp)|P'\rangle\\ &\qquad=e^{iz\cdot(P''-P')}\,\langle P''|\bar\psi_q(w^--z^-,w^\perp-z^\perp,0^+)\gamma^+\psi_q(0)|P'\rangle\end{aligned} \tag{2.78}$$

Then making a change of co-ordinates

$$y\coloneqq w-z; \qquad z'\coloneqq z \tag{2.79}$$

and then integrating out the z' to produce a $\delta^3(P'-P'')$ delta function (had we used pure momentum states in place of wavepackets the delta function would have read $\delta^3(0)$), we find that

$$\begin{aligned}\sum_\alpha\frac{\langle P,\Delta|\,b^\dagger_{k,\alpha,q}b_{k,\alpha,q}\,|P,\Delta\rangle}{2\xi(2\pi)^3}=\sum_{P'}\frac{P^+}{2P'^+(2\pi)^3}|F(P')|^2\\ \cdot\int\mathrm{d}y^-\mathrm{d}^2y_\perp e^{-i\xi P^+y^-+ik_\perp\cdot y_\perp}\cdot\langle P'|\bar\psi_q(0,y^-,y_\perp)\gamma^+\psi_q(0)|P'\rangle\end{aligned} \tag{2.80}$$

We can then meaningfully take the limit of zero width. Doing this, and integrating over all transverse momenta gives

$$\begin{aligned}\int\mathrm{d}^2k_\perp\lim_{\Delta\to0}\sum_\alpha\frac{\langle P,\Delta|\,b^\dagger_{k,\alpha,q}b_{k,\alpha,q}\,|P,\Delta\rangle}{2\xi(2\pi)^3}\\ =\int\frac{\mathrm{d}y^-}{4\pi}e^{-i\xi P^+y^-}\,\langle P|\bar\psi(0,y^-,y_\perp)\gamma^+\psi(0)|P\rangle\end{aligned} \tag{2.81}$$

Thus verifying the number density interpretation of our quark PDF. Note that the bad components of the fermion do not satisfy simple anti-commutation

relations thus obscuring the construction of a corresponding number operator. Also observe that the anti-commutation relations of the renormalized fields $\psi_0 = \sqrt{Z_q(\mu_R)}\psi$

$$\{b_{k,\alpha}, b^\dagger_{l,\alpha'}\} = Z_q^{-1}\delta_{\alpha\alpha'}2k^+\delta(k^+ - l^+)\delta^2(k_\perp - l_\perp), \tag{2.82}$$

spoil the strict number density interpretation. One can carry out similar analyses for the anti-quark and gluon fields again verifying the number density interpretation in lightcone gauge.

2.6.4 Feynman rules for PDF's

In order to calculate the hard co-efficients in factorization formulae, we will need to calculate the PDF's values for *elementary targets* such as quarks and gluons. We will derive here the basic Feynman rules associated with these calculations [46]. To aid the calculation, we first split the Wilson line in two and insert a complete set of states, e.g. for the quark in a nucleon distribution we write

$$\begin{aligned} f_{q/N}(\xi) = \frac{1}{4\pi}\int \mathrm{d}y^-\ e^{-i\xi P^+ y^-} \sum_{\mathcal{X}} \\ \langle P|\bar\psi(0,y^-,0_\perp)\left[\mathcal{P}_\lambda \exp\left\{ig\int_0^\infty \mathrm{d}\lambda\ n\cdot A(y^\mu + n^\mu\lambda)\right\}\right]^\dagger|\mathcal{X}\rangle \\ \gamma^+\langle\mathcal{X}|\mathcal{P}_\lambda\left\{ig\int_0^\infty \mathrm{d}\lambda\ n\cdot A(\lambda n^\mu)\right\}\psi(0)|P\rangle \end{aligned} \tag{2.83}$$

where the vector $n^\mu = g^\mu_-$ points in the direction of the Wilson line. The usual Feynman rules require the matrix elements to be time ordered, however here we have path ordering in x^- instead. But note that all the fields featuring here are all located at the same lightcone time $x^+ = 0$ and hence are automatically time ordered if we work within lightcone quantization. If we work in "Cartesian" quantization the fields are already time ordered in Cartesian time. Thus path ordering and time ordering do not conflict in either quantization scheme and we can derive a perturbation theory for these elements from the usual Feynman rules.

The path ordering gives rise to a new propagator and vertex, as can be most easily seen by examining the second order term of the Wilson line to the right of the cut, whilst expressing the gluon fields in momentum space

$$\begin{aligned} \int_0^\infty \mathrm{d}\lambda_2 \int_0^{\lambda_2}\mathrm{d}\lambda_1 \int \frac{\mathrm{d}^d q_2}{(2\pi)^d}\int\frac{\mathrm{d}^d q_1}{(2\pi)^d} \\ \left(ig\, n\cdot\tilde A(q_2)\, e^{-i\lambda_2 q_2\cdot n}\right)\left(ig\, n\cdot\tilde A(q_1)\, e^{-i\lambda_1 q_1\cdot n}\right) \\ = \int\frac{\mathrm{d}^d q_2}{(2\pi)^d}\int\frac{\mathrm{d}^d q_1}{(2\pi)^d}\left(ig\, n\cdot\tilde A(q_2)\right)\frac{i}{n\cdot q_2 - i\epsilon}\left(ig\, n\cdot\tilde A(q_1)\right)\frac{i}{n\cdot(q_1+q_2)-i\epsilon} \end{aligned} \tag{2.84}$$

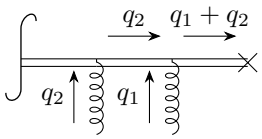

Figure 2.8: Two gluons being absorbed by the Wilson line to the right of the cut, as occuring in Eq.(2.84)

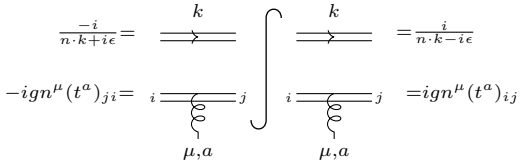

Figure 2.9: Feynman rules for quark-Wilson lines for quark colors i, j and gluon color a. The two sides of the cut are related by Hermitian conjugation. The rules are the same for gluon-Wilson lines except for that the interaction vertex acts in the 8 representation where $(T^a)_{bc} = if_{bac}$.

thus suggesting that the appropriate propagator factor is $\frac{i}{n\cdot q}$. The corresponding Feynman graph for this expression is depicted in Fig(2.84). More generally one can recognize that [46]

$$\int_0^\infty \mathrm{d}\lambda_f e^{-i\lambda_f q_f\cdot n} \ldots \int_0^{\lambda_3} \mathrm{d}\lambda_2\, e^{-i\lambda_2 q_2\cdot n} \int_0^{\lambda_2} \mathrm{d}\lambda_1\, e^{-i\lambda_1 q_1\cdot n} = \prod_{j=1}^{f} \left(\frac{i}{n\cdot(\sum_{i=1}^{j} q_i) - i\epsilon}\right) \quad (2.85)$$

thus verifying the claim that $\frac{i}{n\cdot q}$ is the appropriate propagator factor. Furthermore we recognize from Eq.(2.84) that the gluon attachment vertices's are $ign^\mu t^a_{ij}$ where a is the color of the absorbed gluon, and ij refer to the colors to the left and right of the vertex respectively. The rules for Wilson lines to the left of the cut are given by Hermitian conjugation. We summarize the rules in Fig(2.9). As the gluon parton in the $f_{g/N}$ definition is coupled to the Wilson line by the field strength tensor, the corresponding vertex is $i(k\cdot n g^j_\mu - q^j n_\mu)\delta_{\alpha\beta}$ where k, q are the momenta of the Wilson line and the outgoing gluon respectively, with β, α also respectively denoting their colors.

2.7 Renormalization and evolution equations

The factorization formalism not only makes predictions relating the cross sections of different scattering processes, but can also predict the Q^2 dependence of the structure functions[21]. That is, if one measures the structure functions at a given Q_0, then one can predict the structure functions at another Q. Experimentally the structure functions $F_{1,2}(x, Q^2)$ exhibit a logarithmic Q^2 dependence in which the structure functions shift to lower values of Bjorken-x as Q is increased–indeed the observation of this slow *scale breaking* was the impetus for investigating asymptotically free theories. In this section we will show how the factorization formalism predicts this dependence.

First, notice from Eq.(2.1) that all the PDF's are Q^2 independent and that all of the Q^2 dependence of F_2 is carried by the hard co-efficients. Thus we seek the Q^2 dependence of the hard co-efficients. Now notice that Q always enters H_2 in the ratio $\frac{Q}{\mu_R}$, hence knowing the μ_R dependence of H_2 implies knowledge of its Q dependence. As F_2 is a physical observable it is independent of the UV renormalization scale

$$\mu_R \frac{\mathrm{d}}{\mathrm{d}\mu_R} F_2(x, Q^2, \mu_R) = 0 \tag{2.86}$$

The renormalization scale enters at intermediate stages of the calculation as both the PDF's (whether it be for a real hadron or a quark PDF) and the hard co-efficients contain UV divergences. Thus these two μ_R dependences must mutually cancel one another

$$\left(\mu_R \frac{\mathrm{d}}{\mathrm{d}\mu_R} f\right) \otimes H_2 = -f \otimes \left(\mu_R \frac{\mathrm{d}}{\mathrm{d}\mu_R} H_2\right) \tag{2.87}$$

Evolution is most simply described in Mellin space, where the n^{th} Mellin transform of $g(x)$ is defined as

$$\bar{g}(N) \coloneqq \int_0^1 \mathrm{d}x \; x^{N-1} g(x) \tag{2.88}$$

This is because Mellin transforms undo convolutions of the form Eq.(2.43) into simple products, e.g.

$$\int_x^1 \mathrm{d}y \; g\left(\frac{x}{y}\right) h(y) = \bar{g}(N)\bar{h}(N+1) \tag{2.89}$$

[21] In practice this procedure is stymied by the fact that a given collider is always limited in how low a Bjorken-x region it can probe, and hence one can never measure an entire region of Bjorken-x for a given structure function. This is not an insurmountable problem for intermediate values of Bjorken-x as the structure functions evolution is largely fed by structure functions at higher values of Bjorken-x. However, once one reaches sufficiently low values of Bjorken-x a new regime known as the Color Glass Condensate emerges in which low Bjorken-x partons can feed higher Bjorken-x partons.

and to undo a Mellin transform one uses the inverse Mellin transform

$$g(x) = \frac{1}{2\pi i}\int_{c-\infty}^{c+\infty} \mathrm{d}n\, x^{-n}\bar{g}(n) \tag{2.90}$$

where one takes c such that the complex contour $\Re(n) = c$ is to the right of all singularities of $\bar{g}(n)$. The renormalization equations in Mellin space read

$$\mu_R \frac{\mathrm{d}}{\mathrm{d}\mu_R}\bar{f}_{a/H}(N,\mu_R,...) = -\gamma_{ab}(N,\alpha_s(\mu_R))\bar{f}_{b/H} \tag{2.91}$$

$$\mu_R \frac{\mathrm{d}}{\mathrm{d}\mu_R}\bar{H}_2^a(N,\mu_R,...) = H_2^b\ \gamma_{ba}(N,\alpha_s(\mu_R)) \tag{2.92}$$

where repeated parton indices are summed over. The N^{th} anomalous dimension matrix $\gamma_{ab}(N,\alpha_s\mu_R)$ is a function only of N and $\alpha_s(\mu_R)$ as these are the only two variables which $f_{a/H}$ and H_2 have in common. As H_2 is infrared safe, so must γ be.

Furthermore, one can calculate γ perturbatively using an elementary targets such as individual quarks and gluons, despite the γ in Eq.(2.91) applying to the PDF's of an actual hadron. This can be seen from Eq.(2.92) which indicates that γ is determinable from H_2, which we have already established to be itself determinable from a quark or gluon target. Therefore the same γ applies in Eq.(2.91) whether we are renormalizing an elementary particle's PDF or a real hadron's PDF. This is the so called universality of the DGLAP splitting functions [47, 48, 49].

The solution to Eq(2.91) is given by a μ ordered exponential

$$\begin{aligned}\bar{f}_{a/H}(N,\xi,\mu_F,\mu_R,\alpha_s(\mu_R)) &= \bar{f}_{b/H}(N,\xi,\mu_F,\mu_R^0,\alpha_s(\mu_R)) \\ &\times \mathcal{P}_{\mu'}\left\{\exp\left[-\frac{1}{2}\int_{\mu_R^{0\,2}}^{\mu_R^2}\frac{\mathrm{d}\mu'^2}{\mu'^2}\gamma(N,\alpha_s(\mu'))\right]\right\}_{ba}\end{aligned} \tag{2.93}$$

As the RG fixed point of QCD is at the origin of coupling space, it is an acceptable approximation to retain only the first order term of the anomalous dimension $\gamma = \frac{\alpha_s}{\pi}\gamma^{[1]} + \mathcal{O}\alpha_s^2$, where one must take the initial renormalization point to satisfy $\mu_R^0 \gg \Lambda_{QCD}$. In the vicinity of the fixed point we can use the first order running coupling of QCD

$$\alpha_s(\mu_R) = \frac{2\pi}{b_0\log(\frac{\mu_R}{\Lambda_{QCD}})} \quad ; \quad b_0 = 11 - \frac{2}{3}n_f \tag{2.94}$$

Then if we diagonalize the first order term of the anomalous dimension matrix $\gamma_{ab}^{[1]} = [S^{-1}]_{ac} D_{cd} S_{db}$, we can solve Eq.(2.93) at leading order as

$$\begin{aligned}
\bar{f}_{a/H}(N, \mu_R, ...) &\approx \bar{f}_{b/H}(N, \mu_R^0, ...)[S^{-1}]_{bc} \exp\left[-\frac{D}{2b_0} \int_{\mu_R^{0\,2}}^{\mu_R^2} \frac{\mathrm{d}\mu'^2}{\mu'^2} \frac{1}{\log\left(\frac{\mu'_R}{\Lambda}\right)} \right]_{cd} S_{da} \\
&= \bar{f}_{b/H}(N, \mu_R^0)[S^{-1}]_{bc} \exp\left[-\frac{D}{2b_0} \log\left(\frac{\log(\mu_R^2/\Lambda^2)}{\log(\mu_{R,0}^2/\Lambda^2)} \right) \right]_{cd} S_{da} \\
&= \bar{f}_{b/H}(N, \mu_R^0)[S^{-1}]_{bc} \left[\frac{\log(\mu_R^2/\Lambda^2)}{\log(\mu_{R,0}^2/\Lambda^2)} \right]_{cd}^{-\frac{D}{b_0}} S_{da}
\end{aligned}$$

We therefore see that the PDF's exhibit logarithmic dependence on the renormalization scale. In order to cancel this μ_R dependence, the hard co-efficient must therefore also exhibit logarithmic dependence on μ_R. And as the hard co-efficient depends on μ_R through the ration $\frac{Q}{\mu_R}$ we observe that the structure functions must exhibit logarithmic Q dependence

$$\bar{F}_2(N, x, Q^2) \approx \left[\frac{\log(\mu_R^2/\Lambda^2)}{\log(\mu_{R,0}^2/\Lambda^2)} \right]^{-\frac{D}{b_0}} \tag{2.95}$$

Which demonstrates the logarithmic breaking of Bjorken scaling. Had the RG fixed point not been at $\alpha_s = 0$, one would instead find that F_2 would scale rather as a power of Q.

The implication of the decreasing moments of F_2 with an increase in Q is that the PDF's and structure functions shift from larger values of x_{bj} to smaller values of x_{bj} as Q^2 is increased. If one interprets the scale $\frac{1}{Q^2}$ as the transverse area of the partons, then as one increases Q, the photon resolves the partons on a shorter distance scale, and what was once a single parton, is now viewed as two or more partons with a lower Bjorken-x value than the parent parton.

It should be noted that the anomalous dimension matrix exhibits a strong pole at $\gamma_{gg}(N) \approx \frac{1}{N-1}$. Thus the $N = 1$ moment gives rise to a rapid growth of the low Bjorken x region, which can potentially raise the logarithmic growth to a power law growth.

For numerical computation it easier to implement evolution in x_{bj}-space where the evolution equations take the form of a convolution

$$\mu_R \frac{\mathrm{d}}{\mathrm{d}\mu_R} f_{a/H}(x, Q^2, \mu_R, ...) = \int_0^1 \frac{\mathrm{d}\xi}{\xi} P_{ab}(\frac{x}{\xi}, \alpha_s(\mu_R)) f_{b/H}(\xi, \mu_R) \tag{2.96}$$

where the DGLAP splitting function $P_{ab}(x)$ is related to the N^{th} anomalous dimension matrix via

$$\int_0^1 \mathrm{d}x \; x^{N-1} P_{ab}(x) = -\gamma_{ab}(N) \tag{2.97}$$

We should note that due to the presence of the three mass scales Q, μ_F, μ_R one can avoid potentially large logarithmic ratios of these quantities appearing in a perturbative expansion by setting $\mu_F = \mu_R = Q$. This choice has the effect of shifting all of the Q dependence of F_2 to the PDF's.

2.8 Summary

Let us first offer some partial answers to the questions posed at the beginning of this chapter:

- Why does scattering occur upon a single parton? : This is not actually the case for a theory involving vector fields or any higher rank tensor fields. For those theories, the component of the field which receives the largest enhancement under a boost, will scatter many times with the incoming photon. However, for gauge theories the extra "symmetry" allows one to absorb all of the effects of longitudinal gluon exchanges into one object, a Wilson line. Once this has been done, the hard scattering diagram exhibits a Q power suppression for each extra parton line entering it, thus suppression multiple parton scattering.

- Massless partons? : The PDF's themselves are actually highly sensitive to the non-zero mass of the quarks, as the quark mass sets the distance of closest approach to the PSS's associated with collinear radiation. The question is therefore why the mass in the hard scattering co-efficient is zero? For each PSS of each Feynman diagram which contributes to the leading power of DIS, one classifies all the internal lines as to whether they have virtuality of the order Q^2 or below. The highly virtual lines are then associated with the hard co-efficient, in which case a Taylor expansion in $\frac{m}{Q}$ allows one to neglect the quark masses. By our construction of the hard co-efficient in Sect(2.5), any potentially mass-sensitive contributions to a leading DIS graph are by definition subtracted out of the hard co-efficient. One can however retain the quark masses as described in Chapter 9 of [24].

- On-shell partons? : The leading contributions in a Feynman graph contributing to DIS scattering come from regions in momentum space where two or more propagators approach their mass shell (PSS's). Thus the partons entering the hard subdiagram are approximately on-shell.

- Collinear partons?: At high energies, the only two ways the Landau conditions can be met is either if the two or more on-shell propagators are collinear particles, or if the particle's momenta is soft. In terms of classical scattering diagrams, two lightlike particles can only interact if they are collinear.

- Collinear fraction $0 < \xi < 1$?: In terms of classical scattering diagrams, if a parton carried a momentum fraction outside of these bounds then one of the particles would be traveling backwards in time and hence would not be able to recombine at a later stage as would be necessary for a forward

scattering process. In terms of loop momenta of a Feynman diagram, if a particle has negative energy in a forward scattering diagram, then one of the integration contours will have all of its poles on only one side of its real axis and hence the contour can be closed in the opposite plane to give zero.

- Irrelevance of subsequent evolution?: By unitarity the total DIS cross section is governed by the forward scattering graph of $\gamma^* H \to \gamma^* H$. The only pinched reduced graphs for this process contain a single jet and hard vertex. This indicates that the process of multiple jet production must have no effect on the hard scattering vertex. The physical explanation is that the hard scattering is well localized in spacetime, and hence does not interfere with the subsequent evolution.

In this chapter we also studied some of the properties of the parton distribution functions when defined in terms of hadronic matrix elements of Wilson line operators. We found that the intuitive number density interpretation of the PDF's is approximately realized in lightcone quantization when working in lightcone gauge. However, after renormalizing the fields, we found that the field strength renormalization factors spoiled this interpretation. Furthermore, we indicated how this definition of the PDF's leads to a general iterative procedure for perturbatively calculating the hard scattering co-efficients.

We also derived the evolution equations for the parton distribution functions. Of particular significance was the observation that the DGLAP splitting kernels of a real hadron are the same as those for an elementary quark or gluon. This gives QCD great predictive power as this feature allows one to perturbatively calculate the splitting kernels.

The analysis of this chapter has indicated that it is the infrared singularity structure of quantum field theories in general that leads to the factorization form of scattering amplitudes in certain kinematic regimes. In summary, the factorization formalism provides a powerful framework for making predictions for collider phenomenology.

3 The Cusp Anomalous Dimension

The cusp anomalous dimension [50, 51, 52] is a ubiquitous quantity featuring in gauge theories. It is most simply defined as the anomalous dimension of a Wilson line operator which has a sharp contour. The sharp contour induces UV divergences [50, 53, 54, 55] which are not present for Wilson lines with a smooth contour. As such, the cusp anomalous dimension describes the UV dependence of any amplitude where a Wilson line with sharp kinks features. The UV behavior of the Wilson line can be quantified by the Minkowskian cusp angle $\cosh\theta_{12} = v_1 \cdot v_2$, where v_1^μ, v_2^μ are the unit tangent vectors of the path at the cusped point.

The simplest physical situation where it arises is the scattering of a heavy quark off of an external potential [56, 57, 58]. In the $m_Q \to \infty$ limit, the heavy quark behaves like a classical charged particle which has an incoming classical trajectory with velocity vector $v_1^\mu = \frac{p^\mu}{m_Q}$, which then scatters into a final state with velocity v_2. The instantaneous change in velocity causes the quark to radiate gluons, causing both IR and UV divergences. The anomalous cusp dimension describes the UV behavior of this amplitude through the cusp angle formed by the two velocity vectors. This heavy quark scattering amplitude features in many important physical quantities such as top quark production [59] rates and heavy meson form factors [60].

The cusp anomalous dimension $\Gamma_C(\alpha_s)$ also governs the leading large-x behavior of the DGLAP splitting functions $P_{ii}(x)$ for parton→parton evolution[61, 52]

$$P_{ii}(x) \to \frac{\Gamma_C(\alpha_s)}{2(1-x)_+} + B(\alpha_s)\delta(1-x) + ... \quad \text{for} \quad x \to 1 \tag{3.1}$$

Furthermore, as the anomalous dimensions of the spin-j twist two operators are the j^{th} Mellin moment of the splitting functions $\gamma_2(j) = -\int_0^1 \mathrm{d}x\; x^{j-1} P(x)$, we also see that the cusp anomalous dimension also governs the dominant behavior of the high spin twist two operators[22]

$$\gamma_2(j) = \frac{1}{2}\Gamma_C(\alpha_s)\ln(j) + \mathcal{O}(j^0) \tag{3.2}$$

In this chapter we will describe the cusp anomalous dimension in the context of large-x DIS scattering. In Sect(3.1) we will first indicate why in the large-x region of phase space the factorization formulas derived in the previous chapter require modification. By analyzing the kinematics of this regime we will motivate a new definition of the PDF's, which will now contain Wilson lines with a cusped contour. In Sect(3.2) will then analyze the IR and UV properties of such Wilson lines by calculating their one-loop expectation value. In Sect(3.3)

[22] Here we used that the n^{th} Mellin moment of $[\frac{1}{1-x}]_+$ is $\int_0^1 \mathrm{d}x\; x^{N-1}[\frac{1}{1-x}]_+ = -\log N + \mathcal{O}(\frac{1}{N})$

we will describe the renormalization group properties of Wilson lines in general, which will lead to the definition of the anomalous cusp dimension. We will then study the unique renormalization features of *lightlike* cusped Wilson lines. We will demonstrate that unlike timelike Wilson lines, lightlike Wilson are not multiplicatively renormalizable. We will then demonstrate that we can still derive an RG equation for such Wilson lines, and in so doing we will explain why the PDF's evolution equations are not multiplicative, but convolutional. In Sect(3.4) we will derive the leading order splitting functions for PDF evolution Eq.(3.1).

This chapter is a review of the papers [61, 52, 51, 62]. We have also benefited greatly by reading the master's thesis [63].

3.1 The soft approximation for $x \to 1$

At the phase space boundary $x \to 1$, many of our approximations used in deriving the factorization formula for DIS break down due to a change in kinematics. One example of this is that in the large x region the target remnants are soft as opposed to collinear, due to the parton carrying away most of the hadrons momentum. A clear symptom of this is the appearance of large logarithms of the form $\log(1-x)$ entering the splitting functions in the RG equation for the PDF's [64, 65, 66, 67]. For example, examine Eq(2.50). One of the goals of this chapter is to resum this set of large logarithms. In Sect(3.3) we will demonstrate how to do so.

To understand the kinematics of this region, let us return to our definition of the PDF's at Eq.(2.83)

$$\begin{aligned} f_{q/N}(\xi) = \frac{1}{4\pi}\int_{-\infty}^{\infty} \mathrm{d}y^- \; e^{-ixP^+y^-} \sum_{\mathcal{X}} \\ \langle P|\bar{\psi}(0,y^-,0_\perp)\left[\mathcal{P}_\lambda \exp\left\{ig\int_0^\infty \mathrm{d}\lambda \; v\cdot A(y^\mu + v^\mu\lambda)\right\}\right]^\dagger |\mathcal{X}\rangle \\ \gamma^+ \langle \mathcal{X}|\mathcal{P}_\lambda\left\{ig\int_0^\infty \mathrm{d}\lambda \; v\cdot A(\lambda v^\mu)\right\}\psi(0)|P\rangle \end{aligned} \tag{3.3}$$

If we perform the y^- integral, we see that the parton emits a total amount of $(1-x)P^+$ momentum into the final state $|\mathcal{X}\rangle$. Thus in the large x region the ratio of the momentum of emitted radiation by the parton, to the partons momentum becomes vanishingly small. This then suggests that we can approximate the real gluon emission process by eikonal vertices, in which case the parton is replaced by a Wilson line. Following [61] we will factorize the large Bjorken-x parton-

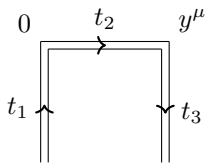

Figure 3.1: The integration contour of $W(C)$. The incoming lines are in the direction of the target hadron, whereas the t_2 contour is on the lightcone opposite to the direction of the hadron. The contour exhibits sharp cusps at time $t = 0$ and $t = 1$ which reflect the hard interaction of the parton with a photon in DIS.

parton PDF as[23]

$$F(x, \mu_R) = H\left(\frac{\mu_R}{M}\right) \int_{-\infty}^{\infty} \frac{\mathrm{d}y^-}{2\pi} P_+ \; e^{iP_+ y_- (1-x)} \; W(C_s), \tag{3.4}$$

where the Wilson line $W(C_s)$

$$W(C_s) \coloneqq \langle \Omega | \mathcal{P} \exp\left(ig \int_{C_s} \mathrm{d}\gamma^\mu A_\mu(\gamma) \right) | \Omega \rangle \tag{3.5}$$

now has a contour γ^μ, depicted in Fig(3.1), which is composed of three segments

$$\gamma^\mu(t) = \begin{cases} n^\mu t_1 & -\infty < t_1 < 0 \\ y^\mu t_2 & 0 < t_2 < 1 \\ y^\mu - (t_3 - 1) n^\mu & 1 < t_3 < \infty \end{cases} \tag{3.6}$$

where the unit tangent vector n^μ is collinear to the incoming hadron, and the lightlike vector y^μ is along the lightcone opposite to the direction of the incoming hadron

$$y^\mu = (0, y^-, 0_\perp) \quad ; \quad y^2 = 0 \quad ; \quad n^\mu = \frac{P^\mu}{M} \quad ; \quad n^2 = 1 \tag{3.7}$$

Eq.(3.4) has segmented the two regions of momentum space: the Wilson line focuses on the soft-collinear gluon radiation process and the function $H(\frac{\mu}{M})$ then accounts for hard virtual gluon loops as well as the details of the incoming hadron. The contour of $W(C_s)$ exhibits two cusps, which represent the hard scattering process of the photon-parton interaction. These two cusps give rise to UV divergences in the Wilson line which are not present for smooth contours[50, 55, 54, 53]. The rest of this chapter will be the study of the UV and IR structure of cusped Wilson lines, and their implications for large-x PDF evolution .

[23] A more rigorous demonstration [52] of the factorization Eq.(3.4) would again require application of Ward identities to disentangle gluon exchanges between soft, collinear and hard subgraphs.

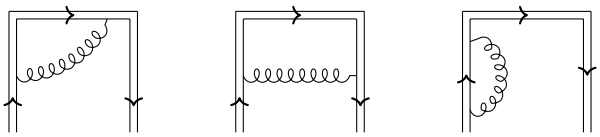

Figure 3.2: First order contributions to $W(C)$. The symmetric diagrams of $W_a^{(1)}$ and $W_b^{(1)}$ are also to be included.

3.2 One loop calculation

To study the IR and UV properties of $W(C_s)$ we will calculate the set of one loop diagrams shown in Fig(3.2), as will as their symmetric contributions. We can omit the self energy diagram along the γ_2 contour as the KLN theorem [42, 43] informs us that the IR singularities associated with final state radiation will cancel amongst one another.

We will parameterize both the UV and IR divergences using dimensional continuation. When we encounter a UV divergent integral, we will evaluate the integral in $D = 4 - \epsilon_{\rm UV} < 4$ dimensions and when we encounter an IR divergence we will evaluate the integral in $D = 4 + \epsilon_{\rm IR} > 4$ dimensions. The reader should pay careful attention as to the nature of each divergence, as renormalization counterterms only apply to the UV singularities.

We will perform the calculation in position space and in Feynman gauge. The position space representation of the D-dimensional gluon propagator is given at Eq.(D.2) as well as the cut propagator at Eq.(D.4).

$W_a^{(1)}$ Cusp Calculation

To evaluate $W_a^{(1)}$ we should sum the two cases where the gluon propagator does, and does not pass through the final state cut. Just as in our example Eq.(3.3) for the PDF definitions, we decompose the γ_2 path into two lines: the first line traverses $z_2 = y^\mu t_2$ for $0 < t_2 < \infty$, we then place the final state cut at this endpoint, and then the second segment of γ_2 is back along the line $z_2 = y^\mu t_2$ for $1 < t < \infty$. Any gluons which attach from γ_1 to the first segment of γ_2 do not pass through the final state cut and hence are virtual, whereas those that attach from γ_1 to the second segment of γ_2 are real. This situation is depicted in Fig(3.3). The two contributions then sum to

$$W_a^{(1)} = -(ig)^2 C_F \; n\cdot y \int_{-\infty}^{0} {\rm d}t_1 \bigg(\int_0^\infty {\rm d}t_2 \; D(z_2 - z_1) + \int_\infty^1 {\rm d}t_2 \; D_+(z_2 - z_1) \bigg) \tag{3.8}$$

We can simplify the calculation considerably by noting that when the separation distance $(z_2 - z_1)^\mu$ is timelike the virtual and cut gluon propagators coincide. By

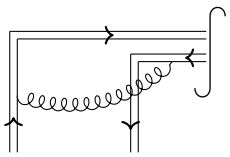

Figure 3.3: Decomposing the γ_2 path into two separate paths: the first segment consists of $z^\mu = y^\mu t_2$ for $0 < t_2 < \infty$, and the second segment traverse back along $z^\mu = y^\mu t_2$ for $1 < t_2 < \infty$. A final state cut is placed at the point at infinity between these two paths, and as such any gluon attaching from γ_1 to the second segment of γ_2 necessarily passes through the final state cut and hence is put on-shell.

noticing that $(z_2 - z_1)^2 = t_1^2 - 2n^+ y^- t_1 t_2$ and $(z_2 - z_1)^0 = \sqrt{2}(y^- t_2 - (n^+ + n^-)t_1)$ are both positive when $y^- > 0$, we can use the virtual gluon propagator for both terms in Eq.(3.8) in the case that $y^- > 0$. The sum of the two terms then simplifies to

$$W_a^{(1)} = -(ig)^2 C_F n \cdot y \int_{-\infty}^{0} \mathrm{d}t_1 \int_0^1 \mathrm{d}t_2 \; D(z_2 - z_1) \tag{3.9}$$

In the case that $y^- < 0$ we can deform the t_1 contour using the following argument: as the poles of the cut propagator both lie in the lower half of the complex t_1 plane we can manipulate the contour as follows

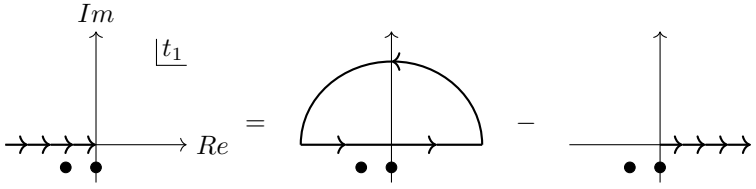

(3.10)

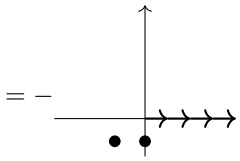

(3.11)

Where in Eq.(3.10) we used that the cut propagator vanishes sufficient fast at $t_1 \to \infty$ for the upper half circle to give a zero contribution to the integral, and in Eq(3.11) we have used that the large semi-circle does not encircle any poles, therefore giving a vanishing integral. From this we can conclude that in the case $y^- < 0$ we can deform the t_1 contour such that it runs from $0 < t_1 < \infty$, with the orientation of the integral bounds being that the path ends at $t_1 = 0$. We then have that the vector $(z_1 - z_2)^\mu$ is again timelike, in which case we can use the virtual propagator for both segments of γ_2. Thus, in both cases we use

the virtual propagator throughout and find

$$W_a^{(1)} = (ig)^2 \mu^{4-D} n_\mu y_\nu \int_0^1 \mathrm{d}t_2 \int_{-\infty}^0 \mathrm{d}t_1 \; D^{\mu\nu}(t_2 y^\alpha - t_1 n^\alpha)$$
$$= \frac{g^2 C_F n \cdot y}{4\pi^{D/2}} \Gamma(D/2-1) \int_0^1 \mathrm{d}t_2 \int_{-\infty}^0 \mathrm{d}t_1 (-t_1^2 + 2t_1 t_2 n \cdot y + i\epsilon)^{1-D/2}$$

where we have modified the coupling at each interaction vertex to include a factor $\mu^{\frac{4-D}{2}}$ in order for the coupling g to remain dimensionless in dimensional continuation. To bring the integral into the form of a representation of the beta function, we make the change of variables $t_1' \coloneqq -\frac{t_1}{(2n\cdot y)t_2}$

$$W_a^{(1)} = \frac{g^2 C_F}{8\pi^{D/2}} \Gamma(D/2-1)(2in\cdot y - i\epsilon)^{4-D}$$
$$\times \int_0^1 \mathrm{d}t_2 \; t_2^{3-D} \cdot \int_0^\infty \mathrm{d}t_1' \; (t_1'(t_1'+1))^{1-D/2} \tag{3.12}$$

We can now evaluate both of the integrals if we work in $D < 4$,

$$\int_0^1 \mathrm{d}t_2 \; t_2^{3-D} = \frac{1}{4 - D_{\mathrm{UV}}}, \qquad D_{\mathrm{UV}} < 4 \tag{3.13}$$

and

$$\int_0^\infty \mathrm{d}t_1' \; (t_1'(t_1'+1))^{1-D/2} = \frac{\Gamma(D-3)\Gamma(2-D_{\mathrm{UV}}/2)}{\Gamma(D/2-1)}$$
$$= \frac{2}{4-D_{\mathrm{UV}}} \cdot \frac{\Gamma(D-3)\Gamma(3-D/2)}{\Gamma(D/2-1)}, \tag{3.14}$$

where in the first and second equality in Eq.(3.14) we used Eq.(D.6) and Eq.(D.9) respectively. Putting it all together one obtains

$$W_a^{(1)} = -\frac{g^2}{4\pi^{D/2}} C_F (2i\mu n\cdot y - i\epsilon)^{4-D} \frac{\Gamma(3-D/2)\Gamma(D-3)}{(4-D_{\mathrm{UV}})^2} \tag{3.15}$$

Let us determine the cause of the double pole arising in Eq.(3.15). The pole in Eq(3.13) arises due to $t_2 \to 0$ in which case the gluon is collinear to the incoming quark. The pole in Eq.(3.14) arises due to the region $t_1' \to 0$ which corresponds to $t_1 \to 0$ in which case the gluon is collinear to the γ_2 path hence forming a lightlike collinear singularity. At the cusp point these two singularities overlap, forming the double pole. We will therefore refer to this singularity as the "cusp singularity". Both these integrals required evaluation in $D < 4$ and hence these singularities are UV in origin.

$W_b^{(1)}$ gluon exchange calculation

In diagram $W_b^{(1)}$, the exchanged gluon necessarily passes through the final state cut. We therefore use the cut propagator Eq.(D.4). Remembering to complex conjugate the gluon vertices one obtains

$$\begin{aligned} W_b^{(1)} &= (ig)(-ig)\mu^{4-D}(-n\cdot n)C_F\int_{-\infty}^{0}\mathrm{d}t_1\int_1^{\infty}\mathrm{d}t_3\ D_+\Big(y^\alpha+n^\alpha(1-t_3)-n^\alpha t_1\Big)\\ &= (-1)^{D/2}\frac{g^2C_F}{4\pi^{D/2}}\mu^{4-D}\Gamma(D/2-1)2^{1-D/2}\\ &\times\int_{-\infty}^{0}\mathrm{d}t_1\int_0^{\infty}\mathrm{d}t_3\ [(y^- - n^-(t_1+t_3)-i\epsilon)(-n^+(t_1+t_3)-i\epsilon)]^{1-D/2}, \end{aligned} \tag{3.16}$$

where at the second equality we performed a shift variables $t_3 \to t_3 - 1$. To evaluate the two integrals, we first perform a change of co-ordinates $t_3 \to t^+ = t_1 + t_3$. The relevant integral then becomes

$$\begin{aligned} &\int_{-\infty}^{0}\mathrm{d}t_1\int_0^{\infty}\mathrm{d}t_3\ [(y^- - n^-(t_1+t_3)-i\epsilon)(-n^+(t_1+t_3)-i\epsilon)]^{1-D/2}\\ &=\int_{-\infty}^{0}\mathrm{d}t_1\int_{t_1}^{\infty}\mathrm{d}t^+\ [t^+]^{1-D/2}[\frac{1}{2}t^+-(n\cdot y-i\epsilon)]^{1-D/2} \end{aligned} \tag{3.17}$$

where we used that $n^+n^- = \frac{1}{2}$. In order to maintain the correct $i\epsilon$ prescription, we noted from Eq.(3.16) that the two poles of t^+ both lie in the lower half of the complex plane. In order to decouple the two integrals in Eq(3.17) we rescale the t^+ co-ordinate as $t^+ \to w = \frac{t_+}{t_1}$

$$\begin{aligned} &\int_{-\infty}^{0}\mathrm{d}t_1\int_{t_1}^{\infty}\mathrm{d}t^+\ [t^+]^{1-D/2}[\ \frac{t^+}{2}-(n\cdot y-i\epsilon)]^{1-D/2}\\ &=\int_{-\infty}^{0}\mathrm{d}t_1\int_1^{-\infty}\mathrm{d}w\ t_1^{2-D/2}w^{1-D/2}[\ \frac{t_1w}{2}-(n\cdot y-i\epsilon)]^{1-D/2} \end{aligned} \tag{3.18}$$

In order to bring the t_1 integral into the form of an integral representation of the beta function we change the t_1 coordinate to $t_1 \to \alpha = -\frac{t_1 w}{2n\cdot y}$

$$\begin{aligned} &\int_{-\infty}^{0}\mathrm{d}t_1\int_1^{-\infty}\mathrm{d}w\ t_1^{2-D/2}w^{1-D/2}[\frac{t_1w}{2}-(n\cdot y-i\epsilon)]^{1-D/2}\\ &\qquad=4\cdot[-n\cdot y]^{4-D}\Big(\int_0^1\frac{\mathrm{d}w}{w^2}\int_0^{\infty}\mathrm{d}\alpha\ \alpha^{2-D/2}(1+\alpha)^{1-D/2}\\ &\qquad\qquad+\int_0^{-\infty}\frac{\mathrm{d}w}{w^2}\int_{-\infty}^{0}\mathrm{d}\alpha\ \alpha^{2-D/2}(1+\alpha)^{1-D/2}\Big) \end{aligned} \tag{3.19}$$

We can evaluate the α integrals, if we work in $D > 4$

$$Eq.(3.19) = 4\cdot[-n\cdot y]^{4-D}\frac{\Gamma(3-D/2)\Gamma(D_{\rm IR}-4)}{\Gamma(D/2-1)}\Big(\int_0^1\frac{\mathrm{d}w}{w^2}-\int_0^{-\infty}\frac{\mathrm{d}w}{w^2}\Big) \tag{3.20}$$

The singularities which arose in the α integrals arise from the region $\alpha = \infty$, which corresponds to $t^+ \to \infty$, which is the case when the emission and absorption sites are infinitely separated. Thus, this is a infrared singularity (which could also be deduced from the integral being finite in $D > 4$). To evaluate the w integrals we put a lower bound ϵ on the two integrals and observe that the two infinities cancel one another

$$\lim_{\epsilon \to 0} \int_\epsilon^1 \frac{\mathrm{d}w}{w^2} - \int_\epsilon^{-\infty} \frac{\mathrm{d}w}{w^2} = \lim_{\epsilon \to 0}(-1 + \frac{1}{\epsilon} - \frac{1}{\epsilon}) \tag{3.21}$$

$$= -1 \tag{3.22}$$

We therefore have that

$$Eq.(3.19) = -4 \cdot [-n \cdot y]^{4-D} \frac{\Gamma(3 - D/2)\Gamma(D_{\text{IR}} - 4)}{\Gamma(D/2 - 1)} \tag{3.23}$$

Putting it all together we find

$$W_b^{(1)} = \frac{g^2}{4\pi^{D/2}} C_F [i\mu(n \cdot y - i\epsilon)]^{4-D} \frac{\Gamma(3 - D/2)\Gamma(D - 3)}{4 - D_{\text{IR}}} \times 2^{3-D/2} \tag{3.24}$$

We note that our answer differs from the result in [61] by a factor of $2^{1-D/2}$. Furthermore, the cancellation of IR divergences described in the following section only occurs if one uses our result.

$W_c^{(1)}$ self energy calculation

Denoting the emission and absorption times of $W_c^{(1)}$ respectively as t_e and t_a we have that

$$W_c^{(1)} = \frac{g^2\mu^{4-D}C_F}{4\pi^{D/2}}\Gamma(D/2-1)\int_{-\infty}^{0}\mathrm{d}t_e\int_{t_e}^{0}\mathrm{d}t_a\ [-(t_e-t_a)^2+i\epsilon]^{1-D/2} \quad (3.25)$$

Changing to the natural set of co-ordinates $t_a \to t^- = t_e - t_a$, the relevant integral becomes

$$\int_{-\infty}^{0}\mathrm{d}t_e\int_{t_e}^{0}\mathrm{d}t_a\ [-(t_e-t_a)^2+i\epsilon]^{1-D/2} = (-1)^{-D/2}\int_{-\infty}^{0}\mathrm{d}t_e\int_{0}^{t_e}\mathrm{d}t^-\ (t_-)^{2-D} \quad (3.26)$$

The region $t^- \to 0$ is highly singular. As this region corresponds to vanishing separation between the absorption and emission sites we recognize this to be a UV singularity. To decouple the two integrals we make the change of variables $t^- \to \alpha \coloneqq \frac{t^-}{t_e}$

$$\int_{-\infty}^{0}\mathrm{d}t_e\int_{0}^{t_e}\mathrm{d}t^-\ (t_-)^{2-D} = \int_{-\infty}^{0}\mathrm{d}t_e\ (t_e)^{3-D}\int_{0}^{1}\mathrm{d}\alpha\ \alpha^{2-D} \quad (3.27)$$

$$= \frac{\Gamma(3-D)}{\Gamma(4-D)}\int_{-\infty}^{0}\mathrm{d}t_e\ (t_e)^{3-D} \quad (3.28)$$

In the second line we used Eq.(D.5) to perform the α integral. The remaining integral is logarithmic and hence receives singular contributions both for the IR region $t_e \to \infty$, and the UV region $t_e \to 0$ where the emission and absorption sites overlap. To clearly separate out these two contributions we partition the integral as

$$\int_{-\infty}^{0}\mathrm{d}t_e\ (t_e)^{3-D} = (-1)^{1-D}\int_{0}^{\infty}\mathrm{d}t_e\ (t_e)^{4-D}\left\{\frac{1}{t_e+1}+\frac{1}{t_e(t_e+1)}\right\} \quad (3.29)$$

$$= (-1)^{1-D}\Big\{\Gamma(5-D)\Gamma(D_{\text{IR}}-4)+\Gamma(4-D_{\text{UV}})\Gamma(D-3)\Big\} \quad (3.30)$$

The first term diverges in the IR region and is finite in the UV, whereas the second term has the opposite singularity structure. Combining Eq.(3.28) and Eq.(3.30) we find

$$\begin{aligned}&\int_{-\infty}^{0}\mathrm{d}t_e\int_{0}^{t_e}\mathrm{d}t^-\ (t_-)^{2-D}\\ &= (-1)^{1-D}\frac{\Gamma(3-D)}{\Gamma(4-D)}\Big\{\Gamma(5-D)\Gamma(D_{\text{IR}}-4)+\Gamma(4-D_{\text{UV}})\Gamma(D-3)\Big\}\\ &= (-1)^{1-D}\Big\{\Gamma(3-D_{\text{UV}})-\Gamma(3-D_{\text{IR}})\Big\}\Gamma(D-3) \quad (3.31)\end{aligned}$$

This indicates that prior to UV renormalization, the self energy graph is formally zero, due to the IR and UV divergences precisely canceling one another. However, after we have renormalized the contribution and subtracted out the UV divergence, one is left with the IR divergence. This is the same cancellations discussed below Eq.(2.50), now carried out in position space. Combing Eq(3.31) with Eq.(3.25) our result for $W_c^{(1)}$ is

$$\begin{aligned} W_c^{(1)} &= \frac{-g^2(i\mu)^{4-D}C_F}{4\pi^{D/2}}\Gamma(D/2-1)\Gamma(D-3) \\ &\times\left\{\Gamma(3-D_{\rm UV})-\Gamma(3-D_{\rm IR})\right\} \end{aligned} \tag{3.32}$$

Cancellation of IR divergences

The first term in Eq.(3.32) is IR divergent, and we will label it $W_c^{(1,{\rm IR})}$. This divergence cancels against the IR divergence in $W_b^{(1)}$. In order to demonstrate the cancellation we expand all terms in powers of $\frac{1}{\epsilon_{\rm IR}}$, taking $D=4+\epsilon_{\rm IR}$. To expand the gamma functions we use Eq.(D.11) and to expand all powers we use Eq(D.12). This yields

$$2W_c^{(1,{\rm IR})} = \frac{g^2C_F}{4\pi^2}\frac{2}{\epsilon_{\rm IR}}+\mathcal{O}(1)+\mathcal{O}(\epsilon) \tag{3.33}$$

$$W_b^{(1)} = -\frac{g^2C_F}{4\pi^2}\frac{2}{\epsilon_{\rm IR}}+\mathcal{O}(1)+\mathcal{O}(\epsilon) \tag{3.34}$$

Thus demonstrating that the IR divergences between these two graphs do cancel. Note that the IR singular terms in $2W_c^1+W_b^{(1)}$ cancel, but the order one terms do not.

First order result

Summing all three contributions, as well as the relevant symmetric contributions one obtains

$$\begin{aligned} W^{(1)} &= 2W_a^{(1)}+W_{(b)}+2W_c^{(1)} \\ &= \frac{g^2C_F}{4\pi^{D/2}}(i\mu^{4-D})\Big\{2(2n\cdot y-i\epsilon)^{4-D}\frac{\Gamma(3-D/2)\Gamma(D-3)}{(4-D_{\rm UV})^2} \\ &- 2\,\Gamma(D/2-1)\Gamma(D-3)\Big(\Gamma(3-D_{\rm UV})-\Gamma(3-D_{\rm IR})\Big) \\ &+ 2^{3-D/2}(n\cdot y-i\epsilon)^{4-D}\frac{\Gamma(3-D/2)\Gamma(D-3)}{4-D_{\rm IR}}\Big\} \end{aligned} \tag{3.35}$$

$\overline{MS}$ Renormalization

Next we subtract out the UV poles in the $\overline{MS}$ renormalization. We will apply the scheme to the $W_a^{(1)}$ term first. Working now in $D = 4 - 2\epsilon$ we have that

$$2W_a^{(1)} = -\frac{\alpha_s C_F}{\pi}\pi^\epsilon (2i\rho)^{2\epsilon}\frac{\Gamma(1+\epsilon)\Gamma(1-2\epsilon)}{2\epsilon^2}, \tag{3.36}$$

where we have defined the dimensionless variable $\rho \coloneqq \mu n \cdot y$. We now expand all small exponents x^ϵ using Eq.(D.12), and all $\Gamma(1+\epsilon)$ gamma functions using Eq.(D.10) to obtain

$$2W_a^{(1)} = -\frac{\alpha_s C_F}{\pi}\exp\left(\epsilon\log(-4\pi\rho^2 e^{\gamma_E}) + \frac{5}{12}\epsilon^2\pi^2\right)\frac{1}{2\epsilon^2} \tag{3.37}$$

$$= -\frac{\alpha_s C_F}{\pi}\left(\frac{1}{2\epsilon^2} + \frac{1}{2\epsilon}\log(-4\pi\rho^2 e^{\gamma_E}) + \frac{1}{4}\log^2(-4\pi e^{\gamma_E}\rho^2) + \frac{5\pi^2}{24} + \mathcal{O}\epsilon\right) \tag{3.38}$$

We now use renormalization counterterms to subtract out the $\frac{1}{\epsilon^2}$ and $\frac{1}{\epsilon}$ pole terms, and in the $\overline{MS}$ scheme we subtract out all terms of the form $\log(-n\pi)$, thus yielding the renormalized result

$$2W_a^{Ren,(1)} = -\frac{\alpha_s C_F}{\pi}\left(\log^2\rho + \frac{5}{24}\pi^2\right) \tag{3.39}$$

Proceeding in analogous fashion for the remaining UV divergence in $W_c^{(1)}$ we obtain our final renormalized result for $W^{(1)}$

$$\boxed{W_{Ren}^{(1)} = \frac{\alpha_s}{\pi}\left(-L^2 + L - \frac{5}{24}\pi^2\right), \qquad L \coloneqq \log(i(\rho - i\epsilon)) + \gamma_E} \tag{3.40}$$

We recall that the double logarithm arose due to the $\frac{1}{\epsilon^2}$ "cusp singularity". It is this term which leads to many of the interesting RG properties of $W(C_s)$. It is also the origin of the plus distribution associated with the large x splitting functions. Note that these as $\rho = \frac{\mu P^+ n^-}{M}$ the $log(\rho)$ terms are large for high energy hadron scattering, and hence need to be resummed.

3.3 Renormalization of lightlike Wilson lines

The renormalization properties of non-lightlike Wilson lines containing a finite number of self-intersection points and cusps have been thoughly studied, e.g.[50, 53, 54, 55]. One of the primary results is that such Wilson lines are multiplicatively renormalizable to all orders in perturbation theory

$$W_{Ren}(g_R, \mu_R, \gamma) = \prod_n Z(\{\,\theta_n\,\}, g_R, \mu_R) W_{bare}(g, \gamma) \tag{3.41}$$

where θ_n denotes the Minkowski angle at the n^{th} cusp point

$$\cosh\theta_n \coloneqq \frac{v_1 \cdot v_2}{\sqrt{v_1^2 v_2^2}} \tag{3.42}$$

where v_1, v_2 denote the tangent vectors at a cusp point. The Z factor contains the counterterms which render the renormalized Wilson line finite, i.e. $Z = (1 + \delta_W)$. A particularly important observation is that Z is only a function of the set of cusped angles, the running coupling, and the renormalization scale. By exploiting the renormalization scale μ_R-independence of the bare Wilson line, one can derive a Callan-Symanzik equation for the renormalized Wilson line

$$\left(\mu\frac{\partial}{\partial\mu} + \beta(g)\frac{\partial}{\partial g}\right)\ln W = -\sum_n \Gamma_{cusp}(\theta_n, g) \tag{3.43}$$

$$\Gamma_{cusp}(\theta_n, g_R) \coloneqq \mu\frac{\mathrm{d}}{\mathrm{d}\mu} Z_n(\theta_n, g_R, \mu_R) \tag{3.44}$$

These equations define the cusp anomalous dimension, and indicate the clear analogy to the anomalous dimension of local operators. As the Mellin moments of the Fourier transform of the Wilson line is related to the local twist two operators, we see that the cusp anomalous dimension encodes the anomalous dimensions of all these twist two operators into a single object. Eq.(3.43) can be used to resum a subset of large logarithms $\log\theta$ occurring in perturbation theory.

However, for lightlike Wilson lines, the Minkowski angle Eq.(3.42) is ill-defined, and therefore so is Γ_{cusp}. Furthermore, in [61], by calculating the two loop order value of $W(C_s)$ it was explicitly demonstrated that the result was inconsistent with the multiplicative renormalizabilty assumption.

In [62] a method was proposed for deriving the renormalization equation for lightlike Wilson lines. We will describe their technique by applying it to our $W(C_s)$ example where the relevant Minkowski angles are

$$\cosh\theta_\pm = \pm\frac{n \cdot y}{\sqrt{y^2}} \tag{3.45}$$

where θ_+ and θ_- refer to the cusps respectively to the left and right of the final state cut. In order to allow for negative values of $n \cdot y$ and y^2 one must

first define the analytic continuation of Eq.(3.45). By examining the gluon propagator's poles in the position space representation one deduces that the correct analytic continuation is

$$\theta_+ = \frac{1}{2}\ln\frac{4(n\cdot y - i\epsilon)^2}{y^2 - i\epsilon}, \qquad \theta_- = \frac{1}{2}\ln\frac{4(n\cdot y - i\epsilon)^2}{y^2 + i\epsilon} \tag{3.46}$$

Next one uses the observation made in [51] that in the limit of a large Minkowski angle, the Γ_{cusp} is at most linear in the Minkowski angle

$$\Gamma_{cusp}(\theta, g) = \theta\ \Gamma_C(g) + \mathcal{O}(\theta^0), \tag{3.47}$$

this equation defines the *lightlike cusp anomalous dimension* Γ_C. As this quantity only depends on the coupling constant and renormalization scale, we recognize it to be a "universal" quantity of QCD. The linearity property of the cusp anomalous dimension was derived from the non-abelian exponentiation theorem [54, 68] which informs us that the dimensionally regularized Wilson line can be written in an exponential form, where the exponent is a weighted sum of a certain set[24] one particle irreducible diagrams containing two external lines. It then follows [51] from the definition of Γ_{cusp} in Eq.(3.44) that Γ_{cusp} is proportional to the R.G. derivative of a sum of $1PI$ graphs with two external lines. And by UV power counting, such graphs are at most double logarithmically divergent (when working in dimensional regularization), thus after taking a derivative we have that Γ_{cusp} can at most be logarithmic, which in turn means linear in the cusp angle.

We can now derive an R.G. equation for a lightlike Wilson line. By using the R.G. equation for $W(C_s)$ for y *not* on the lightcone

$$\left(\mu\frac{\partial}{\partial\mu} + \beta(g)\frac{\partial}{\partial g}\right)\ln\left(W(C_s)\right)\Big|_{y^2\neq 0} = -\Gamma_C(g)(\theta_+ + \theta_-) \tag{3.48}$$

we recognize that the only cause for the equation being ill-defined for $y^2 = 0$ is due to the $\theta_\pm$ containing y^2 factors in their denominators. One can therefore remove all y^2 dependence in the R.G. equation by taking a $n\cdot y$ derivative of Eq(3.48)

$$\begin{aligned}\left(\mu\frac{\partial}{\partial\mu} + \beta(g)\frac{\partial}{\partial g}\right)\frac{\partial}{\partial(n\cdot y)}\ln\left(W(C_s)\right) &= -\Gamma_C(g)\left\{\frac{1}{n\cdot y - \epsilon} + \left(\frac{1}{n\cdot y + i\epsilon}\right)^*\right\} \\ &= -\frac{2\Gamma_C(g)}{n\cdot y - i\epsilon}\end{aligned} \tag{3.49}$$

where the complex conjugation on the second term is due to θ_- occurring to the right of the final state cut. As Eq.(3.49) is y^2 independent, we can now formally set $y^2 = 0$. Furthermore, as $W(C_s)$ only depends on the parameter ρ we can integrate Eq.(3.49) to obtain our final result

[24] That is the set of maximally non-Abelian/web diagrams

$$\boxed{\left(\frac{\partial}{\partial\mu}+\beta(g)\frac{\partial}{\partial g}\right)W(C_s)=-\Big[2\Gamma_C(g)L(\rho)+\Gamma(g)\Big]W(C_s)} \qquad (3.50)$$

where $\Gamma(g)$ is the constant of integration and $L \coloneqq \log(i(\rho - i\epsilon)) + \gamma_E$. We emphasize that whilst $\Gamma(g)$ depends on the specific path of the Wilson line, $\Gamma_C(g)$ is a universal quantity. Unlike the RG equations for multiplicatively renormalizable operators, the RHS of Eq.(3.50) contains a μ dependent term (from the definition of ρ). This is origin of the convolutional as opposed to multiplicative form for the RG equations for PDF's, at least in the large-x region.

We can use our one loop (3.40) result to calculate the anomalous cusp dimension at one loop (suppressing pole prescription $i\epsilon$ factors for notational convenience)

$$-2\Gamma_C(g)\log(i\rho)-\Gamma(g)=\frac{d}{d\log\mu}\log W \qquad (3.51)$$

$$=\left(\frac{\partial}{\partial\log\mu}+\beta(g)\frac{\partial}{\partial g}\right)\log\left(1+\frac{\alpha_s}{\pi}C_F(-\log^2(i\rho)+\log(i\rho)-\frac{5}{24}\pi^2)\right) \qquad (3.52)$$

As $\beta(g)\approx g^3$ and $\frac{\partial}{\partial g}\log W \approx g$ we can ignore running coupling effects at order g^2. Evaluating the derivative then gives

$$-2\Gamma_C(g)\log(i\rho)-\Gamma(g)=\frac{\alpha_s}{\pi}C_F(-2\log(i\rho)+1)+\mathcal{O}\alpha_s^2 \qquad (3.53)$$

We thus find the anomalous dimension at one loop to be

$$\Gamma_C(\alpha_s)=\frac{\alpha_s}{\pi}C_F+\mathcal{O}(\alpha_s^2) \qquad (3.54)$$

$$\Gamma(\alpha_s)=-\frac{\alpha_s}{\pi}C_F+\mathcal{O}(\alpha_s^2) \qquad (3.55)$$

In the next section we will indicate how this results governs the large-x evolution of the parton distribution functions.

3.4 PDF Evolution

With the R.G. properties of $W(C_s)$ determined by Eq.(3.50), we can now infer consequences for parton distribution function evolution at large Bjorken-x. As P and y always feature in the combination $P \cdot y$ in the definition Eq.(3.4) of the PDF, we will work in terms of the dimensionless parameter $\sigma \coloneqq (P \cdot y)$

$$F\left(x, \frac{\mu}{M}\right) = H\left(\frac{\mu}{M}\right) \int_{-\infty}^{\infty} \frac{\mathrm{d}\sigma}{2\pi} e^{i\sigma(1-x)} W\left(\frac{\sigma\mu}{M} - i\epsilon\right) \tag{3.56}$$

The algebra of the derivation of the μ dependence of $F(x)$ is much simpler if we first invert the Fourier transform

$$H\left(\frac{\mu}{M}\right) W\left(\frac{\sigma\mu}{M}\right) = \int_{-\infty}^{\infty} \mathrm{d}x \; e^{-i\sigma(1-x)} F\left(x, \frac{\mu}{M}\right) \tag{3.57}$$

Taking an R.G. derivative on the LHS of Eq.(3.57) produces two terms. The first is

$$\left(\mu \frac{\mathrm{d}}{\mathrm{d}\mu} H\right) W = \left(\mu \frac{\mathrm{d}}{\mathrm{d}\mu} H\right) \frac{1}{H} H \cdot W \tag{3.58}$$

$$= \left(\mu \frac{\mathrm{d}}{\mathrm{d}\mu} \log(H)\right) HW, \tag{3.59}$$

The point of the manipulation was to obtain the LHS of Eq.(3.57) again, times a co-efficient. The second term that arises upon taking an RG derivative is

$$H\mu \frac{\mathrm{d}}{\mathrm{d}\mu} W = -\Big[2\Gamma_C(g) L(\rho) + \Gamma(g)\Big] WH \tag{3.60}$$

where we used the derived RG equation Eq.(3.50) for the lightlike Wilson line. Combing these two results we obtain

$$\left(\mu \frac{\mathrm{d}}{\mathrm{d}\mu} \log H - 2\Gamma_C(g) L(\sigma) + \Gamma(g)\right) \int_{-\infty}^{\infty} \mathrm{d}z \; e^{-i\sigma(1-z)} F(z, \frac{\mu}{M})$$

$$= \int_{-\infty}^{\infty} \mathrm{d}w \; e^{-i\sigma(1-w)} \mu \frac{\mathrm{d}}{\mathrm{d}\mu} F\left(w, \frac{\mu}{M}\right) \tag{3.61}$$

To isolate the term containing the RG derivative of the PDF, we multiply both sides by

$$\int_{-\infty}^{\infty} \frac{\mathrm{d}\sigma}{2\pi} e^{i\sigma(1-x)} \tag{3.62}$$

This then yields the RG equation for the PDF's

$$\boxed{\mu \frac{\mathrm{d}}{\mathrm{d}\mu} F\left(x, \frac{\mu}{M}\right) = \int_x^1 \mathrm{d}z \; P(z-x) F\left(z, \frac{\mu}{M}\right)} \tag{3.63}$$

where the splitting function is defined as

$$P(z-x) \coloneqq \int_{-\infty}^{\infty} \frac{\mathrm{d}\sigma}{2\pi}\, e^{i\sigma(z-x)} \left(\mu \frac{\mathrm{d}}{\mathrm{d}\mu} \log H - 2\Gamma_c(g) L(\sigma + \Gamma(g)) \right) \tag{3.64}$$

and at the last step we used the support properties

$$F(x, \frac{\mu}{M}) = 0 \quad \text{for} \quad z > 1 \tag{3.65}$$

$$P(z-x) = 0 \quad \text{for} \quad x > z \tag{3.66}$$

in order to set the integral bounds on Eq.(3.63). The first support property Eq.(3.65) follows from the definition of the PDF Eq.(3.56) and by recalling that all of the poles of $W(\frac{\sigma\mu}{M} - i\epsilon)$ lie in the upper half of the complex σ plane. Hence for $1 - x > 0$, the exponential in Eq.(3.56) tells us that we can close the σ contour in the upper half plane with the added contour lines giving a vanishing contribution. As this contribution encircles the poles of W, one obtains a non-zero value for the integral. Whereas for $(1 - x) < 0$ we can close the contour in the lower half plane, encircling no poles, and thus giving a zero result. The exact same reasoning applied to the definition of the splitting function in Eq(3.64) establishes the second support property Eq.(3.66).

We can use our one loop result Eq.(3.55) to calculate the splitting function to leading order. As all terms in Eq.(3.64) are σ independent, the only non-trivial Fourier transform is that of the logarithm [61]

$$\int_{-\infty}^{\infty} \frac{\mathrm{d}\sigma}{2\pi}\, e^{i\sigma(z-x)} \log(i\sigma e^{\gamma_E}) = \left[\frac{\theta(1-z)}{1-z} \right]_+ \tag{3.67}$$

where $(...)_+$ denotes the plus distribution. The splitting function at leading order is therefore

$$P(z) = 2\Gamma_C(g) \left[\frac{\theta(1-z)}{1-z} \right]_+ + \delta(1-z) h(g) \tag{3.68}$$

$$h(g) \coloneqq -\Gamma(g) + 2\Gamma_C(g) \ln \frac{M}{\mu} + \mu \frac{\mathrm{d}}{\mathrm{d}\mu} H(\frac{\mu}{M})$$

We therefore conclude that the lightlike cusp anomalous dimension controls the large x asymptotics of the parton distribution functions. The analysis also demonstrates that it is the loss of multiplicative renormalizabilty of cusped lightlike Wilson lines which leads to the convolutional form of the evolution equations of parton distribution functions.

3.5 Summary

In this chapter we have introduced an important universal quantity of QCD, the lightlike cusp anomalous dimension. We have demonstrated that this quantity governs the UV dependence of many important physical quantities such as

the large Bjorken-x DGLAP splitting functions and heavy meson form factors. We performed the first order calculation of this quantity and found it to be $\frac{\alpha_s C_F}{\pi}$. We note that cusp anomalous dimension continues to be considered an important quantity of Yang-Mills theory with it calculation to the four loop level recently completed [69].

4 Conclusion

In this thesis we have outlined the general framework of factorization used in making predictions for collider experiments. We introduced and developed some of the important tools that can be used in proving factorization theorems, such as power counting, Lorentz transformation properties of fields, the study of pinch singular surfaces and the Landau conditions. We indicated how pinch singular surfaces offer a powerful tool for analyzing the infrared singularity structure of quantum field theories in general. For example, we described how infrared singularities give rise to the jet structures observed in collider events. PSS's also guide us in the search for infrared finite observables, and provide a helpful intuition for understanding the cancellation of infrared divergences. We provided a more formal explanation for why partons can be treated as massless, onshell and target collinear in high energy scattering events. We then established a factorization theorem for DIS scattering. The proof indicated how essential gauge symmetry is in establishing useful factorization theorems. We noted that the factorization formalism would offer very little predictive power for tensor fields without the added gauge symmetry. With a proof of factorization in DIS outlined, we were able to decide on an appropriate set of definitions for the parton distribution functions and hard scattering co-efficients. We then derived the renormalization group properties of these quantities. One of the most interesting features of this renormalization group study was the observation that the DGLAP splitting kernels are " universal ". That is, the same kernels apply for the PDF of a parton-in-a-parton as for a parton in a hadron. This is the feature which enables one to perturbatively calculate the splitting functions and is one of the properties which gives QCD great predictive power despite many of the quantities involved in scattering events being non-perturbative.

We then analyzed the kinematics of the large-x regime of DIS scattering and found that a PDF with a cusped Wilson line captured many of the essential kinematic features of this region of phase space. We calculated this quantity to the one loop level and found that the presence of large logarithms required us to derive an RG equation for such Wilson line operators. By studying the renormalization properties of such operators we found that lightlike cusped Wilson lines exhibit interesting R.G. features such as the loss of multiplicative renormalizability. We described how, despite the loss of multiplicative renormalizability, one can nevertheless derive an R.G. equation for these operators. This lead us to an important universal object in perturbative QCD, the cusp anomalous dimension. We calculated this quantity to the one loop level and demonstrated

that it governs the large-x splitting functions. This analysis demonstrated that it was the loss of multiplicative renormalizability which leads to the convolutional form for the evolution of parton distribution functions.

Perturbative QCD continues to provide deep insights into the subatomic structure of matter, and it is hoped that the tools outlined in this thesis will help the student of QCD to begin exploring this open landscape for themselves.

Appendices

A Parameterizing Deep Inelastic Scattering

We aim to parameterize the inclusive deep inelastic cross section in terms of variables that can be inferred from knowledge of only the momentum of the incoming and outgoing electron. The transfer matrix amplitude for $eP \to e\mathcal{X}$ can be written as

$$i\mathcal{T} = \bar{u}(k_f)(-ie\gamma_\mu)u(k_i)\int d^4x\, e^{iq\cdot x}\ \langle \mathcal{X}|\hat{A}^\mu(x)|P\rangle \tag{A.1}$$

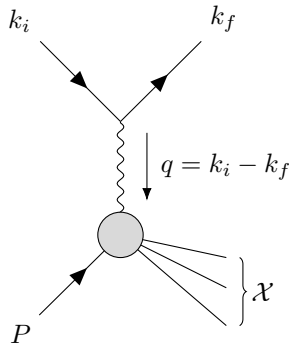

The variables are displayed in the Feynman diagram. We have ignored contributions from electron Bremsstrahlung and electron form factor corrections. The hadronic matrix element $\langle \mathcal{X}|\tilde{A}^\mu(q)|P\rangle$ is equal to the sum of all Feynman diagrams with a single external photon line carrying momentum q^μ and two external lines corresponding to the in proton state and final out state $\mathcal{X}$. This matrix element contains the photons external line factor of $\frac{-i}{q^2}$ which we can extract by multiplying the exponential by $-\eta_{\mu\lambda}\frac{\Box^{\gamma\lambda}_x}{q^2}$, where

$$\Box^{\gamma\lambda} \coloneqq \left(\Box g^{\gamma\lambda} - (1-\frac{1}{\xi})\partial^\gamma\partial^\lambda\right) \tag{A.2}$$

$$\eta_{\mu\lambda} \coloneqq \left(g_{\mu\lambda} - (1-\xi)\frac{q_\lambda q_\mu}{q^2}\right) \tag{A.3}$$

followed by integrating by parts, thus yielding

$$i\mathcal{T} = \frac{ie\eta_{\mu\nu}}{q^2+i\epsilon}\bar{u}(k_f)\gamma^\mu u(k_i)\int d^4x\, e^{iq\cdot x}\,\Box_{\nu\gamma}\,\langle \mathcal{X}|\hat{A}^\gamma(x)|P\rangle \tag{A.4}$$

We can then use the Schwinger-Dyson equations of QED

$$\begin{aligned}\Box_x^{\mu\nu} \langle\Omega|T\{A_\mu(x), \hat{\mathcal{O}}_1(x_1), ..., \hat{\mathcal{O}}_n(x_n)\}|\Omega\rangle \\ = \langle\Omega|T\{J_\nu(x), \hat{\mathcal{O}}_1(x_1), ..., \hat{\mathcal{O}}_n(x_n)\}|\Omega\rangle \\ - i\sum_{j=1}^{n} \langle\Omega|T\{\hat{\mathcal{O}}_1(x_1), ... \frac{\delta\hat{\mathcal{O}}_j(x_j)}{\delta A_a^\nu(x)} ..., \hat{\mathcal{O}}_n(x_n)\}|\Omega\rangle \quad \text{(A.5)}\end{aligned}$$

In our case we will have contact terms arising from the fields which interpolate the in/out states when using the LSZ reduction formula. The field which interpolates the proton is independent of the photon field operator and hence the proton contact term vanishes. The operator which interpolates the out state $\langle\mathcal{X}|$ may contain factors of the photon field, however, once the functional derivative with respect to the photon field has been taken, the pole structure of the operator will have been modified and thus this contact term will vanish when multiplied through by the $P_{\mathcal{X}}^2 - M_{\mathcal{X}}^2$ term featuring in the LSZ formula[25]. We therefore have that the transfer matrix element can be written as

$$\mathcal{T} = \frac{e^2\eta_{\mu\nu}}{q^2 + i\epsilon}\bar{u}(k_f)\gamma^\mu u(k_i)\int d^4x\, e^{iq\cdot x}\ \langle\mathcal{X}|\hat{J}^\nu(x)|P\rangle \quad \text{(A.6)}$$

Where $J^\mu(x)$ is the electromagnetic current in units of e, which contains all particles which couple to the photon directly. Using translational invariance we can factor out an overall momentum conserving delta function and thus extract the invariant matrix element $\mathcal{M}$. Choosing to work in Feynman gauge $\xi = 1$ we then have

$$\mathcal{M} = \frac{e^2}{q^2 + i\epsilon}\bar{u}(k_f)\gamma_\mu u(k_i)\ \langle\mathcal{X}|\hat{J}^\mu(0)|P\rangle \quad \text{(A.7)}$$

Squaring the amplitude, averaging over incoming electron spins and averaging over outgoing electron spins gives

$$\begin{aligned}\frac{1}{2}\sum_{spins}|\mathcal{M}|^2 = \frac{2e^4}{q^4}L_{\mu\nu}\ \langle\mathcal{X}|\hat{J}^\mu(0)|P\rangle\langle P|\hat{J}^\nu(0)|\mathcal{X}\rangle \\ L_{\mu\nu} \coloneqq k_f^\mu k_i^\nu + k_f^\nu k_i^\mu - g^{\mu\nu}k_f\cdot k_i\end{aligned}$$

Turning this into an inclusive cross section by including flux factors and summing over all possible out states gives

$$\begin{aligned}\sum_{\mathcal{X}}\sigma(e^-P \to e^-\mathcal{X}) = \frac{e^4}{2EE_P|v_i - v_p|}\int\frac{d^3k}{(2\pi)^3}\frac{1}{2E'}L_{\mu\nu}\int d\Pi_{\mathcal{X}} \\ (2\pi)^4\delta(k_i + P - P_{\mathcal{X}} - k_f)\ \langle P|\hat{J}^\nu(0)|\mathcal{X}\rangle\langle\mathcal{X}|\hat{J}^\mu(0)|P\rangle \quad \text{(A.8)}\end{aligned}$$

[25]Equivalently, we could argue that the momentum space delta function induced by the commutator of the photon field with the out state photon fields represents disconnected Feynman graphs, which one removes when calculating the S-matrix.

We then define the hadronic tensor $W^{\mu\nu}$ as

$$\begin{aligned} W^{\mu\nu} &\coloneqq \int d\Pi_{\mathcal{X}} (2\pi)^4 \delta(k_i + P - P_{\mathcal{X}} - k_f) \, \langle P|\hat{J}^\nu(0)|\mathcal{X}\rangle \langle \mathcal{X}|\hat{J}^\mu(0)|P\rangle \\ &= \int d\Pi_{\mathcal{X}} \int d^4x \, e^{k_i + P - P_{\mathcal{X}} - k_f} \, \langle P|\hat{J}^\nu(0)|\mathcal{X}\rangle \langle \mathcal{X}|\hat{J}^\mu(0)|P\rangle \end{aligned} \tag{A.9}$$

We can then use the momentum operator to write

$$\begin{aligned} \langle P|\hat{J}^\nu(0)|\mathcal{X}\rangle &= \langle P|e^{-i\hat{P}\cdot x}\hat{J}^\nu(x)e^{i\hat{P}\cdot x}|\mathcal{X}\rangle \\ &= e^{-ix\cdot(P-P_{\mathcal{X}})} \langle P|\hat{J}^\nu(x)|\mathcal{X}\rangle \end{aligned}$$

So that the hadronic tensor becomes

$$W^{\mu\nu} = \int d^4x e^{iq\cdot x} \langle P|J^\nu(x)J^\mu(0)|P\rangle \tag{A.10}$$

where we have used the completeness of the final set of states. Returning to our expressions for the cross section Eq.(A.8), if we specify the outgoing electrons energy E' and outgoing angle, then the differential cross section is

$$\frac{d\sigma}{dE'\, d\Omega} = \frac{\alpha_e^2}{2E_P}\frac{E'}{E}\frac{1}{|v_i - v_p|}\frac{1}{q^4} L_{\mu\nu}W^{\mu\nu} \tag{A.11}$$

We next wish to parameterize the tensor structure of $W^{\mu\nu}$. By the QED Ward identity we have that

$$\int d^4x \, e^{iq\cdot x} q_\mu \, \langle P|\hat{J}^\mu(x)|\mathcal{X}\rangle = 0 \tag{A.12}$$

Thus constraining $q_\mu W^{\mu\nu} = q_\nu W^{\mu\nu} = 0$. Thus the most general parameterization is

$$W^{\mu\nu} = W_1\bigg(- g_{\mu\nu} + \frac{q^\mu q^\nu}{q^2}\bigg) + W_2\bigg(P^\mu - \frac{P\cdot q}{q^2}q^\mu\bigg)\bigg(P^\nu - \frac{P\cdot q}{q^2}q^\nu\bigg) \tag{A.13}$$

The structure functions $W_{1,2}$ depend on the two invariants in the problem $P\cdot q$ and q^2. Contracting the lepton tensor with the hadron tensor gives

$$L_{\mu\nu}W^{\mu\nu} = 2W_1 \, k_f\cdot k_i + W_2(2P\cdot k_f P\cdot k_i - M_P^2 k_f\cdot k_i) \tag{A.14}$$

The differential cross section in an arbitrary frame is therefore

$$\begin{aligned} \frac{d\sigma}{dE'\, d\Omega} = \frac{\alpha_e^2}{2E_P}\frac{E'}{E}\frac{1}{|v_i - v_p|}\frac{1}{q^4} \\ \cdot\bigg\{2W_1(k_f\cdot k_i) + W_2\bigg(2P\cdot k_f P\cdot k_i - M_P^2 k_f\cdot k_i\bigg)\bigg\} \end{aligned} \tag{A.15}$$

If we then specify to the proton/lab frame we arrive at

$$\left(\frac{d\sigma}{dE'\,d\Omega}\right)_{Lab} = \frac{\alpha_e^2}{4E^2}\frac{\cos^2\frac{\theta}{2}}{\sin^4\frac{\theta}{2}}\left[W_2 + 2W_1\tan^2\frac{\theta}{2}\right] \tag{A.16}$$

Results are also sometimes reported in terms of the dimensionless structure functions:

$$F_1(Q^2,\nu) \coloneqq \frac{1}{4\pi}W_1(Q^2,\nu) \tag{A.17}$$

$$F_2(Q^2,\nu) \coloneqq \frac{\nu M_P}{4\pi}\,W_2(Q^2,\nu) \tag{A.18}$$

The Virtual Photon Cross Section

The subprocess of photon emission by the electron in DIS represents well understood and experimentally verified physics. Thus it is customary to extract this piece out of the cross section and report only the interesting subprocess of the virtual photon-proton scattering cross section $\sigma^{\gamma^* P}$. Note that, by the definition of the hadron tensor Eq.(A.9), the hadron tensor is equal to the sum of the square of all Feynman diagrams in which a virtual photon strikes a proton and produces any final state $\mathcal{X}$. By working with $\hat{J}$ matrix elements as opposed to $\hat{A}$ matrix elements we have also stripped of the $\frac{1}{q^2}$ propagator factors of the incoming and outgoing photons, thus the hadron tensor is related to the total virtual photon-proton cross section in the proton rest frame by

$$\sigma^{\gamma^* P}(x,Q^2) = \frac{\pi\alpha_e}{M_P\sqrt{\nu^2+Q^2}}\sum_\lambda \epsilon_\lambda^\mu \epsilon^{\nu *}_\lambda\; W_{\mu\nu}(x,Q^2) \tag{A.19}$$

where $\lambda = T, L$ denotes the transverse and longitudinal polarizations of the photon. There is an inherent ambiguity in the definition of the flux for a virtual particle. Here we have used Gilman's convention [70]. Let us introduce the helicity projectors of the photon

$$d_{\mu\nu}^{(L)} = \epsilon_\mu^L \epsilon_\nu^{L^*} = \frac{Q^2}{M_P^2(\nu^2+Q^2)}\left(P_\mu + \frac{P\cdot q}{Q^2}q_\mu\right)\left(P_\nu + \frac{P\cdot q}{Q^2}q_\nu\right) \tag{A.20}$$

$$d_{\mu\nu}^{(T)} = \epsilon_\mu^T \epsilon_\nu^{T^*} = -\frac{1}{2}\left(g_{\mu\nu} + \frac{q_\mu q_\nu}{Q^2}\right) - \frac{1}{2}d_{\mu\nu}^{(L)} \tag{A.21}$$

Contracting the projectors onto the hadron tensor (which is made easier by noting that $W^{\mu\nu}$ is orthogonal to q^μ)

$$\sigma_L^{\gamma^* P} = \frac{4\pi^2\alpha_e}{\sqrt{\nu^2+Q^2}}\left[-W_1 + \left(1+\frac{\nu^2}{Q^2}\right)W_2\right] \tag{A.22}$$

$$\sigma_T^{\gamma^* P} = \frac{4\pi^2\alpha_e}{\sqrt{\nu^2+Q^2}}W_1 \tag{A.23}$$

Neglecting Q^2 with respect to ν^2, which is appropriate in the low Bjorken x limit, and working with the dimensionless structure functions gives

$$\sigma_L^{\gamma^* P} = \frac{4\pi^2\alpha_e}{Q^2}(F_2 - 2xF_1) \tag{A.24}$$

$$\sigma_T^{\gamma^* P} = \frac{4\pi^2\alpha_e}{Q^2}2xF_1 \tag{A.25}$$

Then taking the sum of the two cross sections gives our final result for the total virtual photon-proton cross section in terms of the dimensionless structure functions

$$\sigma_{tot}^{\gamma^* P}(x, Q^2) = \frac{4\pi^2\alpha_e}{Q^2}F_2(x, Q^2) \tag{A.26}$$

$$W_1(\nu, Q^2) = \frac{K}{4\pi^2\alpha}\sigma_T(\nu, Q^2) \tag{A.27}$$

$$W_2(\nu, Q^2) = \frac{K}{4\pi^2\alpha}\left(\frac{Q^2}{Q^2+\nu^2}\right)[\sigma_T(\nu, Q^2) + \sigma_L(\nu, Q^2)] \tag{A.28}$$

$$K \coloneqq \frac{(W^2 - M^2)}{2M} \tag{A.29}$$

Where σ_T and σ_L refer respectively to the total virtual photon-proton cross section for transverse or longitudinal photon polarization. We have defined the mass of the hadronic system $W^2 \coloneqq (P+q)^2$.

The Dispersion Relation

We seek to show

$$Disc[T_{\mu\nu}] = iW_{\mu\nu} \tag{A.30}$$

where the forward Compton amplitude $T_{\mu\nu}$ is defined in Eq.(1.31). Writing the time ordering in terms of step functions

$$T_{\mu\nu}(\nu, Q^2) = i\int d^4x e^{iq\cdot x}\Big(\theta(x_0)\langle P|J_\mu(x)J_\nu(0)|P\rangle + \theta(-x_0)\langle P|J_\nu(0)J_\mu(x)|P\rangle\Big) \tag{A.31}$$

we note that the second term vanishes in the Bjorken limit as can be seen by inserting a complete set of intermediate states and then by translating

$$\begin{aligned}\int d^4x e^{iq\cdot x}\langle P|J_\nu(0)J_\mu(x)|P\rangle &= \int d^4x \int d\Pi_{\mathcal{X}} e^{iq\cdot x}\langle P|J_\nu(0)|\mathcal{X}\rangle\langle\mathcal{X}|J_\mu(x)|P\rangle \\ &= \int d^4x \int d\Pi_{\mathcal{X}} e^{ix\cdot(q+P_{\mathcal{X}}-P)}\langle P|J_\nu(0)|\mathcal{X}\rangle\langle\mathcal{X}|J_\mu(0)|P\rangle\end{aligned} \tag{A.32}$$

Integrating out x^0 yields a $\delta(P^0_{\mathcal{X}} + q^0 - P^0)$ which in the rest frame of the proton implies that the intermediate state has an energy $E_{\mathcal{X}} = M_P - \nu$. In the Bjorken limit we send $\nu \to \infty$, hence there are no physical intermediate states

contributing to this term and thus it vanishes.
Using the representation

$$\theta(x^0) = \frac{1}{2\pi i}\int_{-\infty}^{\infty}\frac{ds}{s-i\epsilon}e^{isx^0} \tag{A.33}$$

for the first term in Eq.(A.31) and again inserting a complete set of states followed by using the momentum operator to translate the current, we find

$$\begin{aligned} T_{\mu\nu}(\nu,Q^2) =& \frac{1}{2\pi}\int d^4x \int d\Pi_{\mathcal{X}} \int_{-\infty}^{\infty}\frac{ds}{s-i\epsilon}e^{isx^0}e^{ix\cdot(q-P_{\mathcal{X}}+P)} \\ & \cdot \langle P|J_\mu(0)|\mathcal{X}\rangle \langle \mathcal{X}|J_\nu(0)|P\rangle \end{aligned} \tag{A.34}$$

Integrating out x and s yields

$$T_{\mu\nu}(\nu,Q^2) = \int d\Pi_{\mathcal{X}} \frac{(2\pi)^3\delta^3(\vec{q}+\vec{P}-\vec{P}_{\mathcal{X}})}{P^0_{\mathcal{X}}-q^0-P-i\epsilon}\cdot\langle P|J_\mu(0)|\mathcal{X}\rangle\langle\mathcal{X}|J_\nu(0)|P\rangle \tag{A.35}$$

Then using that

$$Disc[\,\frac{1}{P^0_{\mathcal{X}}-q^0-P-i\epsilon}\,] = 2\pi i\,\delta(P^0_{\mathcal{X}}-q^0-P) \tag{A.36}$$

we have that

$$\begin{aligned} Disc[T_{\mu\nu}] &= i\int d\Pi_{\mathcal{X}}\ (2\pi)^4\delta^4(q+P-P_{\mathcal{X}})\,\langle P|J_\mu(0)|\mathcal{X}\rangle\langle\mathcal{X}|J_\nu(0)|P\rangle \\ &= iW_{\mu\nu} \end{aligned}$$

Which is what we sought to prove. The analyticity of the S-matrix implies that the discontinuity of any amplitude is $2i$ times its imaginary part [38], thus we can also write are derived relation as

$$2\,Im[T_{\mu\nu}] = W_{\mu\nu} \tag{A.37}$$

B Quantization of QCD on the lightcone

In the Bjorken limit, the currents featuring in the DIS hadronic tensor approach a lightlike separation, see the discussion at Eq.(1.34) This motivates the use of lightcone quantization. We will find in Sect that this approach most closely captures most of the intuitive features of the parton model, such as the number density interpretation of the PDF's. Furthermore, lightcone quantization, when used with an old fashioned pertrubation theory approach can simplify some of the features of perturbative calculations. The founding paper is [71]

Canonical quantization

Let us briefly review the canonical quantization procedure. One first picks an arbitrary $d-1$ dimensional sub-manifold which splits spacetime in two. The directions orthogonal to this quantization surface then define the direction of time, which we will denote by x^t. To evolve fields away from the quantization surface one uses Heisenbergs evolution equations

$$i\frac{\partial \hat{O}(x)}{\partial x^t} = [\hat{O}(x), g^{t\mu}\hat{P}_\mu] \tag{B.1}$$

where this equation defines the unitary operator $\hat{P}^t$ to be the generator of translations orthogonal to the quantization surface. One determines the commutation/anti-commutation of the fields on the equal time surface by requiring that Eq.(B.1) reproduces the classical equations of motion for the elementary fields. The unitarity of the evolution then guarantees that the commutation relations will continue to hold when evaluated on any other equal time surface.

Lightcone quantization

In "light front" quantization one uses a lightlike surface $x^+ := x^0 + x^3 = \text{constant}$ as the initial surface upon which the commutation relations are determined. One then uses the lightcone Hamiltonian $\hat{P^-} := \hat{P^0} - \hat{P^3}$ to evolve away from the surface. Note that we therefore identify $\hat{P^-}$ and not $\hat{P^+}$ with the energy of the system as $\hat{P^-}$ generates translations orthogonal to the initial surface of quantization whereas $\hat{P^+}$ translates along the initial surface. The co-ordinate x^+ therefore referred to as "lightcone time" and henceforth we will refer to it as the time co-ordinate, see Fig(B.1).

Fermions on the lightcone

Unlike in the instant approach, each Dirac spinor only has two degrees of freedom in the lightcone approach, with the other two components being determined by a constraint equation. To see this, we note that the classical QCD equations of motion for the fermion fields read

$$(i\gamma^\mu D_\mu - m)\psi = 0 \tag{B.2}$$

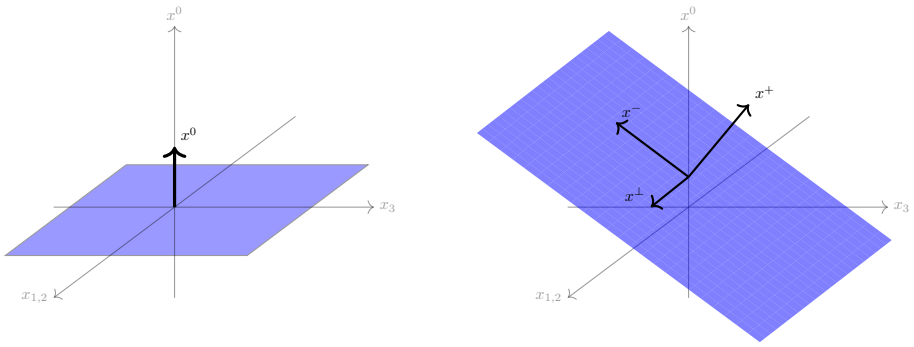

Figure B.1: The blue surfaces represents the "quantization" surfaces upon which the equal "time" commutation relations are determined. They also serve as the surfaces where the initial conditions of the fields are imposed. The left and right panels respectively refer to the "instant" and "lightfront" schemes of quantization.

which unlike in Cartesian co-ordinates, the term containing a time derivative $\gamma^+\partial_+$ only affects two of the four components of ψ. This can be seen by defining the so-called good and bad projection operators

$$\mathcal{P}_G = \frac{1}{2}\gamma^-\gamma^+ \qquad \mathcal{P}_B = \frac{1}{2}\gamma^+\gamma^- \tag{B.3}$$

which satisfy the usual properties of projectors ($\mathcal{P}_G + \mathcal{P}_B = \mathbb{1}$, $\mathcal{P}_G^2 = \mathcal{P}_G$, $\mathcal{P}_B\mathcal{P}_G = 0$ etc). Then we define the good and bad components of the fermion field by

$$\psi_G = \mathcal{P}_G\psi, \qquad \psi_B = \mathcal{P}_B\psi \tag{B.4}$$

so that $\bar{\psi}_G = \bar{\psi}\mathcal{P}_B$.
The equations of motion then take the form

$$2iD_+\psi_G + \gamma^-(i\gamma_\perp^j D_j - m)\psi_B = 0 \tag{B.5}$$

$$2iD_-\psi_B + \gamma^+(i\gamma_\perp^j D_j - m)\psi_G = 0 \tag{B.6}$$

The first equation gives the x^+ evolution of the good components of the field. The second equation does not contain any ∂_+ terms and is therefore to be treated as a constraint equation. The bad fields do not have any dynamics of their own. They are to be expressed as a function of the dynamical fields

$$\psi_B = \gamma^+\frac{i}{2D_-}(i\gamma_\perp^j D_j - m)\psi_G \tag{B.7}$$

This presents a problem which as of yet is not resolved. Eq.(B.7) is not uniquely determined by the values of the ψ_G and A_a^μ fields on an initial surface of constant

x^+. This can be seen by working in lightcone gauge $A_- = A^+ = 0$ where the solution to Eq.(B.7) is

$$\psi_B(x) = \frac{i\gamma^+}{4}\int_{-\infty}^{\infty} dy^- \theta(x^- - y^-)(i\gamma_\perp^j D_j - m)\psi_G(x^+, y^-, x_\perp) + C_\psi(x^+, x_\perp) \tag{B.8}$$

The x^- independent term $C_\psi(x^+, x_\perp)$ indicates that the equations of motion and initial conditions are not sufficient for determining evolution in x^+. By Fourier transforming C_ψ in x^- we see that this term only contributes to the zero energy k^+ mode and hence is related to the structure of the vacuum. Henceforth we will ignore this complication.
We can construct the Hamiltonian P^- from the Lagrangian

$$P^- = \int dx^- d^2x_\perp [\bar{\psi}(-i\gamma^- D_- - i\gamma_\perp^j D_j + m)\psi] \tag{B.9}$$

We can now determine the equal time commutation relations of the fields by requiring that the Heisenberg equations

$$i\frac{\partial \hat{A}(x)}{\partial x^+} = [\hat{A}(x), \hat{P^-}] \tag{B.10}$$

correctly reproduce the Euler-Lagrange equations for the fields. Thus we have

$$\{\psi_G(x^+, x^-, x_\perp), \bar{\psi}_G(x^+, w^-, w_\perp)\} = \frac{\gamma^-}{2}\delta(x^- - w^-)\delta^2(x_\perp - w_\perp) \tag{B.11}$$

The constraint equation for ψ_B is non-linear in the fields implying that the equal time commutator of these components are not $c-$number functions multiplying a delta function, but instead are operator valued. Current algebra relies on these commutation relations being $c-$valued, hence one can only apply current algebra to the good fields. Furthermore, without simple commutation relations, one cannot construct physically intuitive operators such as the number operator $N \sim a_p^\dagger a_p$ which rely on these commutators. These are the primary reasons for referring to the ψ_B as the bad components of the fields.

B.0.1 Light front annihilation and creation operators

We can now express the interaction picture components of the good fields in terms of annihilation and creation operators

$$\psi_G(x) = \sum_\alpha \int_0^\infty \frac{dk^+}{2k^+}\int \frac{d^2k_\perp}{(2\pi)^3}\Big(b_{k,\alpha}(x^+)u_{k,\alpha}e^{-ik^+x^- + ik_\perp\cdot x_\perp} + d_{k,\alpha}^\dagger(x^+)u_{k,-\alpha}e^{ik^+x^- ik_\perp\cdot x_\perp}\Big) \tag{B.12}$$

Note that the Hamiltonian Eq.(B.9) does not contain any terms linear in ∂_+ and hence the linearly solvable part of the evolution does not contain any x^+

dependence. This is the reason for having the annihilation and creation operators carry the x^+ dependence and not in the exponential factors.
The label α corresponds to "light-front helicity" in the sense that

$$\sigma^{x_\perp y_\perp}\, u_{k,\alpha} = 2\alpha\, u_{k,\alpha} \tag{B.13}$$

where $\sigma^{x_\perp y_\perp} \coloneqq \frac{i}{2}[\gamma^{x_\perp}, \gamma^{y_\perp}]$ and $\alpha = \pm 1$. The bounds on the k^+ integral follow from the phase space associated with 1-particle states of the Poincaré group

$$\begin{aligned}\int d^4k\, \delta(k^2 - m^2)\theta(k^0) &= \int_{-\infty}^{\infty} dk^- \int_{-\infty}^{\infty} \frac{dk^+}{2|k^+|} \int d^2k_\perp \delta(k^- - \frac{k_\perp^2 + m^2}{k^+})\theta(k^+ + k^-) \\ &= \int \frac{dk^+}{2|k^+|} \int_{-k^+}^{\infty} \mathrm{d}k^- \int d^2k_\perp\ \delta\left(k^- - \frac{k_\perp^2 + m^2}{k^+}\right)\end{aligned} \tag{B.14}$$

Clearly the only region of integration where the Dirac delta function has support is $k^+ > 0$. Also note that although k^+ features in many places where k^0 usually features such as $\frac{\theta(k^+)}{2k^+}$ it is not to be mistaken for the energy co-ordinate.

Interestingly, the measure associated with the one particle phase space does not require the specification of a particle mass, unlike in the instant form of quantization in which $\sqrt{\vec{k}^2 + m^2}$ features. This is an advantage since there is an inherent ambiguity in deciding which mass to use: the bare, physical and $\bar{M}S$ renormalized mass all being different and the latter two not being known prior to solving the theory. Moreover, confined particles such as quarks do not have a definite physical mass
Examination of Eq.(B.5,B.6) motivates us to define the wavefunctions of the "good" components of the Dirac free field to be massless with zero transverse momentum. Furthermore we normalize them to obey

$$\bar{u}_{k,\alpha}\gamma^+ u_{k,\alpha'} = 2k^+\delta_+\alpha\alpha' \tag{B.15}$$

and hence

$$\sum_\alpha u_{k,\alpha}\bar{u}_{k,\alpha} = k^+\gamma^- \tag{B.16}$$

With these relations we can invert the Fourier transform Eq.(B.12) to find

$$b_{k,\alpha}(x^+) = \int dx^- d^2\mathbf{x}_\perp e^{ik^+x^- - ik_\perp\cdot x_\perp}\bar{u}_{k,\alpha}\gamma^+\psi_G(x) \tag{B.17}$$

$$d_{k,\alpha}(x^+) = \int dx^- d^2\mathbf{x}_\perp e^{ik^+x^- - ik_\perp\cdot x_\perp}\bar{\psi}_G(x)\gamma^+ u_{k,-\alpha} \tag{B.18}$$

Then using the anticommutation relations of the good components of the fields Eq.(B.11) the anticommutation relations of the creation and annihilation operators follow

$$\{b_{k,\alpha}, b^\dagger_{l,\alpha'}\} = \{d_{k,\alpha}, d^\dagger_{l,\alpha'}\} = (2\pi)^3 2k^+\delta(k^+ - l^+)\delta^{(2)}(k_\perp - l_\perp)\delta_{\alpha\alpha'} \tag{B.19}$$

with the other anti-commutators all zero. These simple commutation relations imply that we can readily construct the number operator for the good quark and anti-quark fields at Eq.(2.73).

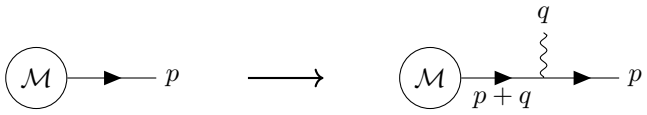

Figure C.1: Feynman diagram contributing to the modification of an amplitude to include a real final state soft photon. This diagram is specific to emission by a final state particle.

C The Summation of Soft-Collinear Radiation

QED Example

Denoting the amplitude for an arbitrary process involving a final state electron of momentum p as $\mathcal{M} \coloneqq \bar{u}(p)\tilde{\mathcal{M}}(p)$, the amplitude for the same process but with the electron radiating a real final state soft photon of momentum k^μ is

$$\begin{aligned}
\text{Fig.(C.1)} &= \tilde{\mathcal{M}}(p+q)\bar{u}(p)(-ie\gamma^\alpha\epsilon^*_\alpha(q))\frac{i(\not{p}+\not{q})+m}{(p+q)^2-m^2+i\epsilon} \\
&\overset{q\ll p}{\approx} \tilde{\mathcal{M}}(p)\bar{u}(p)e\gamma^\alpha\epsilon^*_\alpha(q)\frac{\not{p}+m}{2p\cdot q+i\epsilon} + \mathcal{O}q^\alpha\frac{\partial}{\partial p^\alpha}\tilde{\mathcal{M}}(p) \\
&= \tilde{\mathcal{M}}(p)\bar{u}(p)e\frac{p\cdot\epsilon^*(q)}{p\cdot q+i\epsilon} \\
&= \left(e\frac{p\cdot\epsilon^*(q)}{p\cdot q+i\epsilon}\right)\mathcal{M}(p)
\end{aligned} \tag{C.1}$$

To obtain the second line one uses that the final state particles are on-shell ($q^2 = 0$ and $p^2 = m^2$). The third line follows by commuting the $\not{p}$ past the γ^α and then by use of the Dirac equation $\bar{u}(p)(\not{p}-m) = 0$. To obtain the full amplitude for single photon emission we must sum over all all external[26] state particles in $\mathcal{M}$ as sources of the photon. For emission by an initial state electron, the fermionic propagator has momentum $(p-q)^\mu$ giving the same result but with a denominator $(-p\cdot q+i\epsilon)$. For emission by an anti-particle the propagator acquires a minus sign as per the usual Feynman rules. The net amplitude for single photon emission in the $q \to 0$ limit during the process $\mathcal{M}$ is then

$$\mathcal{M}(\{p\};k) = \left(\sum_i e_i\eta_i\frac{p_i\cdot\epsilon^*(k)}{p_i\cdot q+i\eta\epsilon}\right)\mathcal{M}(\{p\}) \tag{C.2}$$

where $\eta = +1$ and -1 for final and initial state particles respectively and $e = +1$ and -1 for particles and anti-particles respectively. The eikonal factor $\frac{p\cdot\epsilon^*(q)}{p\cdot q}$ exhibits many interesting features and is in fact common to charged particles

[26] Of course the photon could also be emitted by an internal line, but in that case there is no factor that goes as $(p\cdot q)^{-1}$ for $q \to 0$

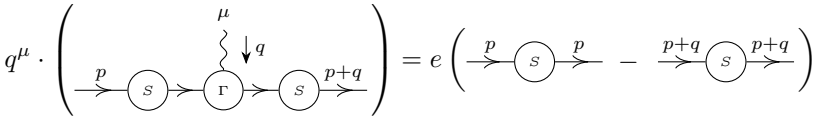

Figure C.2: Diagrammatic representation of the Ward-Takahashi identity applied to the electron-photon three point function.

of any spin [**?**] interacting with a massless spin one gauge boson[27]. Firstly, it is diagonal in spinor indices — as one might intuitively expect that soft radiation is unable to flip spin. It is also dependent only on the direction and not the energy of the emitting particle. We will make this second feature manifest by rewriting the eikonal factor in terms of the emitting particles direction vector $n^\mu := \frac{p^\mu}{p^0}$

$$\frac{p \cdot \epsilon^*(q)}{p \cdot q} = \frac{n \cdot \epsilon^*(q)}{n \cdot q} \tag{C.3}$$

By far the most important feature for our purposes of the eikonal factor is its divergence structure. Furthermore, Eq.(C.2) is correct to all orders in perturbation theory in the soft limit $q \to 0$. This can be seen by applying the Ward-Takahashi identity to the three point function of an incoming electron, an outgoing electron and an absorbed photon. The identity is represented diagrammatically in Fig.(C.2) and it states that, for not necessarily on-shell momenta,

$$q_\mu \Gamma^\mu(p+q,p) = i\Big(S^{-1}(p+q) - S^{-1}(p)\Big) \tag{C.4}$$

Where $\Gamma^\mu(p, p+q)$ denotes the sum of all amputated one particle irreducible contributions to the electron-photon interaction vertex, $S(p)$ denotes the full fermion propagator,

$$S^{-1}(p) = -i(\not{p} - m_{\mathcal{L}} - \Sigma(p)) \tag{C.5}$$

$\Sigma(p)$ denotes the sum of all amputated one particle irreducible contributions to the fermion two point function and $m_{\mathcal{L}}$ denotes the mass featuring in the Lagrangian. In the limit of infinitely soft radiation $q^\mu \to 0$, the Ward identity Eq.(C.4) reads

$$\begin{aligned}\Gamma^\mu(p,p) &= i\frac{\partial}{\partial p^\mu} S^{-1}(p) \\ &= \gamma^\mu + \frac{\partial}{\partial p^\mu}\Sigma(p)\end{aligned}$$

[27]The stated reference also demonstrates that one can use the eikonal factor along with its Lorentz transformation properties to derive the conservation of charge, the equivalence principle of gravitation and the prohibition of spin $j \geq 3$ particles at low energies in a rather expedient fashion.

However, when calculating S-matrix elements we work with renormalized fields $\psi_R = Z_\psi^{1/2}\psi$, choosing the rescaling constant to ensure that the full fermion propagator has unit residue at the location of the mass shell pole—which is precisely the statement that

$$\frac{\partial}{\partial p^\mu}\Sigma(p)\bigg|_{p=m_R} = 0 \tag{C.6}$$

Therefore, in the case of an onshell outgoing electron, the emission vertex for soft radiation in the limit that $q \to 0$ is

$$\bar{u}(p)\Gamma^\mu(p,p)u(p) = \bar{u}(p)\gamma^\mu u(p) \tag{C.7}$$

This then guarantees that all higher order corrections to the eikonal identity vanish in this limit. Note that had we not used a renormalized fermion field then the correction to the vertex function would have canceled the corrections due to radiative corrections to the external fermion lines, leaving the electric charge again unchanged.

Before turning to multiple photon emissions, let us establish where the connection between eikonal factors and Wilson Lines will emerge from. For this, we will need to use the result that for a renormalized field[28] $\hat{A}^\mu(y)$ and a final state photon of momentum q^μ we have

$$\langle q|\hat{A}_\mu(y)|\Omega\rangle = e^{ik\cdot y}\epsilon^*_\mu(q) \tag{C.8}$$

With this, and by making use of Schwinger's integral trick, we can rewrite the eikonal factor as

$$\begin{aligned} e\frac{n\cdot\epsilon^*(q)}{n\cdot q + i\epsilon} &= ie\, n\cdot\epsilon^*(k)\int_0^\infty dT\ e^{iT(n\cdot k)}e^{-\epsilon T} \\ &= \langle k|ie\int_0^\infty dT\ n\cdot\hat{A}(n^\nu T)e^{-\epsilon T}|\Omega\rangle \end{aligned} \tag{C.9}$$

We will come to recognize Eq.(C.9) as the first order Taylor expansion of a Wilson line matrix element. We can account for the minus sign of initial state particles by setting the bounds on the Schwinger integral to $\int_{-\infty}^0$, thus also mimicking the naive 'times' of emission. Anti-particles are again accommodated by the sign of e_i. Now let us consider the effects of including two photon emissions. In the case that the photons are emitted by two different external legs, the matrix element is simply multiplied by a product of two eikonal factors. Perhaps surprisingly, the same neat factorization occurs for emission from the same external leg. Taking Figure (C.3) as an example

[28] Indeed Eq.(C.8) is the condition one aims to satisfy when choosing the field strength renormalization constant.

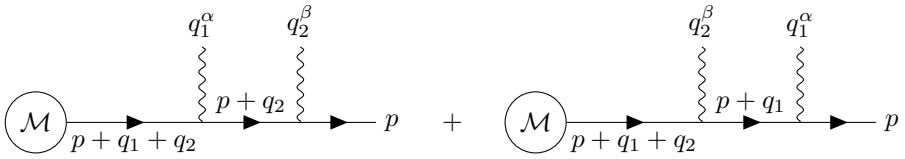

Figure C.3: Double photon emmision from the same external final state leg. The two possible orderings of the emissions give rise to two diagrams

$$\begin{aligned}
\text{Fig.(C.3)} &= (-ie)^2\bar{u}(p)\left[\gamma^\beta\frac{i(\not{p}+\not{q}_2+m)}{(p+q_2)^2-m^2}\gamma^\alpha+\gamma^\alpha\frac{i(\not{p}+\not{q}_1+m)}{(p+q_1)^2-m^2}\gamma^\beta\right]\tilde{\mathcal{M}}\\
&\approx e^2\bar{u}(p)\left[\frac{1}{p\cdot q_2}+\frac{1}{p\cdot q_1}\right]\frac{p\cdot\epsilon^*(q_1)p\cdot\epsilon^*(q_2)}{p\cdot(q_1+q_2)}\tilde{\mathcal{M}}\\
&= e^2\left(\frac{p\cdot\epsilon^*(q_1)}{p\cdot q_1}\right)\left(\frac{p\cdot\epsilon^*(q_2)}{p\cdot q_2}\right)\mathcal{M} \qquad \text{(C.10)}
\end{aligned}$$

This neat factorization of eikonal terms continues to hold for any number of final state photon emissions, as is readily proved by mathematical induction[29]. It follows then that the amplitude $\mathcal{M}_{\alpha\beta}(q_1,..,q_N)$ for emitting N final state photons of momenta $\{\,q_i\,\}$, during the process $\alpha\to\beta$, in the limit that $q_i\to 0$ is obtained simply by multiplying the $\mathcal{M}_{\alpha\beta}$ amplitude by the factorized product of eikonal factors

$$\mathcal{M}_{\alpha\beta}(q_1,...,q_N)=\mathcal{M}_{\alpha\beta}\left[\prod_{r=1}^{N}\left(\sum_i\eta_i e_i\frac{p_i\cdot\epsilon^*(q_r)}{p_i\cdot q_r+i\eta_i\epsilon}\right)\right] \qquad \text{(C.11)}$$

Using the same manipulations as in Eq.(C.9) we can rewrite this as the matrix element of a product of Wilson Line operators. For example the eikonal factors

[29]We have already seen that it is true for 2 photons. Suppose that it is true for $N-1$ photons. For N photons we may write the sum over permutations as a sum over the choice of the first emitted photon q_r which has the associated propagator factor of $\left[p\cdot\sum_{s=1}^N q_s\right]^{-1}$ together with a sum over the permutations of the remaining $N-1$ photons

$$\begin{aligned}
&\left[p\cdot q_1\right]^{-1}\left[p\cdot(q_1+q_2)\right]^{-1}...\left[p\cdot(q_1+q_2...+q_N\right]^{-1}+\text{permutations}\\
&=\sum_{r=1}^{N}\left[p\cdot\left(\sum_{s=1}^{N}q_s\right)\right]^{-1}\prod_{s\neq r}\left[p\cdot q_s\right]^{-1}\\
&=\sum_{r=1}^{N}\left[p\cdot\left(\sum_{s=1}^{N}q_s\right)\right]^{-1}\left[p\cdot q_r\right]\prod_{s=1}^{N}\left[p\cdot q_s\right]^{-1}=\prod_{s=1}^{N}\left[p\cdot q_s\right]^{-1}
\end{aligned}$$

as was to be proved.

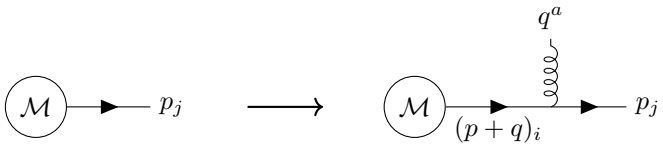

Figure C.4: Feynman diagram contributing to the modification of an amplitude to include a real final state soft gluon. The a index indicates the color generator associated with the gluon and the the ij indicate the color of the fermions.

associated with 2 photons emitted from the same leg of direction n_i we can write

$$e_i^2\left(\frac{n_i\cdot\epsilon^*(q_1)}{n_i\cdot q_1+i\epsilon}\right)\left(\frac{n_i\cdot\epsilon^*(q_2)}{n_i\cdot q_2+i\epsilon}\right)=\frac{1}{2!}\,\langle q_1q_2|\left[ie_i\int_0^\infty dT_1\;n_i\cdot\hat{A}(n_i^\mu T_1)e^{-\epsilon T_1}\right]\left[ie_i\int_0^\infty dT_2\;n_i\cdot\hat{A}(n_i^\mu T_2)e^{-\epsilon T_2}\right]|\Omega\rangle \tag{C.12}$$

The $\frac{1}{2!}$ is necessary for the two possible sets of contractions of the A fields onto the out state photons. For any number of final state photons emitted from the same leg we observe

$$\prod_{r=1}^{N}\eta_i e_i\frac{n_i\cdot\epsilon^*(q_r)}{n_i\cdot q_r+i\eta_i\epsilon}=\langle q_1...q_N|\exp\left[ie_i\int_{\eta_i}dT\;n_i\cdot\hat{A}(n_i^\mu T)e^{-\epsilon\eta_i T}\right]|\Omega\rangle \tag{C.13}$$

$$\coloneqq\langle q_1...q_N|U(n_i,\eta_i,e_i)|\Omega\rangle \tag{C.14}$$

Where the integral bounds $\int_{\eta_i}$ are $\int_0^\infty$ and $\int_{-\infty}^0$ for final and initial state particles respectively. The only non-zero term in the expansion of the exponential is the term containing N gauge fields $\hat{A}$. We can therefore write Eq.(C.11) in terms of Wilson Lines as

$$\mathcal{M}_{\alpha\beta}(q_1,..,q_N)=\langle\beta|\alpha\rangle\,\langle q_1...q_N|\prod_{i\,\epsilon\,\beta,\alpha}U(n_i,\eta_i,e_i)|\Omega\rangle \tag{C.15}$$

Non-Abelian Example

The effect of soft gluon radiation on hard amplitudes is similar to the effects of photon radiation discussed in the previous section,however there are some interesting subtle differences. For the case of one gluon emission into the final state, the modification of the amplitude is

$$\text{Fig.(C.4)}=\sum_i\left(gt_{ij}^a\frac{p\cdot\epsilon^*(q)}{p\cdot q+i\epsilon}\right)\mathcal{M} \tag{C.16}$$

The two immediate differences are the presence of a $\mathfrak{su}[N_c]$ lie algebra element (thus the soft radiation does not rotate the spin degrees of freedom but does

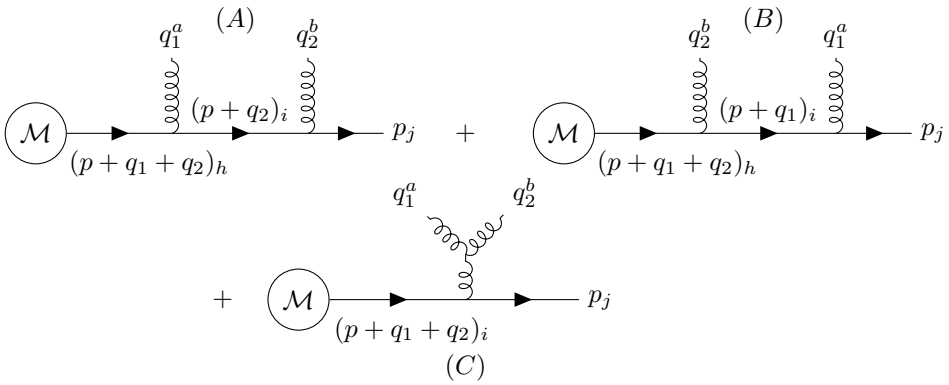

Figure C.5: Diagrams contributing to double gluon emission from the same external final state leg.

cause the rotation of the color of the hard particle) and a trivial change of sign relative to the QED eikonal factor, due to the difference in conventions between the signs of the interaction vertex of the two. In the case of two gluons in the final state, there are now three contributing graphs Fig.(C.5)

Graphs (A) and (B) of Fig.(C.5) sum to

$$(A)+(B) = g^2\left(t^b t^a \frac{p\cdot\epsilon^*(q_2)}{p\cdot q_2}\frac{p\cdot\epsilon^*(q_1)}{p\cdot(q_1+q_2)} + t^a t^b \frac{p\cdot\epsilon^*(q_1)}{p\cdot q_1}\frac{p\cdot\epsilon^*(q_2)}{p\cdot(q_1+q_2)}\right) \quad \text{(C.17)}$$

Due to the non-commutative nature of the algebra elements, this term does not factorize into the simple product of the form of Eq.(C.10), nevertheless the result still does co-coincide with the matrix element of a Wilson Line, as long as we include the important feature of path ordering. Evaluating the following matrix element demonstrates the point

$$\begin{aligned}
&\langle q_1^a q_2^b|\,(ig)^2\int_0^\infty dT_1\int_0^{T_1} dT_2\ \ n\cdot\hat{A}^c(nT_1)\ \ n\cdot\hat{A}^d(nT_2)\ t^c t^d\,|\Omega\rangle \\
&= (ig)^2\int_0^\infty dT_1\int_0^{T_1} dT_2\ n\cdot\epsilon^*(q_1)\ n\cdot\epsilon^*(q_2)\left(t^a t^b\ e^{in\cdot(T_1 q_1+T_2 q_2)} + t^b t^a\ e^{in\cdot(T_2 q_1+T_1 q_2)}\right) \\
&= g^2\left(t^b t^a \frac{p\cdot\epsilon^*(q_2)}{p\cdot q_2}\frac{p\cdot\epsilon^*(q_1)}{p\cdot(q_1+q_2)} + t^a t^b \frac{p\cdot\epsilon^*(q_1)}{p\cdot q_1}\frac{p\cdot\epsilon^*(q_2)}{p\cdot(q_1+q_2)}\right) = \text{Eq.(C.17)}
\end{aligned}$$

Generalizing to any number of final state soft gluons, the relevant Wilson Line definition must be

$$U(n_i,\eta_i,e_i) \coloneqq \mathcal{P}\exp\left(ig_i\int_{\eta_i} dT\ n\cdot\hat{A}^a(n_i T)t^a e^{-\epsilon\eta_i T}\right) \quad \text{(C.18)}$$

and with this definition of the Wilson Line, the QCD generalization of Eq.(C.15) holds for final state gluons. There is a subtle difference however in the evaluation

of the matrix elements of the QCD and QED Wilson Lines; in the case of gluons one must include gluon self interactions such as in diagram (C) of Fig.(C.5) . One can appreciate why such diagrams are not factored into the Wilson Line; the eikonal factors arise due to the simplifications occurring between the interaction of soft radiation with hard matter, whereas in diagram (C) there is no such separation of energy scales as all gluons are presumed to be soft.

D Useful Formulae

- Propagators

  The Virtual Boson Propagator in Covariant gauge is

$$D^{\mu\nu}(x) = i \int \frac{\mathrm{d}^d k}{(2\pi)^d} e^{-ik\cdot x} \frac{1}{k^2 + i\epsilon} \tag{D.1}$$

$$= (-1)^{2-\frac{D}{2}} \eta^{\mu\nu} \delta_{ab} \frac{\Gamma(\frac{D}{2} - 1)}{4\pi^{\frac{D}{2}}} (x^2 - i\epsilon)^{1-\frac{D}{2}} \tag{D.2}$$

  The cut propagator, in the case of zero displacement in the transverse directions $x_\perp = 0$)

$$D_+(x) = \int \frac{\mathrm{d}^d k}{(2\pi)^d} e^{-ik\cdot x} 2\pi\theta(k^0)\delta(k^2) \tag{D.3}$$

$$= -\eta^{\mu\nu} \delta_{ab} \frac{\Gamma(\frac{D}{2} - 1)}{4\pi^{\frac{D}{2}}} (-2(x^+ - i\epsilon)(x^- - i\epsilon))^{1-\frac{D}{2}} \tag{D.4}$$

  In the case that $x^2 > 0$ and $x^0 > 0$ we have that the cut and virtual propagators coincide.

- Beta-function

$$B(\mu, \nu) = \int_0^1 dx\, x^{\mu-1}(1-x)^{\nu-1} \tag{D.5}$$

$$= \int_0^\infty dx\, x^{\nu-1}(1+x)^{-\mu-\nu} \tag{D.6}$$

$$= \frac{\Gamma(\mu)\Gamma(\nu)}{\Gamma(\mu+\nu)} \tag{D.7}$$

- Gamma-function
  - Integral Representation

$$\Gamma(z) = \int_0^\infty dx\, x^{z-1} \exp(-x) \tag{D.8}$$

  - Recursion Relation

$$z\Gamma(z) = \Gamma(z+1) \tag{D.9}$$

  - Expansion

$$\Gamma(1+\epsilon) = \exp(-\epsilon\gamma_E + \frac{1}{12}\epsilon^2\pi^2 + \mathcal{O}\epsilon^3) \tag{D.10}$$

  - Pole expansions: Near $x = -n$

$$\Gamma(x) = \frac{(-1)^n}{n!}\left(\frac{1}{x+n} - \gamma + 1 + ... + \frac{1}{n} + \mathcal{O}(x+n)\right) \tag{D.11}$$

- Useful Expansions

$$A^{\epsilon} = 1 + \epsilon \log A + \frac{\epsilon^2}{2!} \log^2 A + \frac{\epsilon^3}{3!} \log^3 A + \mathcal{O}\epsilon^3 \tag{D.12}$$

References

[1] H. Geiger and E. Marsden. On a Diffuse Reflection of the α -Particles. *Proceedings of the Royal Society of London Series A*, 82:495–500, July 1909.

[2] Professor E. Rutherford F.R.S. Lxxix. the scattering of and particles by matter and the structure of the atom. *The London, Edinburgh, and Dublin Philosophical Magazine and Journal of Science*, 21(125):669–688, 1911.

[3] Dr. H. Geiger and E. Marsden. Lxi. the laws of deflexion of a particles through large angles. *The London, Edinburgh, and Dublin Philosophical Magazine and Journal of Science*, 25(148):604–623, 1913.

[4] R. W. McAllister and R. Hofstadter. Elastic Scattering of 188-Mev Electrons from the Proton and the Alpha Particle. *Phys. Rev.*, 102:851–856, May 1956.

[5] E. B. Hughes, T. A. Griffy, M. R. Yearian, and R. Hofstadter. Neutron Form Factors from Inelastic Electron-Deuteron Scattering. *Phys. Rev.*, 139:B458–B471, Jul 1965.

[6] W Albrecht, HJ Behrend, FW Brasse, W Flauger, H Hultschig, and KG Steffen. Elastic electron-proton scattering at momentum transfers up to 245 f- 2. *Physical Review Letters*, 17(23):1192, 1966.

[7] Elliott D. Bloom et al. High-Energy Inelastic e p Scattering at 6-Degrees and 10-Degrees. *Phys. Rev. Lett.*, 23:930–934, 1969.

[8] M. Breidenbach, J. I. Friedman, H. W. Kendall, E. D. Bloom, D. H. Coward, H. DeStaebler, J. Drees, L. W. Mo, and R. E. Taylor. Observed Behavior of Highly Inelastic Electron-Proton Scattering. *Phys. Rev. Lett.*, 23:935–939, Oct 1969.

[9] J. I. Friedman. Deep inelastic scattering: Comparisons with the quark model. *Reviews of Modern Physics*, 63:615–628, July 1991.

[10] J. D. Bjorken. Asymptotic sum rules at infinite momentum. *Phys. Rev.*, 179:1547–1553, Mar 1969.

[11] Curtis G. Callan and David J. Gross. Bjorken scaling in quantum field theory. *Phys. Rev. D*, 8:4383–4394, Dec 1973.

[12] Sidney Coleman and David J. Gross. Price of asymptotic freedom. *Phys. Rev. Lett.*, 31:851–854, Sep 1973.

[13] George F. Sterman. *An Introduction to quantum field theory.* Cambridge University Press, 1993.

[14] K. Symanzik. Small distance behaviour in field theory and power counting. *Comm. Math. Phys.*, 18(3):227–246, 1970.

[15] Curtis G. Callan. Broken scale invariance in scalar field theory. *Phys. Rev. D*, 2:1541–1547, Oct 1970.

[16] K. Symanzik. Small-distance-behaviour analysis and Wilson expansions. *Comm. Math. Phys.*, 23(1):49–86, 1971.

[17] N. Christ, B. Hasslacher, and A. H. Mueller. Light-cone behavior of perturbation theory. *Phys. Rev. D*, 6:3543–3562, Dec 1972.

[18] Paul G. Federbush and Kenneth A. Johnson. Uniqueness property of the twofold vacuum expectation value. *Phys. Rev.*, 120:1926–1926, Dec 1960.

[19] David J. Gross. Nobel lecture: The discovery of asymptotic freedom and the emergence of qcd. *Rev. Mod. Phys.*, 77:837–849, Sep 2005.

[20] Gerard 't Hooft. Renormalization of Massless Yang-Mills Fields. *Nucl. Phys.*, B33:173–199, 1971.

[21] David J. Gross and Frank Wilczek. Ultraviolet Behavior of Nonabelian Gauge Theories. *Phys. Rev. Lett.*, 30:1343–1346, 1973. [,271(1973)].

[22] H. David Politzer. Reliable Perturbative Results for Strong Interactions? *Phys. Rev. Lett.*, 30:1346–1349, 1973. [,274(1973)].

[23] John C. Collins, Davison E. Soper, and George F. Sterman. Factorization of Hard Processes in QCD. *Adv. Ser. Direct. High Energy Phys.*, 5:1–91, 1989.

[24] John Collins. Foundations of perturbative QCD. *Camb. Monogr. Part. Phys. Nucl. Phys. Cosmol.*, 32:1–624, 2011.

[25] George F. Sterman. QCD and jets. In *Physics in D >= 4. Proceedings, Theoretical Advanced Study Institute in elementary particle physics, TASI 2004, Boulder, USA, June 6-July 2, 2004*, pages 67–145, 2004.

[26] Geoffrey T. Bodwin, Stanley J. Brodsky, and G. Peter Lepage. Initial State Interactions and the Drell-Yan Process. *Phys. Rev. Lett.*, 47:1799, 1981.

[27] Geoffrey T. Bodwin. Factorization of the Drell-Yan Cross-Section in Perturbation Theory. *Phys. Rev.*, D31:2616, 1985. [Erratum: Phys. Rev.D34,3932(1986)].

[28] John C. Collins, Davison E. Soper, and George F. Sterman. Factorization for Short Distance Hadron - Hadron Scattering. *Nucl. Phys.*, B261:104–142, 1985.

[29] John C. Collins, Davison E. Soper, and George F. Sterman. Soft Gluons and Factorization. *Nucl. Phys.*, B308:833–856, 1988.

[30] L. D. Landau. On analytic properties of vertex parts in quantum field theory. *Nucl. Phys.*, 13:181–192, 1959.

[31] Richard John Eden, Peter V. Landshoff, David I. Olive, and John Charlton Polkinghorne. *The analytic S-matrix*. Cambridge Univ. Press, Cambridge, 1966.

[32] S. Coleman and R. Norton. Singularities in the physical region. *Nuovo Cimento Serie*, 38:438–442, July 1965.

[33] Stephen B. Libby and George Sterman. Mass divergences in two-particle inelastic scattering. *Phys. Rev. D*, 18:4737–4745, Dec 1978.

[34] George Sterman. Mass divergences in annihilation processes. i. origin and nature of divergences in cut vacuum polarization diagrams. *Phys. Rev. D*, 17:2773–2788, May 1978.

[35] George Sterman. Mass divergences in annihilation processes. ii. cancellation of divergences in cut vacuum polarization diagrams. *Phys. Rev. D*, 17:2789–2799, May 1978.

[36] Steven Weinberg. *The Quantum theory of fields. Vol. 1: Foundations*. Cambridge University Press, 2005.

[37] John C. Collins, Leonid Frankfurt, and Mark Strikman. Factorization for hard exclusive electroproduction of mesons in QCD. *Phys. Rev.*, D56:2982–3006, 1997.

[38] Michael E. Peskin and Daniel V. Schroeder. *An Introduction to quantum field theory*. Addison-Wesley, Reading, USA, 1995.

[39] J. M. F. Labastida and George F. Sterman. Inclusive Hadron - Hadron Scattering in the Feynman Gauge. *Nucl. Phys.*, B254:425–440, 1985.

[40] P V. Landshoff. The propagator in axial gauge. 169:69–72, 03 1986.

[41] Guido Altarelli, R. Keith Ellis, and G. Martinelli. Large Perturbative Corrections to the Drell-Yan Process in QCD. *Nucl. Phys.*, B157:461–497, 1979.

[42] T. Kinoshita. Mass singularities of Feynman amplitudes. *J. Math. Phys.*, 3:650–677, 1962.

[43] T. D. Lee and M. Nauenberg. Degenerate Systems and Mass Singularities. *Phys. Rev.*, 133:B1549–B1562, 1964. [,25(1964)].

[44] George F. Sterman. Summation of Large Corrections to Short Distance Hadronic Cross-Sections. *Nucl. Phys.*, B281:310–364, 1987.

[45] John C. Collins and Davison E. Soper. Parton Distribution and Decay Functions. *Nucl. Phys.*, B194:445–492, 1982.

[46] Igor Olegovich Cherednikov, Tom Mertens, and Frederik F. Van der Veken. *Wilson lines in quantum field theory*, volume 24. De Gruyter, 2014.

[47] Yuri L. Dokshitzer. Calculation of the Structure Functions for Deep Inelastic Scattering and e+ e- Annihilation by Perturbation Theory in Quantum Chromodynamics. *Sov. Phys. JETP*, 46:641–653, 1977. [Zh. Eksp. Teor. Fiz.73,1216(1977)].

[48] Guido Altarelli and G. Parisi. Asymptotic Freedom in Parton Language. *Nucl. Phys.*, B126:298–318, 1977.

[49] V. N. Gribov and L. N. Lipatov. Deep inelastic e p scattering in perturbation theory. *Sov. J. Nucl. Phys.*, 15:438–450, 1972. [Yad. Fiz.15,781(1972)].

[50] Alexander M. Polyakov. Gauge Fields as Rings of Glue. *Nucl. Phys.*, B164:171–188, 1980.

[51] G. P. Korchemsky and A. V. Radyushkin. Renormalization of the Wilson Loops Beyond the Leading Order. *Nucl. Phys.*, B283:342–364, 1987.

[52] G. P. Korchemsky. Asymptotics of the Altarelli-Parisi-Lipatov Evolution Kernels of Parton Distributions. *Mod. Phys. Lett.*, A4:1257–1276, 1989.

[53] I. Ya. Arefeva. Quantum Contour Field Equations. *Phys. Lett.*, 93B:347–353, 1980.

[54] V. S. Dotsenko and S. N. Vergeles. Renormalizability of Phase Factors in the Nonabelian Gauge Theory. *Nucl. Phys.*, B169:527–546, 1980.

[55] Richard A. Brandt, Filippo Neri, and Masa-aki Sato. Renormalization of Loop Functions for All Loops. *Phys. Rev.*, D24:879, 1981.

[56] Matthias Neubert. Heavy quark symmetry. *Phys. Rept.*, 245:259–396, 1994.

[57] Aneesh V. Manohar and Mark B. Wise. Heavy quark physics. *Camb. Monogr. Part. Phys. Nucl. Phys. Cosmol.*, 10:1–191, 2000.

[58] A. G. Grozin. Heavy quark effective theory. *Springer Tracts Mod. Phys.*, 201:1–213, 2004.

[59] Michal Czakon, Alexander Mitov, and George F. Sterman. Threshold Resummation for Top-Pair Hadroproduction to Next-to-Next-to-Leading Log. *Phys. Rev.*, D80:074017, 2009.

[60] Adam F. Falk, Howard Georgi, Benjamin Grinstein, and Mark B. Wise. Heavy Meson Form-factors From QCD. *Nucl. Phys.*, B343:1–13, 1990.

[61] G. P. Korchemsky and G. Marchesini. Structure function for large x and renormalization of Wilson loop. *Nucl. Phys.*, B406:225–258, 1993.

[62] I. A. Korchemskaya and G. P. Korchemsky. On lightlike Wilson loops. *Phys. Lett.*, B287:169–175, 1992.

[63] Rikkert Frederix. Wilson lines in qcd. *nikhef/masters-thesis*, 2005.

[64] Alfred H. Mueller. Perturbative QCD at High-Energies. *Phys. Rept.*, 73:237, 1981.

[65] Guido Altarelli. Partons in Quantum Chromodynamics. *Phys. Rept.*, 81:1, 1982.

[66] A. Bassetto, M. Ciafaloni, and G. Marchesini. Jet Structure and Infrared Sensitive Quantities in Perturbative QCD. *Phys. Rept.*, 100:201–272, 1983.

[67] Yuri L. Dokshitzer, Valery A. Khoze, S. I. Troian, and Alfred H. Mueller. QCD Coherence in High-Energy Reactions. *Rev. Mod. Phys.*, 60:373, 1988.

[68] J. G. M. Gatheral. Exponentiation of Eikonal Cross-sections in Nonabelian Gauge Theories. *Phys. Lett.*, 133B:90–94, 1983.

[69] Zvi Bern, Michael Czakon, Lance J. Dixon, David A. Kosower, and Vladimir A. Smirnov. The Four-Loop Planar Amplitude and Cusp Anomalous Dimension in Maximally Supersymmetric Yang-Mills Theory. *Phys. Rev.*, D75:085010, 2007.

[70] Elliot Leader and Enrico Predazzi. *An Introduction to Gauge Theories and Modern Particle Physics*, volume 2 of *Cambridge Monographs on Particle Physics, Nuclear Physics and Cosmology.* Cambridge University Press, 1996.

[71] P. A. M. Dirac. Forms of relativistic dynamics. *Rev. Mod. Phys.*, 21:392–399, Jul 1949.